Final Report 2002-06

Research

Analysis Tools and Rapid Screening Data for Distortional Fatigue in Steel Bridge Girders

Technical Report Documentation Page

1. Report No.	2.	3. Recipients Accession No.
MN/RC –2002-06		

4. Title and Subtitle	5. Report Date
ANALYSIS TOOLS AND RAPID SCREENING DATA FOR DISTORTIONAL FATIGUE IN STEEL BRIDGE GIRDERS	December 2001
	6.

7. Author(s)	8. Performing Organization Report No.
Evan Berglund Arturo E. Schultz	

9. Performing Organization Name and Address	10. Project/Task/Work Unit No.
Department of Civil Engineering University of Minnesota 122 Civil Engineering 500 Pillsbury Drive SE Minneapolis, MN 55455	11. Contract (C) or Grant (G) No. (C) 74708 wo) 177

12. Sponsoring Organization Name and Address	13. Type of Report and Period Covered
Minnesota Department of Transportation 395 John Ireland Boulevard Mail Stop 330 St. Paul, Minnesota 55155	Final Report 2001 14. Sponsoring Agency Code

15. Supplementary Notes

16. Abstract (Limit: 200 words)

Fatigue cracking often occurs in composite bridges with unstiffened girder web gaps at the ends of transverse stiffeners. In this project, researchers sought to better understand bridge diaphragm deflection behavior and advance the ability to estimate web gap distortional stress. Trends from the parametric studies led to general observations that may assist in identifying fatigue-prone bridges.

Variables that influence diaphragm deflection behavior include girder spacing, bridge skew, span length, and deck thickness. Transverse load distribution properties appear to play the most significant role in determining the magnitude of differential deflection. Parameter study stress trends indicate that out-of-plane distortional stress in fatigue prone web gaps primarily depends on web gap properties, bridge span length, and angle of skew.

Differential deflection and web gap dimension trends apply to a varied spectrum of bridge configurations. The research resulted in a method to assess bridge girder differential deflection and distortional stress in actual steel bridges without complex analysis and modeling. Proposed procedures for evaluating out-of-plane stress should prove practical and aid in screening, identifying, and assessing bridges vulnerable to distortion –induced fatigue cracking.

17. Document Analysis/Descriptors	18. Availability Statement
Fatigue Cracking Bridge Girder	No restrictions. Document available from: National Technical Information Services, Springfield, Virginia 22161

19. Security Class (this report)	20. Security Class (this page)	21. No. of Pages	22. Price
Unclassified	Unclassified	103	

Analysis Tools and Rapid Screening Data for Assessing Distortional Fatigue in Steel Bridge Girders

Final Report

Prepared by:

Evan Berglund

Arturo E. Schultz

Department of Civil Engineering
University of Minnesota
Minneapolis, Minnesota 55455

December 2001

Published by:

Minnesota Department of Transportation
Office of Research and Strategic Services
Transportation Building
395 John Ireland Boulevard
St. Paul, Minnesota 55155-1899

ACKNOWLEDGEMENTS

This research would not have been possible without the generous support of the Minnesota Department of Transportation (Mn/DOT) and the Graduate School of the University of Minnesota. Special thanks are also extended to the American Institute of Steel Construction (AISC) and to the US Steel Corporation for their generous financial support through the AISC-US Steel Graduate Fellowship to Evan Berglund during the fall semester 2001. The authors would like to give thanks to Paochen Mma, Joe Louis, and Gary Peterson from the Mn/DOT Office of Bridges and Structures. Their knowledge and direction was instrumental to the progress and success of this project.

Many thanks also to Eric Corwin, Altan Altay, Paul Bergson, Ted Galambos, and Robert Dexter for their assistance in finite element modeling, fatigue information, bridge visits, and their knowledge and ideas in regard to the content and direction of this project. Without their assistance, this project could not have been completed in a timely manner and their time and effort deserve special thanks.

Table of Contents

List of Figures

List of Tables

List of Equations

Executive Summary

Displacement-induced fatigue cracking has developed in many types of steel bridges. Steel bridge design prior to 1985 discouraged the welding of girder web stiffeners to tension flanges, which resulted in a prevalent, fatigue prone detail. Unstiffened girder web gaps at the ends of transverse stiffeners, which also serve as diaphragm connection plates, are subjected to high stress from cyclic, out-of-plane distortion. Fatigue cracking often occurs in composite bridges with this detail because girders undergoing differential vertical displacement have rigid diaphragms between the girders that rotate and force large out-of-plane distortions in the web gap. This phenomenon is considered the most significant source of fatigue damage in U.S. steel bridges.

Past research has focused on understanding the extent of the distortional stress problem and assessing the effectiveness of retrofit solutions to alleviate web-gap distortion and stress. Previous Minnesota Department of Transportation (Mn/DOT) research advanced the understanding of web gap behavior in skewed, steel bridges with staggered, rigid plate diaphragms. A simple equation for estimating the magnitude of web gap stress was proposed which can be used to accurately estimate web gap stress given bridge properties and the magnitude of diaphragm differential deflection. Despite this research attention, no recommendations exist for evaluating the magnitude of girder differential deflection, which correspond directly with the web gap stresses that govern the remaining life in many steel bridges. There is in essence no guidance for bridge owners to identify and assess which structures are in jeopardy of developing web cracks and which are not. Although observations have been made of bridge characteristics that contribute to the problem of distortional fatigue in steel bridges, the technical literature offers scant publications on research efforts directed at a comprehensive understanding of bridge characteristics responsible for distortional fatigue.

The need for a reliable method to assess distortional fatigue susceptible bridges prompted Mn/DOT to fund the current research. Full-scale, three-dimensional finite element models were developed for analysis to accurately predict bridge girder deflection behavior. A parametric study was conducted to determine bridge characteristics that have significant impact on girder

relative deflection, and, therefore, also have strong influence on out-of-plane stress and distortion-induced fatigue. Bridges were modeled to have all possible combinations of parameters thought to have significant effect on differential deflection. Other parameters, believed to have less influence on bridge deflection behavior, were investigated in secondary modeling studies.

The research findings within this study further the understanding of bridge diaphragm deflection behavior and advance the ability to estimate web gap distortional stress and assess distortional fatigue. Behavior in bridges with unique configurations may be analyzed using the finite element modeling techniques reported in this study. Trends from the parametric studies lead to general observations that can assist in identifying fatigue prone bridges. Variables that influence diaphragm deflection behavior include: girder spacing, bridge skew, span length, and deck thickness. Transverse load distribution properties appear to play the most significant role in determining the magnitude of differential deflection. Trends identified in the parameter study stress indicate that out-of-plane distortional stress in fatigue-prone web-gaps is primarily dependent on web gap properties, bridge span length, and angle of skew.

Trends concerning differential deflection and web gap dimensions should be applicable to a varied spectrum of bridge configurations. Analysis of results generated simple formulas for estimating differential vertical deflection and characterizing web-gap geometry. These formulas and the web-gap stress formula developed in the previous study renders a method by which bridge girder differential deflection and distortional stress may be assessed in steel bridges without the need for complex modeling and analysis. Proposed procedures for evaluating out-of-plane stress should prove practical and aid in screening, identifying, and assessing bridges vulnerable to distortion-induced fatigue cracking.

Chapter 1
Introduction

1.1 Background

Steel bridges with multiple girders are a commonly used structural system for highways in the United States and throughout the world. These bridges have functioned well in the past and are an efficient structure for spans common within our nation's infrastructure. The composite steel bridge is a system that incorporates a reinforced concrete deck attached to girder flanges by shear studs embedded in the concrete. The deck and steel girders behave in a composite manner that aids in resisting bridge loads while maintaining serviceability requirements. Transverse loads are distributed to the bridge girders via the concrete deck and steel members oriented transverse to the girders. These transverse steel members, often known as diaphragms, tie girders together, provide resistance for lateral loads, and serve as bracing during construction.

It is common in the design of steel plate girders to terminate or cope transverse stiffeners near the girder flanges to avoid intersecting web to stiffener welds with welds at the flange and web connection. Bridge design prior to 1985 discouraged the welding of web stiffeners to girder tension flanges due to fatigue considerations. Since 1985, such connections have typically been welded or rigidly bolted. The transverse stiffener weld was terminated short of the girder flange to provide a coped weld access hole and to avoid welding in an already heat-affected weld zone.

Diaphragms connect adjacent girders by means of connection plates that also serve as girder transverse stiffeners. In such cases, the short 2.5 to 5 cm (1 to 2 in) unbraced portion of the girder web, or web-gap, between the tension flange and the web stiffener must accommodate all movement due to diaphragm rotation caused by differential vertical deflection of adjacent girders. This is especially the case in negative moment regions where the top flange is fully restrained by a stiff concrete deck.

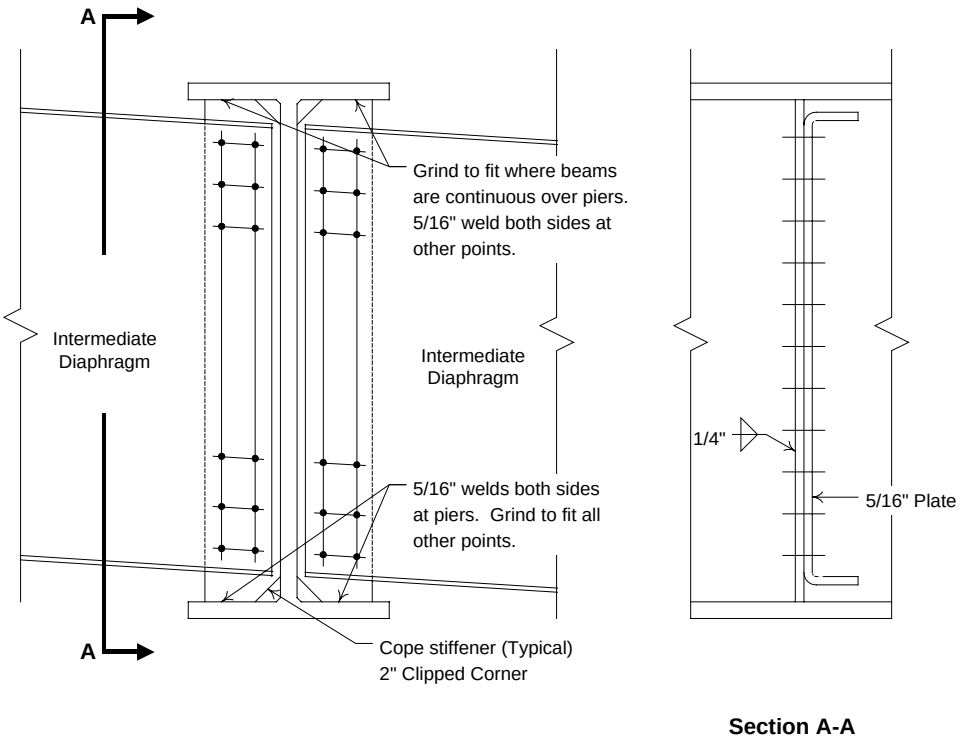

Figure 1.1 Typical Intermediate Diaphragm Detail

Fatigue cracks in steel bridges often result from out-of-plane distortion. Web gap out-of-plane distortion at the toe of the web stiffener leads to stresses several times larger than flange stresses and cracking may occur well within the design life of a bridge structure due to the high cyclic stresses that occur under normal bridge loading. Much research has been conducted to address the magnitude of distortional stress and fatigue cracking and a variety of solutions have been proposed and implemented to alleviate the problem. Although existing design recommendations offer solutions to mitigate distortional fatigue damage, design procedures do not directly address out-of-plane deformations and no guidance exists for evaluating the magnitude of web gap stresses that govern the fatigue and remaining life of many steel girder bridges.

1.2 Objective

Although observations have been made of basic bridge characteristics that contribute to distortional fatigue in steel bridges, the research literature indicates there has been little research effort expended toward a comprehensive understanding of bridge characteristics responsible for this phenomenon. Recent research funded by the Minnesota Department of Transportation

(Mn/DOT) furthered the understanding of the web gap distortion mechanism and led to the development of a simple equation for estimating stress magnitudes [1]. This prompted Mn/DOT to fund further study aimed at understanding which bridges may be susceptible to distortional fatigue. The research objectives included (1) the development of three-dimensional finite element models for bridge analysis to accurately predict differential vertical deflection between adjacent girders, (2) a parametric study to determine bridge characteristics that significantly impact diaphragm relative deflection and therefore also have strong influence on out-of-plane stress and distortion-induced fatigue, and (3) provide a means to assess bridge girder differential deflection and distortional stress.

1.3 Outline

This report begins with a brief introduction to the topic of distortional stress in steel bridges. Also included are the objectives of this research project and a brief outline of the contents of this report.

Chapter 2 presents a literature review of the problems associated with web gap out-of-plane distortion and research that has been conducted to understand and correct the problem. Issues regarding a previous Mn/DOT research project, which is the foundation of this present research, are discussed, as are bridge models that have been used to study composite steel bridge behavior.

Chapter 3 discusses the finite element model that was formulated and calibrated to study the deflection behavior of the previously instrumented and studied Mn/DOT bridge. Verification of the model to provide confidence in its predictive ability is given to ensure its reliability in future modeling studies.

Chapter 4 introduces the preliminary finite element studies that were conducted. Information was gathered to establish guidelines for the generation of bridge characteristics to ensure the systematic proportioning of bridge models was consistent with the Mn/DOT bridge inventory.

Chapter 5 documents the primary parameter study. Parameters deemed to have significant effect on diaphragm relative deflection are discussed. In addition, results are presented from the finite element study of models having all possible combinations of these primary parameters.

Chapter 6 outlines the secondary parameter study. Secondary parameters were not included in the primary parameter study to limit the number of finite element analyses needed to address all bridge parametric combinations. They were instead investigated selectively to determine how significant their role can be in bridge deflection behavior.

Chapter 7 presents trends for stresses calculated within the primary parameter study. Three-dimensional plots of stress are provided to accurately illustrate the trends present. The assumptions made within the stress equations are also discussed.

Chapter 8 describes the proposed assessment tools by which distortional stress may be estimated in existing bridges. The assumptions made in developing the equations and the identified trends are also discussed to identify the usefulness and limitations of the assessment tools.

Chapter 9 reviews the findings of this study as well as the implications, conclusions, and importance of this research.

Chapter 2
Literature Review

2.1 Overview

Displacement-induced fatigue cracking has developed in many types of bridges, including trusses, suspension bridges, girder/floor-beam bridges, multi-beam bridges, tie arch bridges, and box girder bridges [2]. The technical literature regarding distortion-induced fatigue damage may be placed into two separate categories. The first class of literature documents cases of distortional stress, fatigue damage, and features common to damaged bridges. The second class includes laboratory research into the origin and magnitude of the distortional stresses. Although less common than field research, laboratory experimentation has been conducted to provide detailed insight into the causes of distortion-induced cracking and assessing retrofit designs. Retrofit solutions proposed to alleviate the distortional stresses that cause cracking have been common in research investigations. Field observations and experimental research has prompted code changes and provided design guidelines. Field studies and experimental research can greatly enhance the understanding of the nature and severity of the distortional fatigue problem, as well as help guide the maintenance and design of steel bridges.

2.2 Web Gap Behavior

A small gap in the girder web between the girder flange and the termination of transverse stiffeners is commonly found in multi-girder bridges to provide access to the flange-web connection and to avoid further welding in a region with high local stresses (Figure 1.1). Bridge design prior to 1985 discouraged the welding of web stiffeners to girder tension flanges due to fatigue considerations. Since 1985, connections have typically been welded, as permitted by fatigue design considerations, or have been rigidly bolted. Many designers prefer to bolt the stiffener to the flange to completely avoid possible fatigue issues. The lack of a positive connection between transverse stiffener connection plates and the girder tension flange has rendered this detail susceptible to out-of-plane distortion. When bridge girders undergo vertical displacements, stiff diaphragms between girders force the transverse stiffener to displace and

rotate (Figure 2.1). All deformation of the web-gap must be accommodated by the short 2.5 to 5 cm (1 to 2 in) web gap.

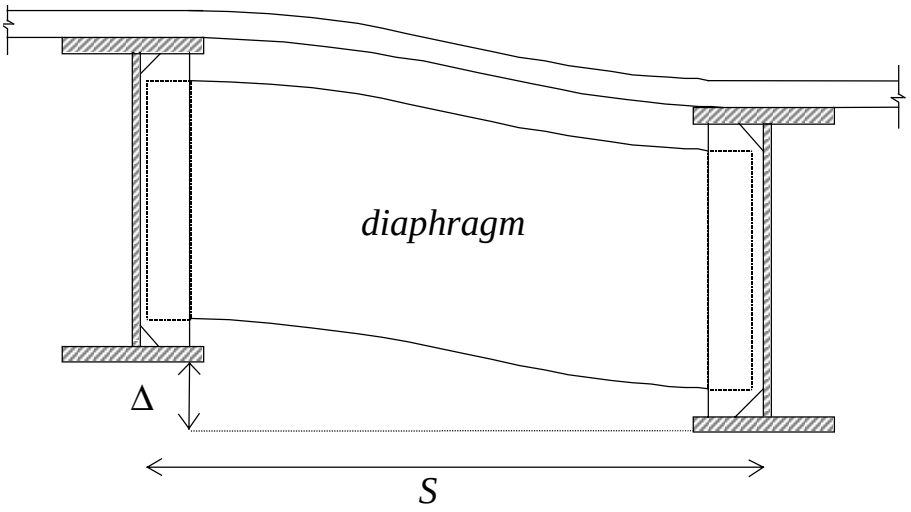

Figure 2.1 Girder Differential Deflection

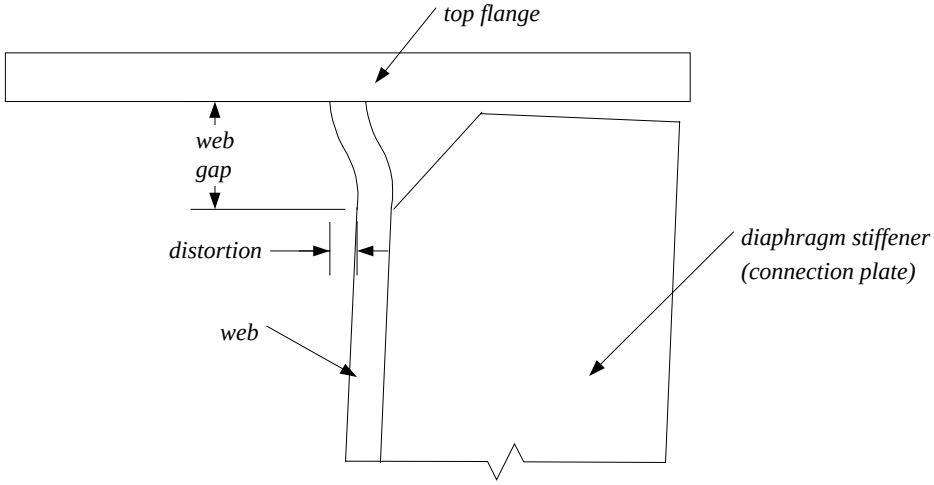

Figure 2.2 Girder Web Gap Distortion

Due to the severity of the cyclic stresses and the prevalence of this detail, distortion-induced fatigue cracking in unstiffened web gaps is considered the largest source of fatigue cracking in steel bridges [3]. Girder vertical movements and the diaphragm rotation mechanism forcing out-of-plane secondary stresses have resulted in documented cases of fatigue cracking in hundreds of bridges. Fatigue cracks due to secondary stresses in the web typically run parallel to primary bridge stresses (i.e., in the longitudinal direction) and are not detrimental to the performance of

the structure providing they are discovered and retrofitted before turning perpendicular (i.e., vertical or inclined) to the applied stresses from primary loads. Web gaps have been confirmed to possess fatigue strengths comparable to the AASHTO Category C fatigue resistance S-N curve for hot-spot stresses in the transverse connection plate detail [2]. It is interesting to note that a transverse stiffener welded to the tension flange (i.e., the fatigue detail designers were intentionally avoiding) has the same fatigue resistance as the problematic web gap detail. Although the measured web gap stress range is often higher at the web-flange weld, the smooth weld profile of that region results in much higher fatigue resistance than the weld termination at the transverse stiffener. In short web gaps, most cracking originates in the weld bead extending beyond the end of the connection plate, while in gaps greater than 3.8 cm (1.5 in) the cracks tend to form at the connection plate weld toe [2].

Web gap stresses have been investigated in the field often. The case studies documenting distortional fatigue cracking of unstiffened web gaps confirm the behavior described earlier and reinforce the view that this problem warrants further research attention [4, 5, 6, 7, 8, 9].

Field investigations and experimental studies have shown that the magnitude of distortional stresses in web gaps is difficult to predict. It has been postulated that web gaps may behave much like short, fixed-fixed beams that undergo relative displacements (without rotation) at each end. Although equations for estimating stresses have been proposed [10], laboratory experiments demonstrate that a wide variability in response can be expected, which makes it difficult to model web gap behavior [2]. Other reports have noted erratic cracking behavior for web gaps less than five times the web thickness [11].

2.3 Retrofitting

Distortional fatigue crack retrofit solutions for distortional fatigue have been a frequent topic in the research literature considering the severity of the distortional fatigue problem. One such retrofitting procedure involves the drilling of holes at crack tips, provided distortional stress levels are below 103 MPa (15 ksi) [2]. Removing part of the transverse stiffener plate to lengthen the web gap and improve flexibility has proven successful in reducing stresses and crack growth since bending stresses decrease in an inverse geometric manner with web gap

length. Research into partial stiffener removal has shown that increase in gap length must be at least $20t_w$, where t_w is the web plate thickness, to be fully effective in stopping distortion and crack growth. Various types of positive attachments have been proposed and have been shown to be effective. These include plates (Figure 2.3), angles, tees, either bolted or welded to bridge the web gap [2, 12, 13]. Figure 2.3 is a laboratory example of a stiffener to flange connection in the positive moment region of a girder.

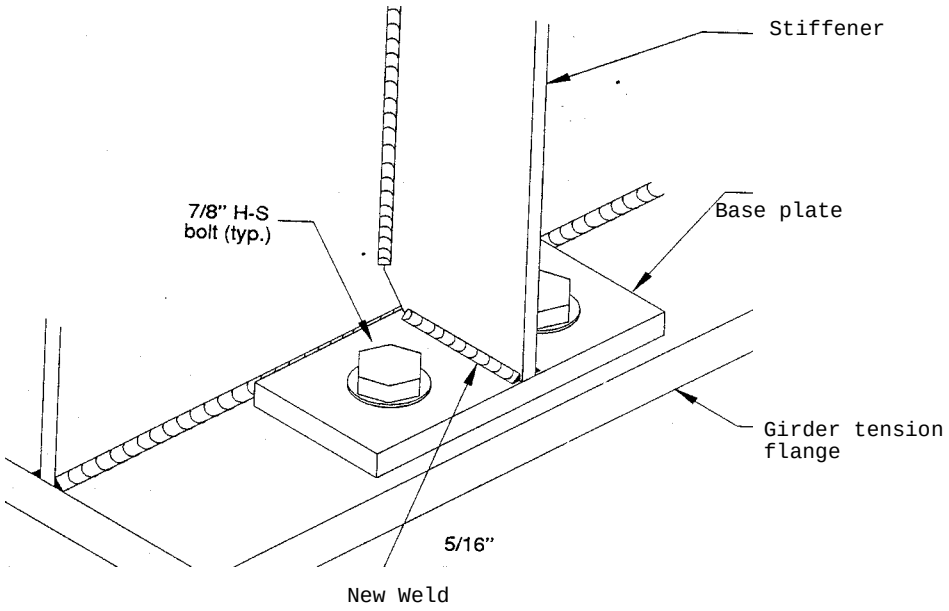

Figure 2.3 Retrofit Example, Bolted Base Plate [2]

Although many retrofit solutions may successfully reduce distortional stress and arrest crack growth, implementation of these solutions proves to be expensive and challenging. Welding of reinforcement details proves difficult in the field because of overhead positions, dirt accumulation, preheat weld requirements, and corrosion from service conditions. Traffic must be stopped to minimize structure movement if welds are placed while the bridge is in service. Research indicates that a welded joint between connection plates and girder flanges is the most rigid of retrofits and therefore the most effective in bridging web gaps. When less rigid bolted connections are utilized, rigid splice components are recommended, such as 1.9 cm (0.75 in) thick angles or built-up components. Applying new bolted connections in negative moment regions is undesirable in the field because accessing the girder top flange requires removal of the reinforced concrete deck.

A different approach toward solving the out-of-plane distortion problem is the removal of diaphragm bolts so the connection can accommodate out-of-plane displacements without generating web gap stresses, or the complete removal of diaphragms, thereby eliminating distortion imposed by diaphragm rotations. The Iowa Department of Transportation (Iowa DOT) is currently testing the feasibility of loosening bolts to reduce connection restraint and alleviate distortional stresses [14]. The Iowa DOT believes the new, semi-rigid connection, with diaphragms in place, may still distribute lateral load due to wind or collision and provide bracing support. Instrumentation of a bridge before and after the removal of diaphragms indicated that the absence of diaphragms had negligible impact on capacity [15]. Although a successful solution, the impact of complete diaphragm removal on lateral support should be carefully considered. In addition, nuts on loosened bolts can become completely free due to traffic vibrations, creating a hazardous situation with falling nuts and bolts.

Due to field observations and recommendations based on laboratory work, current AASHTO design provisions specify a positive attachment between girder flanges and the transverse connection plate for diaphragms and X-frames. Fatigue and fracture studies of welded details have verified that welded attachments on the tension flange are not any more severe than similar attachments to the web [2]. This positive attachment decreases the web gap distortion to acceptable levels provided the web gap at the cope is at least 5.1 cm (2 in) or four times the web plate thickness, whichever is larger. In addition to AASHTO design guidelines regarding distortional fatigue, NCHRP Report 229, *Fatigue Evaluation Procedures for Steel Bridges* [16], provides guidance for fatigue evaluation of existing bridges, including assessing fatigue loading, stress ranges, and remaining life.

2.4 Mn/DOT Project Background

Given the importance of web gap out-of-plane distortion and the number of steel bridges susceptible to fatigue damage, Mn/DOT funded research in 1995 to (1) instrument/field monitor a typical, skew supported, multi-girder steel bridge, (2) assess the frequency and magnitude of distortional fatigue stresses at web-stiffener connections, and (3) evaluate the impact of these stresses on fatigue life [1]. The project included the instrumentation of Mn/DOT Bridge No.

27734 at the intersection of Interstate Highways 94 (I-94) and 694 (I-694) in the Minneapolis-St. Paul metropolitan area to determine girder stresses and web gap stresses from daily traffic over a period of several months. In addition to this long-term monitoring, truck tests at highway speeds were conducted to determine bridge stresses and deflection under known loads.

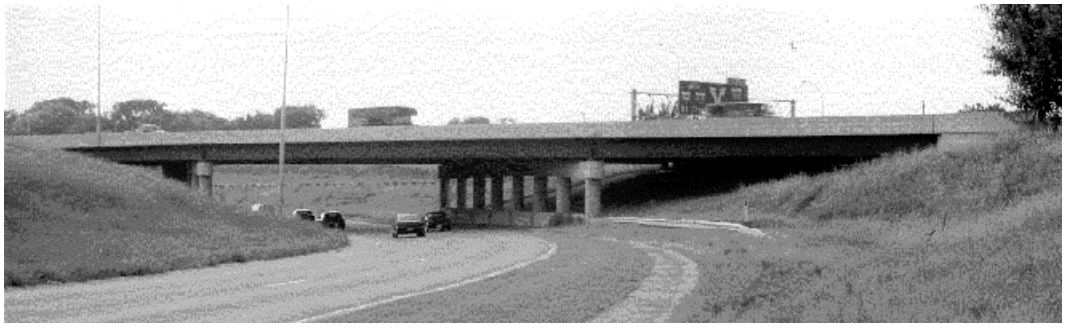

Figure 2.4 Mn/DOT Bridge No. 27734

Typical loading resulted in web gap stresses that were 2 to 2.5 times that of flange stresses. Finite element analysis of the web gap detail indicated that actual stresses were higher than those measured in the field. This apparent discrepancy was explained by the existence of rapidly changing stress gradients in the vicinity of the web gap, as well as the location of the strain gages in the field. In actual bridges, the diaphragm, stiffeners, and surrounding structural elements absorb some of the out-of-plane forces, and the out-of-plane displacement of the lower flange can accommodate most of the diaphragm rotation. The study revealed that the web gap distortion mechanism causing a majority of the stress was best described as a small fixed-pinned beam pivoting about the toe of the stiffener.

With this mechanism known, a simple equation for predicting web gap stresses was obtained on the basis of beam theory applied to the portion of the web in the gap region, and maximum stress at the termination of the stiffener was obtained assuming a linear, elastic material [1]. Combining these expressions and the diaphragm rotation ($\theta = \Delta/S$, where S is equal to the diaphragm length, also equal to the girder spacing, and Δ is girder differential deflection) gives the following expression for maximum web gap stress, σ_{wg}

$$\sigma_{wg} = 2E \cdot \left(\frac{t_w}{g}\right)\left(\frac{\Delta}{S}\right) \qquad \text{Eq. 2.1}$$

where E is modulus of elasticity, t_w is web thickness, and g is web gap length. This simple, approximate equation correlates well with the field data and web gap stress estimates from finite element analysis for this detail. The approximation is solely dependent on steel modulus, web gap dimensions, girder spacing, and the differential deflection between adjacent girders. A clear understanding of the parameters affecting differential vertical deflection between adjacent bridge girders would improve greatly the ability to assess distortional fatigue cracking of girder web gaps.

2.5 Bridge Models

The magnitude of out-of-plane movement between girders has been conjectured to depend on girder spacing, angle of skew of bridge supports, and the geometry and type of diaphragm [6]. As a rule, it has been observed that skewed bridges experience larger differential deflections between girders since the distance from applied loads to the supports differs for adjacent girders. Despite these observations, the research literature on distortional fatigue in steel bridges indicates there has been little research effort expended toward identifying and quantifying basic bridge characteristics responsible for the girder relative deflections that lead to this phenomenon.

Bridge models are a common vehicle by which bridge behavior is tested and confirmed. Simple, analytical models involving bridges prove successful in analyzing loads, forces, and bridge behavior only if a bridge is uncomplicated in its configuration. Simple line girder models developed to predict the deflection behavior of Mn/DOT Bridge No. 27734 were unable to

predict deflections with reasonable accuracy [1]. The complexities in load distribution, especially in multi-span continuous composite steel bridges, is not well represented by simple models. Structural components, their elaborate connectivity, and their behavior in skewed bridges are too complex to be modeled without either intricate grillage models or three-dimensional finite element models.

Finite element models have been often used in the study of bridges. Recent research aimed at developing more precise AASHTO wheel distribution factors has utilized finite element modeling [17, 18]. Actual, small-scale bridge models have been used in parametric tests to determine lateral load distribution factors [19]. These models, confirmed with finite element models, indicated that parameters found to influence lateral distribution factors included: skew angle, girder spacing, bridge aspect ratio (long span length/bridge width), span length ratio (long span length/short span length), and intermediate transverse diaphragms. More than 600 finite element parameter study models were utilized incorporating four-node shell elements and two-node three-dimensional beam elements with six-degrees of freedom at each node [19]. Rigid constraint between the deck and girder assured the simulation of full bridge composite action.

A number of different finite element schemes have been tested to determine wheel load distribution factors. In one such study [20], four commonly used finite element modeling techniques were tested to compare calculated distribution factors to those obtained from the *Guide Specification for Distribution of Loads for Highway Bridges* [21]. The AASHTO guide is based on the NCHRP 12-26 research project [22] and different than those specified in the *Standard Specifications for Highway Bridges* [23]. The first method to configure finite element bridge models was idealized with quadrilateral shell elements for the deck and space frame members for the steel girders. In this model, the centroid of each girder coincided with the centroid of the concrete slab. The second model was idealized as deck shell elements eccentrically connected to girder frame elements. Rigid links were applied to accommodate the eccentricity of the girders with respect to the slab and simulate composite action. In the third model, the concrete slab and steel girder webs were assigned shell elements, while girder flanges were modeled as frame elements. A flange to deck shear connection was again modeled via a rigid link. The fourth finite element model incorporated an eight-node solid element for the

concrete slab, and girder flanges and webs were modeled using shell elements. All finite element models produced load distribution factors similar to the NCHRP 12-26 formula but less than the AASHTO specification formula.

Similar finite element studies using the methods above have been conducted to study the influence of multi-span continuous steel girders and when sidewalks and integral railings are present in steel bridges [24]. Integral sidewalks and rails were shown to increase the load-carrying capacity of a bridge by as much as 30% when they are included in bridge strength evaluations [25]. Overall, the many finite element studies mentioned above provide a high degree of confidence when adopting a modeling technique for analyzing the behavior of new and existing steel girder bridges.

Chapter 3

Finite Element Bridge Modeling

3.1 Overview

The mechanism that causes distortional fatigue is the direct result of diaphragm rotation between adjacent bridge girders that undergo differential vertical deflection. Finite element models were formulated and calibrated in efforts to predict bridge girder vertical deflections. These studies were also conducted in an attempt to reproduce the truck test deflection data obtained from Mn/DOT Bridge No. 27734 [1]. A summary of model characteristics and modifications to refine its accuracy is presented and output is compared to experimental data from the truck tests. Final model sensitivity is discussed and results are presented to confirm the reliability of the finite element technique to simulate entire, composite steel bridge behavior.

3.2 Model Formulation

Finite element model formulation included the selection of elements required to correctly model bridge behavior. The analysis program *SAP2000 Nonlinear* [26] was utilized to create finite element models of simple structures. Appropriate elements were selected by comparing the displacement response of the finite element models for the simple structures subjected to point loads with the known analytical solutions. Skewed, two girder configurations were also analyzed at this stage to verify the sizes and selection of elements. Mesh convergence studies indicated the appropriate refinement in element mesh size. This exercise established confidence in the future large-scale skewed bridge model.

Plans for Bridge No. 27734, the overpass at the I-94/I-694 junction in Brooklyn Center, were acquired from Mn/DOT and a geometric analysis was conducted in order to create a full, three-dimensional bridge model, including all girders, deck, diaphragms, and J-rails (Figure 3.1). Shell elements were used to represent the bridge deck and girder webs, and frame elements were chosen to model girder flanges, diaphragms, and the rail (Figure 3.2). Rigid elements connected points that were to act integrally with one another (i.e., between slab and top girder flange, between rail and concrete slab). Previous Mn/DOT research indicated that diaphragms rotate essentially as pinned elements with little moment developed since rotation is resisted only by the flexible web and the girder flange displacing out-of-plane. The diaphragms in the finite element

models simulate these conditions since the diaphragms were connected solely at one point in the middle of the web. An integral edge rail (Figure 3.3) was included since studies have found integral non-structural components, such as sidewalks and railings, can have significant effect on load capacity [25]. This model configuration is similar in nature to one of the finite element methods used in studying wheel load distribution factors [20].

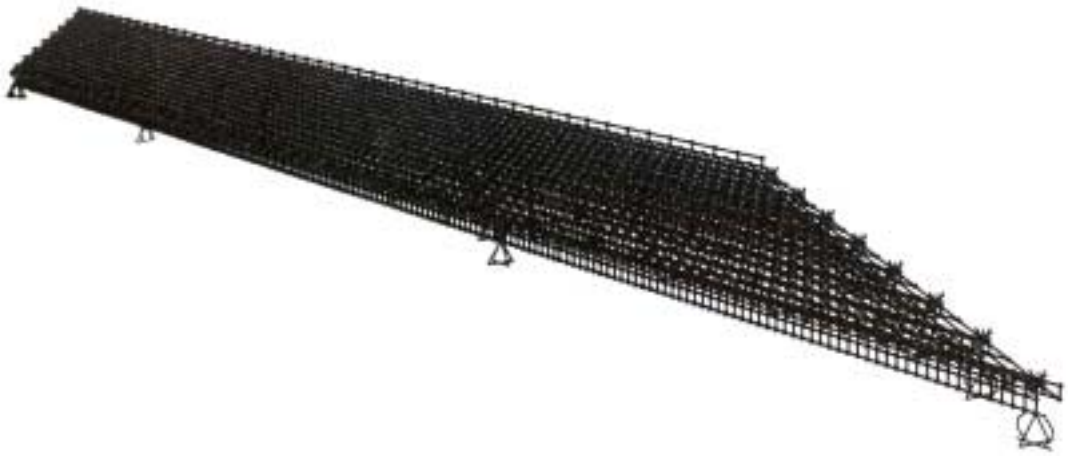

Figure 3.1 Finite Element Model of Mn/DOT Bridge No. 27734

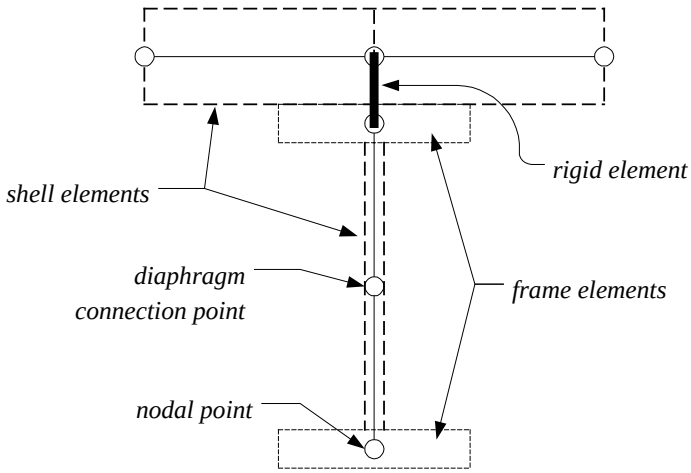

Figure 3.2 Finite Element Model of Typical Partial Cross-Section

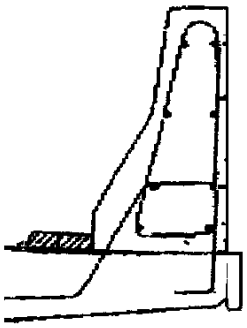

Figure 3.3 Typical Cross-Section of Mn/DOT Integral J-rail

3.3 Model Modification and Verification

A total of seven different load configurations were reported by Jajich, et al. for the truck tests in the previous research phase [1]. Truck configurations consisted of two 222-kN (50-kip) sand trucks crossing the bridge, either side by side in adjacent lanes, or one following the other in a single lane (Figure 3.4). The relationship between girder and lane numbering is given in Figure 3.5.

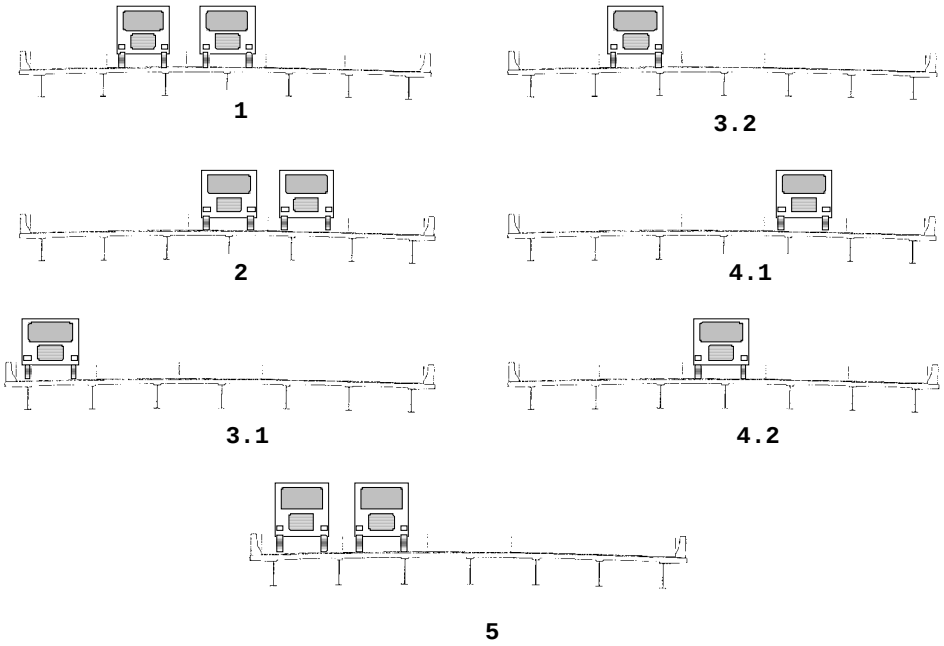

Figure 3.4 Truck Test Configurations

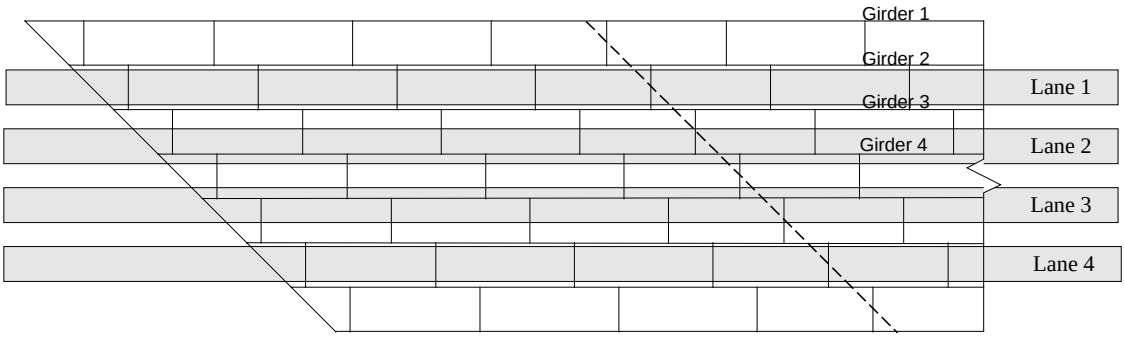

Figure 3.5 Bridge Lane Position and Girder Numbers

Each load case was applied as a sweep on the finite element model to compare model vertical deflection to truck test deflection. In the cases of two trucks in a single lane, only one 222-kN truck was applied to the finite element model. Data for comparison with each configuration included differential deflection of two diaphragms as well as mid-span deflections for the first four girders.

Initial models did not produce results with great accuracy and more detailed information on the bridge was sought. This information included: edge rail dimensions, deck concrete modulus, edge rail concrete modulus, and support details. Support conditions, unknown at the time, were changed to the proper roller/pin combinations after support details were acquired from Mn/DOT and significantly aided in model adjustment. Normal concrete strength, f'_c, was assumed equal to 33.1 MPa (4800 psi), while the high-strength wearing surface was assumed to have a strength of 48.3 MPa (7000 psi). Using the American Concrete Institute Building Code 318-99 equation for concrete modulus of elasticity, $E_c = 57000(f''_c)^{0.5}$, edge rail modulus of elasticity was set equal to 24.8 MPa (3600 psi), while the concrete deck modulus was set higher at 28.3 MPa (4100 psi) to account for the high-strength wearing surface. Steel modulus of elasticity was taken as a constant 200 GPa (29000 ksi). A visit to the bridge allowed the measurement of values that were not specified on the bridge plans, including diaphragm depth and plate thickness, and J-rail dimensions. Calibrated model geometry and properties are presented in Table 3.1. With refined bridge dimensions and proper support conditions, the finite element model predicted vertical deflections with reasonable accuracy (Figure 3.6 to Figure 3.12).

Calibrated Finite Element Model of Mn/DOT Bridge No. 27734	
West Span Length	32.92 m (108 ft.)
Main (Center) Span Length	42.06 m (138 ft.)
East Span Length	24.38 m (80 ft.)
Girder Depth	1.016 m (40 in.)
Girder Spacing	2.82 m (9 ft.- 3 in.)
Angle of Skew	60 deg.-27'-25.5"
Concrete Modulus of Elasticity	28.3 MPa (4100 psi)
Edge Rail Modulus of Elasticity	24.8 MPa (3600 psi)
Edge Rail Height	0.86 m (34 in.)
Edge Rail Deflection Joint	every 4.88 m (16 ft.)
Steel Modulus of Elasticity	200 GPa (29000 ksi)
Deck Thickness	22.86 cm (9 in.)
Diaphragm Depth	0.76 m (30 in.)
Diaphragm Thickness	7.94 mm (0.3125 in.)
Girder Flange Width	0.35 - 0.56 m (14 - 22 in.)
Flange Thickness (w/ cover plates)	2.22 - 9.53 cm (0.875 - 3.75 in.)
Deck Cantilever Length to Edge Rail	1.016 m (40 in.)
West Abutment Support	elastomeric bearing pad (free)
West Pier Support	elastomeric bearing pad (pin)
East Pier Support	elastomeric bearing pad (free)
East Abutment Support	elastomeric bearing pad (free)

Table 3.1 Material and Geometric Properties

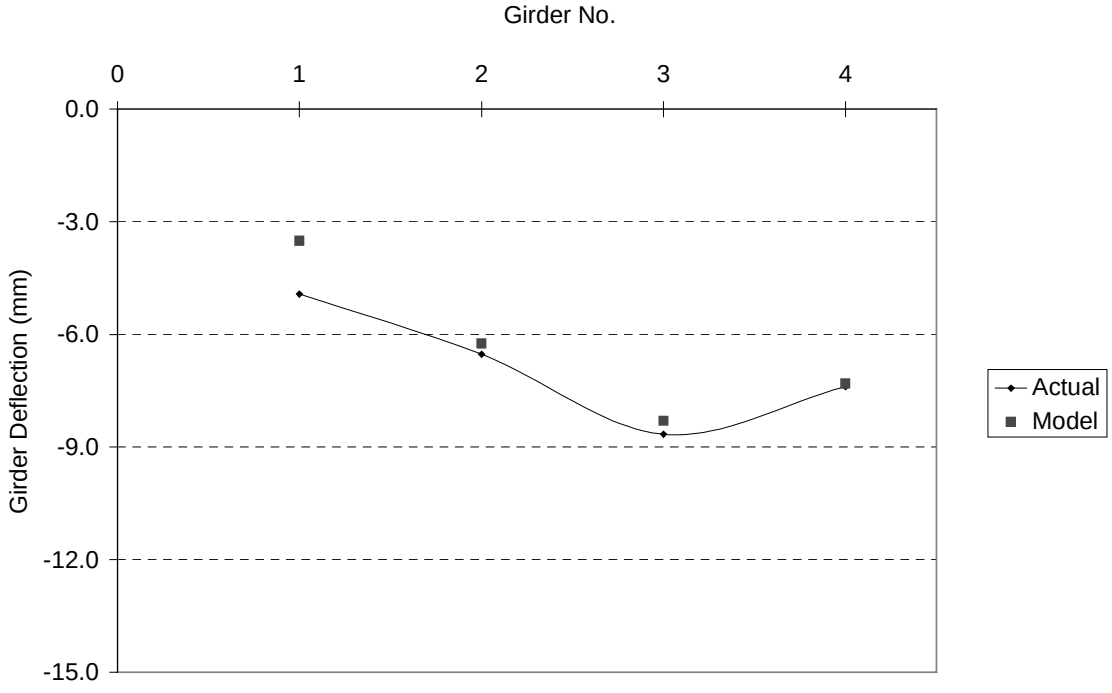

Figure 3.6 Mid-Span Deflection, Sweep #1

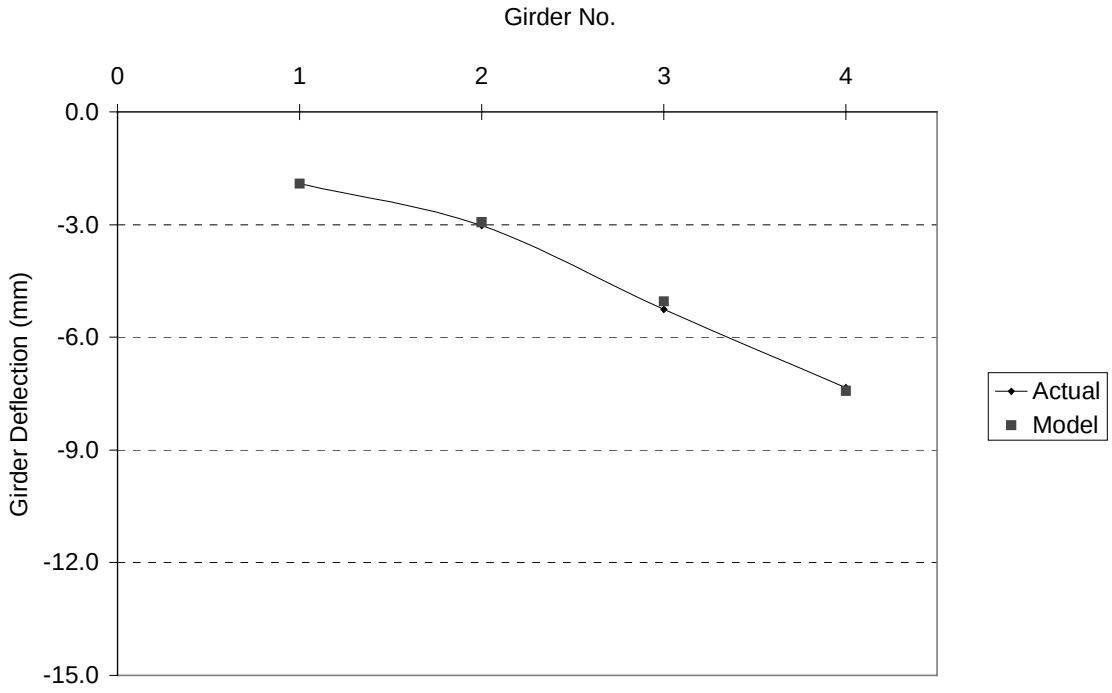

Figure 3.7 Mid-Span Deflection, Sweep #2

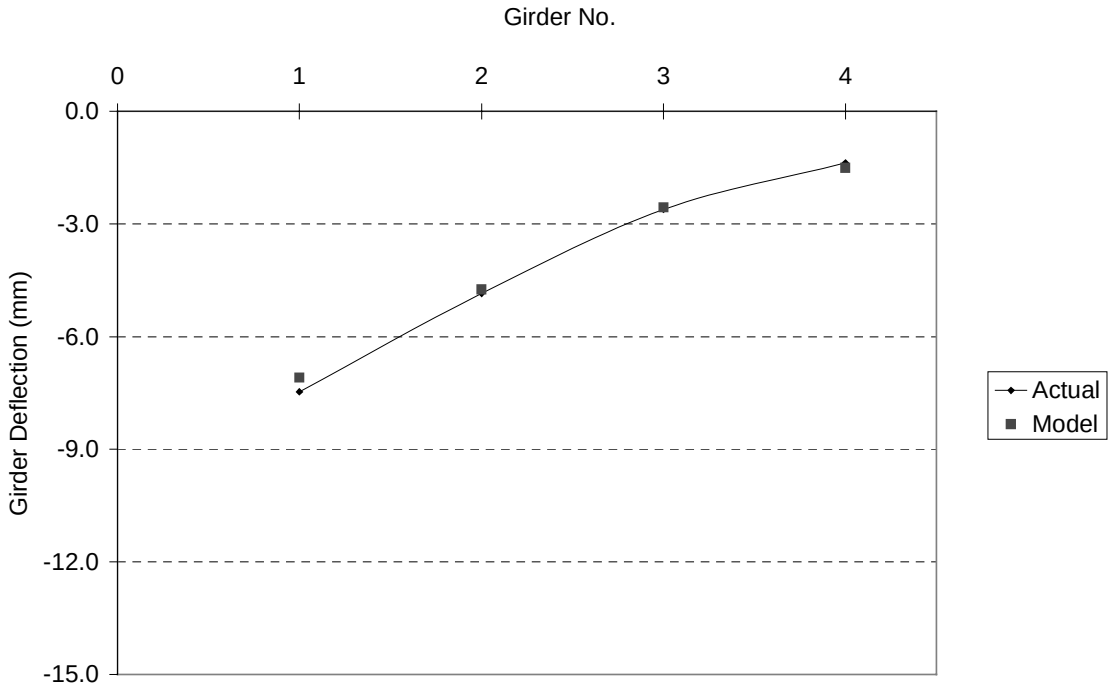

Figure 3.8 Mid-Span Deflection, Sweep #3.1

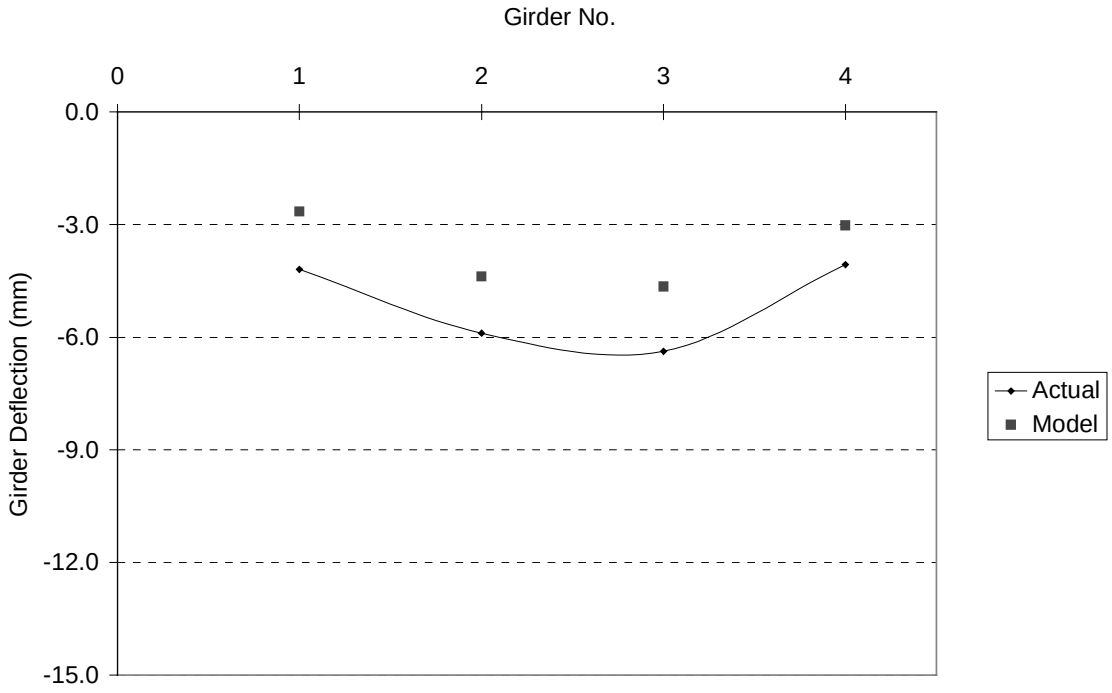

Figure 3.9 Mid-Span Deflection, Sweep #3.2

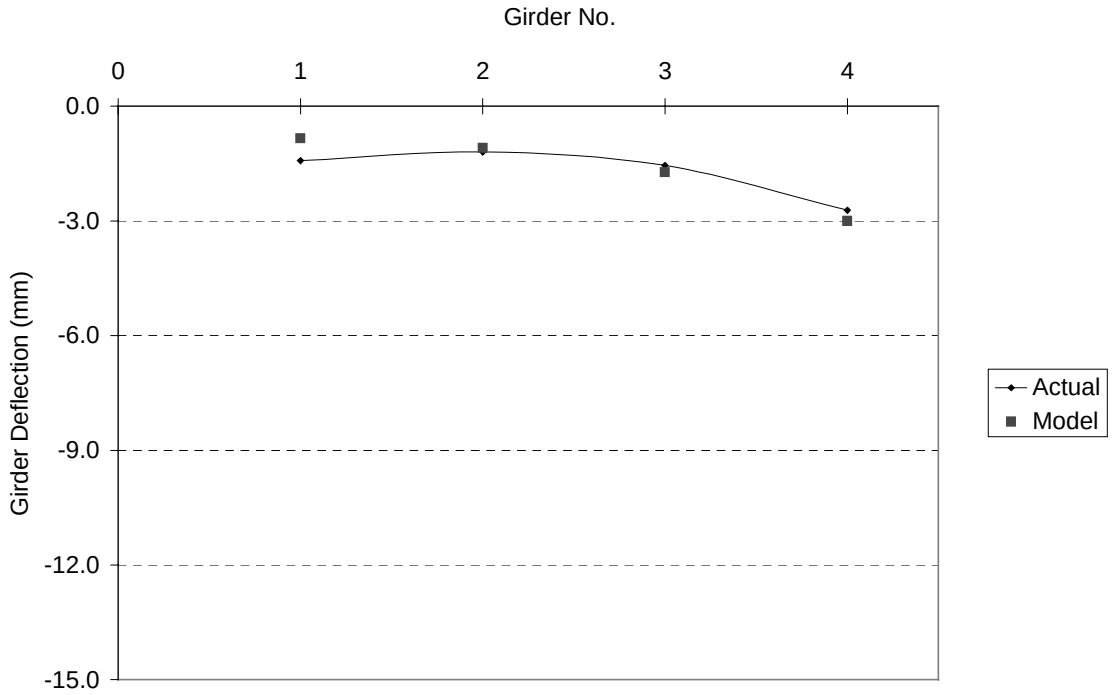

Figure 3.10 Mid-Span Deflection, Sweep #4.1

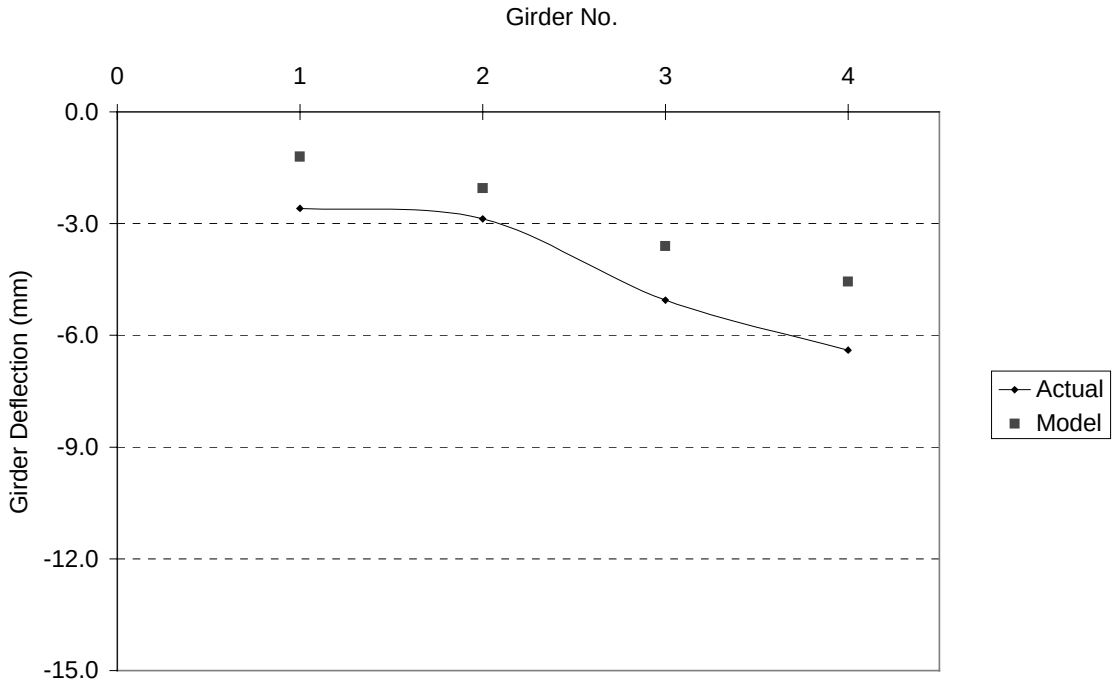

Figure 3.11 Mid-Span Deflection, Sweep #4.2

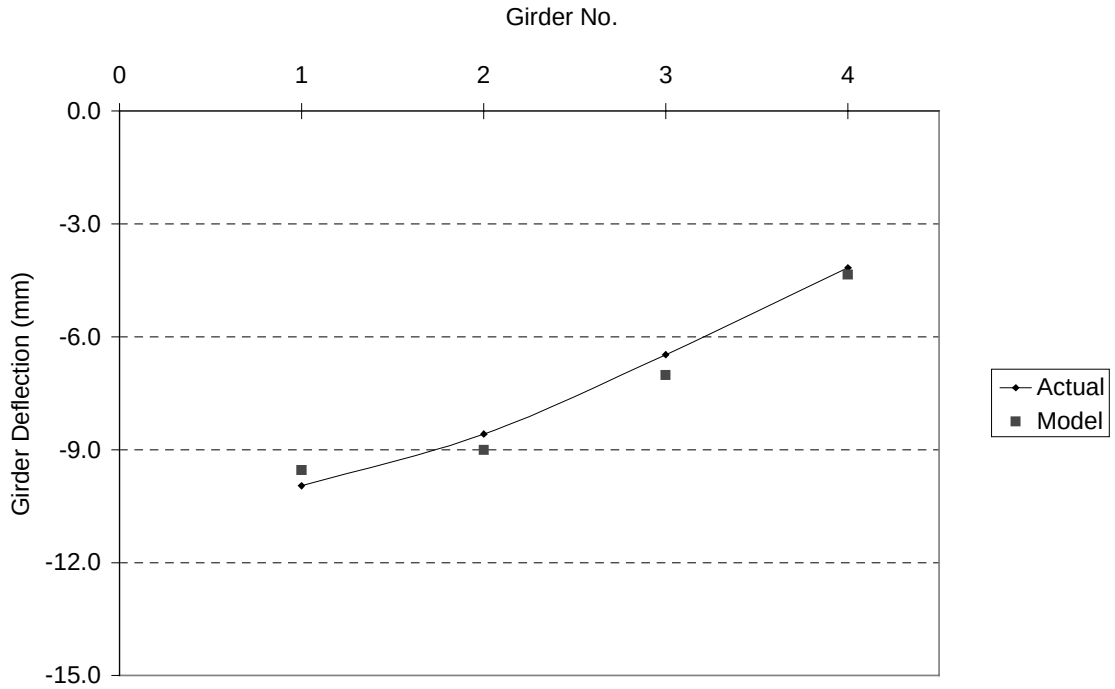

Figure 3.12 Mid-Span Deflection, Sweep #5

3.4 Model Sensitivity and Results

Data for comparison with data from all seven truck configurations was generated using the finite element model. For some load cases, to be as precise as possible, bridge elements were subdivided beyond the usual mesh size to apply truck axle loads at more exact locations. Computed deflection response indicated that the integral edge rail conditions do not appear to be modeled as accurately as other components of the bridge. Evidence of this fact can be observed for most instances in Girder 1 deflection. A deflection joint is present in the actual bridge rail and consists of a V-groove in the upper half of the rail. There was concern that cracks existed in the rail in the bridges negative moment region. Node constraint conditions for the finite element model were changed in an attempt to improve the modeling of rail deflection joints since these joints and potential cracks in the negative moment region could affect deflection. Modeling cracked deflection joints did not improve computed model deflection accuracy. No further model refinements were made since continuous steel reinforcement is provided along the length of the rail (both top and bottom) and in the concrete deck and deflection results were reasonable. Most model and truck test midspan deflections were typically within 5% of measured values. The magnitude of this 5% variance was approximately 0.25-0.5 mm (0.01-0.02 in).

Mid-span deflection profiles that did not match the exact deflection magnitude did match the shape of the deflection profile and should be, therefore, satisfactory in predicting differential deflections. The cases with lower deflection accuracy are restricted to truck test sweeps with the two trucks in a single line. The separation of the trucks in these sweeps was sufficiently large that both vehicles were not on the bridge simultaneously. However, since the trucks were traveling at typical highway speeds, the bridge was most likely vibrating from the dynamic (impact) loading of the first truck when the second truck passed over the bridge. Consequently, the measured deflection would include contributions from both trucks. These conditions are difficult, if not impossible, to simulate in a static finite element analysis. Yet, these single-line truck sweeps (Sweeps 3.1, 4.1 and 4.2 in Fig. 3) generated smaller deflections and distortional fatigue stresses than the side-by-side sweeps, so a high degree of accuracy in these cases is not considered as important. In addition to the uncertainty in truck loading, all truck tests were

conducted in the presence of normal traffic, although the superimposed effects of light traffic elsewhere on the bridge is believed to be negligible.

Bridge instruments were configured differently during truck testing to gather both mid-span girder deflections (morning truck sweeps) and select diaphragm differential deflections (afternoon truck sweeps). All truck sweeps were tested in the finite element model to determine diaphragm differential deflection. Figure 3.13 summarizes the differential deflection of the diaphragm nearest the first bridge pier, between Girders 1 and 2, for all truck sweeps analyzed in this study. Calculated deflection results for sweeps with side-by-side trucks (Sweeps 1, 2, and 5) were the most accurate. In general, deflection results are reasonably accurate with the smallest error accompanying the largest deflections (Sweep 1, 3.2, and 5), which are directly related to the largest out-of-plane distortion and fatigue stress.

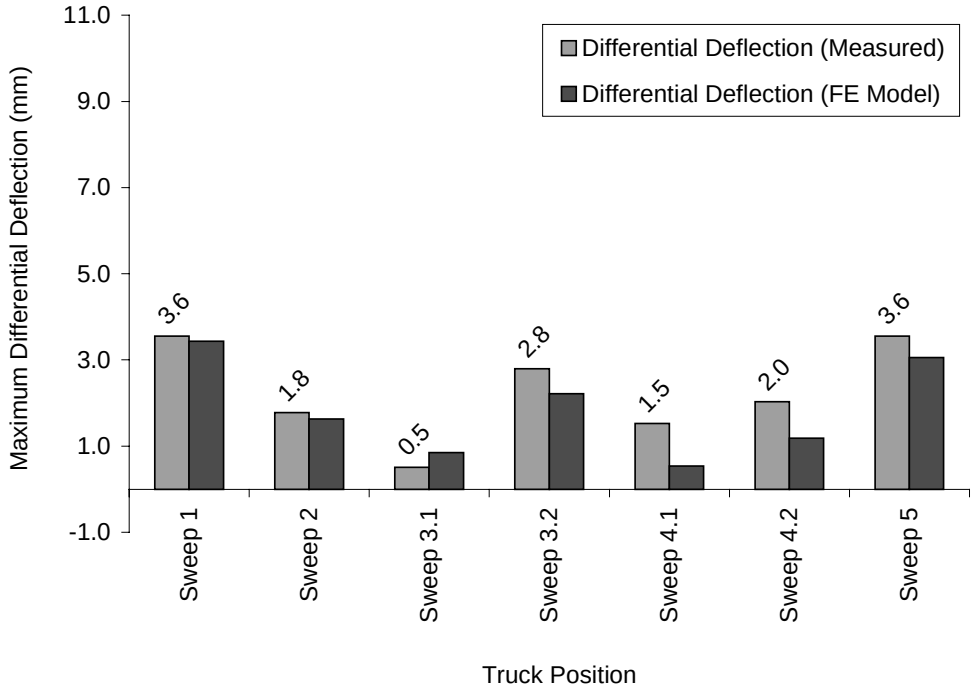

Figure 3.13 Maximum Diaphragm Differential Deflection, Girders 1-2

Deflection predictions using simple models of transverse sections of the deck in the previous Mn/DOT study by Jajich, et al [1] exhibited as much as 100% error. The finite element model

demonstrates remarkable improvements upon this error. Observed mid-span and diaphragm deflections suggest that precise conditions of supports and the integral edge rail are difficult to simulate, but their effects are minimized within a short distance away from them. The match in deflection profile at girder mid-spans between the finite element models and the truck tests indicates that differential deflection is predicted well at locations away from the supports.

3.5 Conclusions

The refinements afforded by the finite element modeling technique provide confidence in the predictive ability of this method. In addition, it provides a basis by which the parametric study may be conducted to determine which bridge properties and configurations have significant effects on girder relative deflection and out-of-plane distortion.

Chapter 4
Preliminary Study and Modeling Guidelines

4.1 Overview

This chapter discusses the preparatory study that served to define and focus the parameter study. In order to define bridges that are consistent with Mn/DOT design practice, a variety of bridge parameters were researched to help identify trends in the Mn/DOT bridge inventory. A description is presented that elucidates the procedures and methodology by which the finite element parameter study models were created. This chapter also reviews the range of variables in the parameter study, the decisions made regarding their study, and how they were incorporated in the parameter study.

4.2 Preliminary Modeling

Prior to the formulation of the models in the parameter study, research into skew bridge models and lane loading was conducted. Bridge models using the finite element girder from the calibrated bridge model were modified with various angles of skew for a preliminary foray into the parameter study. Bridge angle of skew is measured from a line perpendicular to the direction of traffic. Deck and girder discretization and diaphragm locations at which deflections were recorded were exactly the same for all models. Results from this preliminary skew study prompted questions regarding the location at which displacement data should be gathered within the parameter study. Data in Figure 4.1 indicate the trends in differential deflection for bridge models that are the same in all manners except for skew.

Analysis with HS-20 truck loading (Figure 4.2) was conducted for the span of the three-span calibrated bridge model in which each of four lanes were loaded one at a time in the west span. All diaphragms in the three-span bridge were identified as indicated in Figure 4.3. Results from lane loading analysis (Figure 4.4) indicate that for skewed spans the location of maximum differential girder deflection for a loaded lane occurs in the obtuse corner of that lane for a skewed span (Figure 4.5).

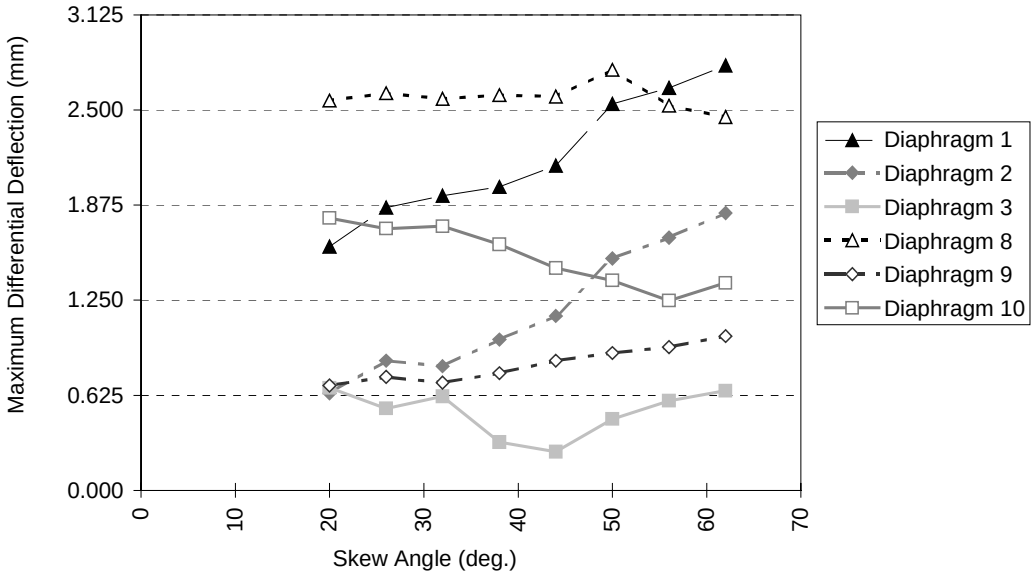

Figure 4.1 Results of Preliminary Skew Study

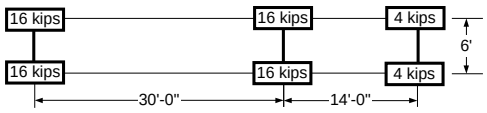

Figure 4.2 AASHTO HS-20 Axle Load Configuration

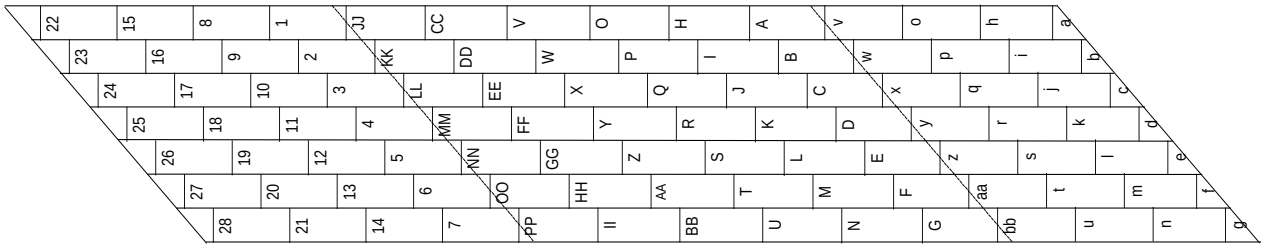

Figure 4.3 Calibrated Bridge Diaphragm Arrangement

The obtuse corner effect is the result of loads being transferred from the diaphragms near the obtuse corner (e.g., diaphragms 1 and 8 for Lane 1 loading in Figure 4.5) in the direction nearly perpendicular to the closest line of supports towards the opposite end of the span (e.g., diaphragms 17 and 24 in Figure 4.5).

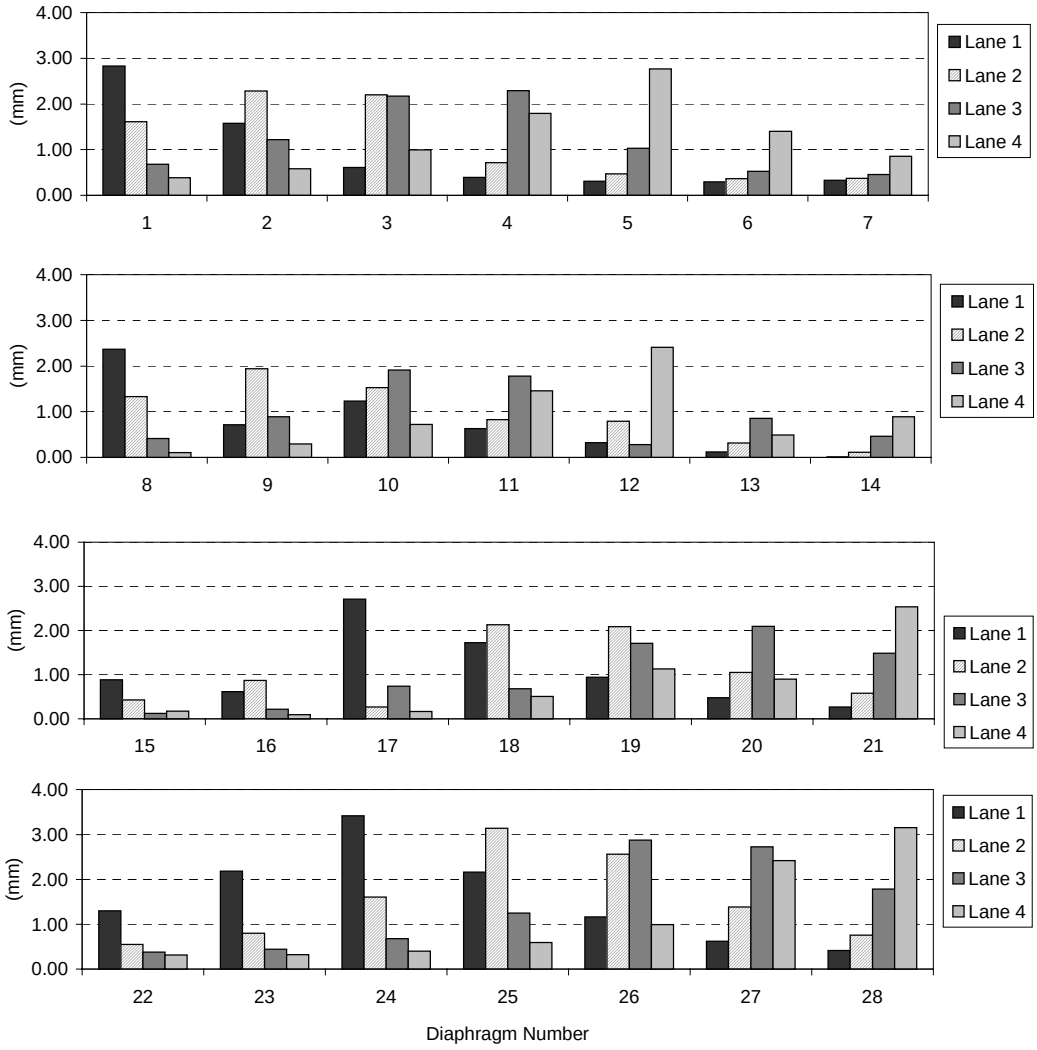

Figure 4.4 West Span Diaphragm Differential Deflection

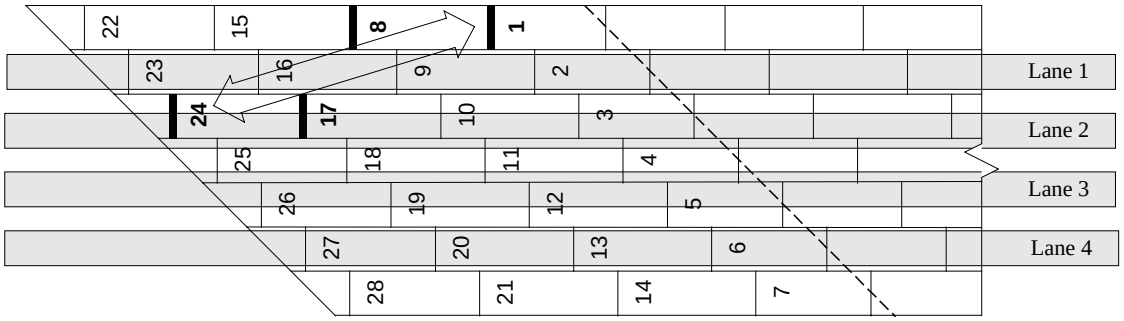

Figure 4.5 Lane 1 Loading Obtuse Corner Effect

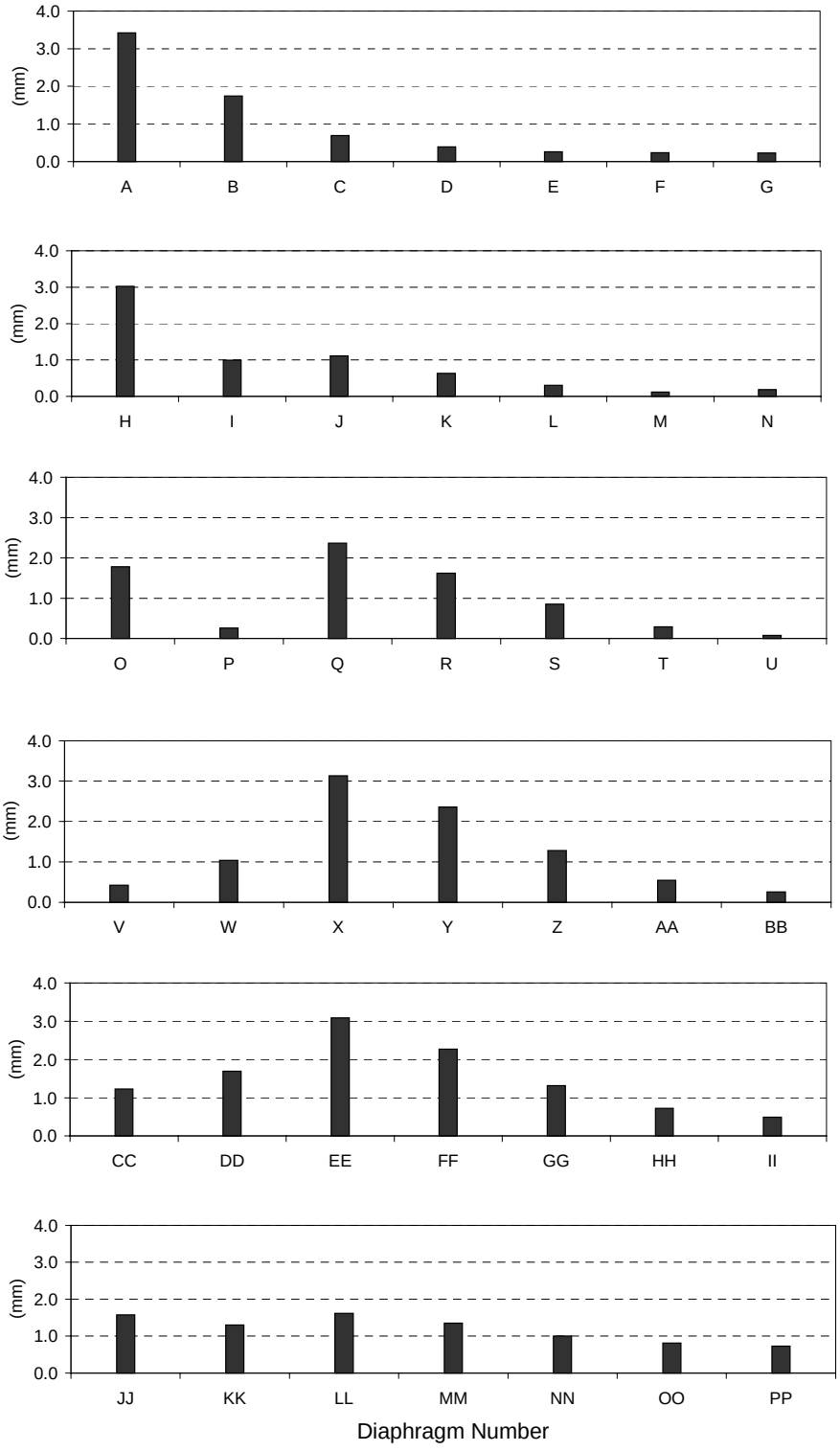

Figure 4.6 Main Span Diaphragm Differential Deflection for Lane 1 Loading

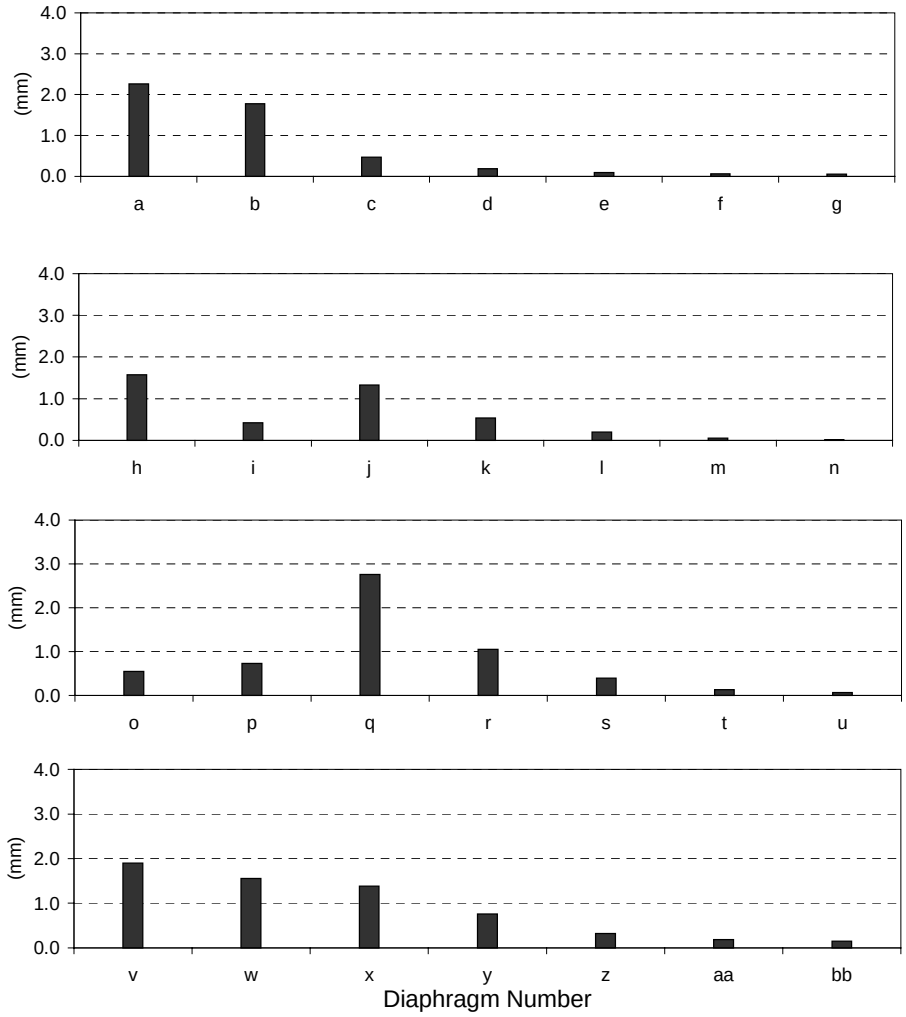

Figure 4.7 East Span Diaphragm Differential Deflection for Lane 1 Loading

The obtuse corner effect was also observed upon review of loading in the main span (Figure 4.6) and the east span (Figure 4.7). As with loading in the west span, the obtuse corner effect may be explained by loads flowing perpendicular to the supports (Figure 4.5). Results indicate that maximum values for diaphragm differential deflections have approximately the same magnitude and frequency for all lane load cases, and they differ only in the locations that attain these maxima. Distortional fatigue will therefore likely occur in the obtuse corner of the most frequently loaded lane. Thus, the parameter study included a single truck load in the north outside edge lane and diaphragm deflections would be recorded in and near the obtuse corner nearest the north edge lane of the main span.

In addition to single truck loads, side-by-side HS-20 trucks were applied to the finite element model. Results again illustrate the obtuse corner effect, but the maximum diaphragm deflection occurs at the discontinuous end of the span which is roller-supported (Figure 4.8), and not in the negative moment region where distortional fatigue has been noted to be most significant. Girder continuity near the first pier appears to reduce diaphragm differential deflection from side-by-side trucks as compared with the rotationally free conditions at the discontinuous end of the span.

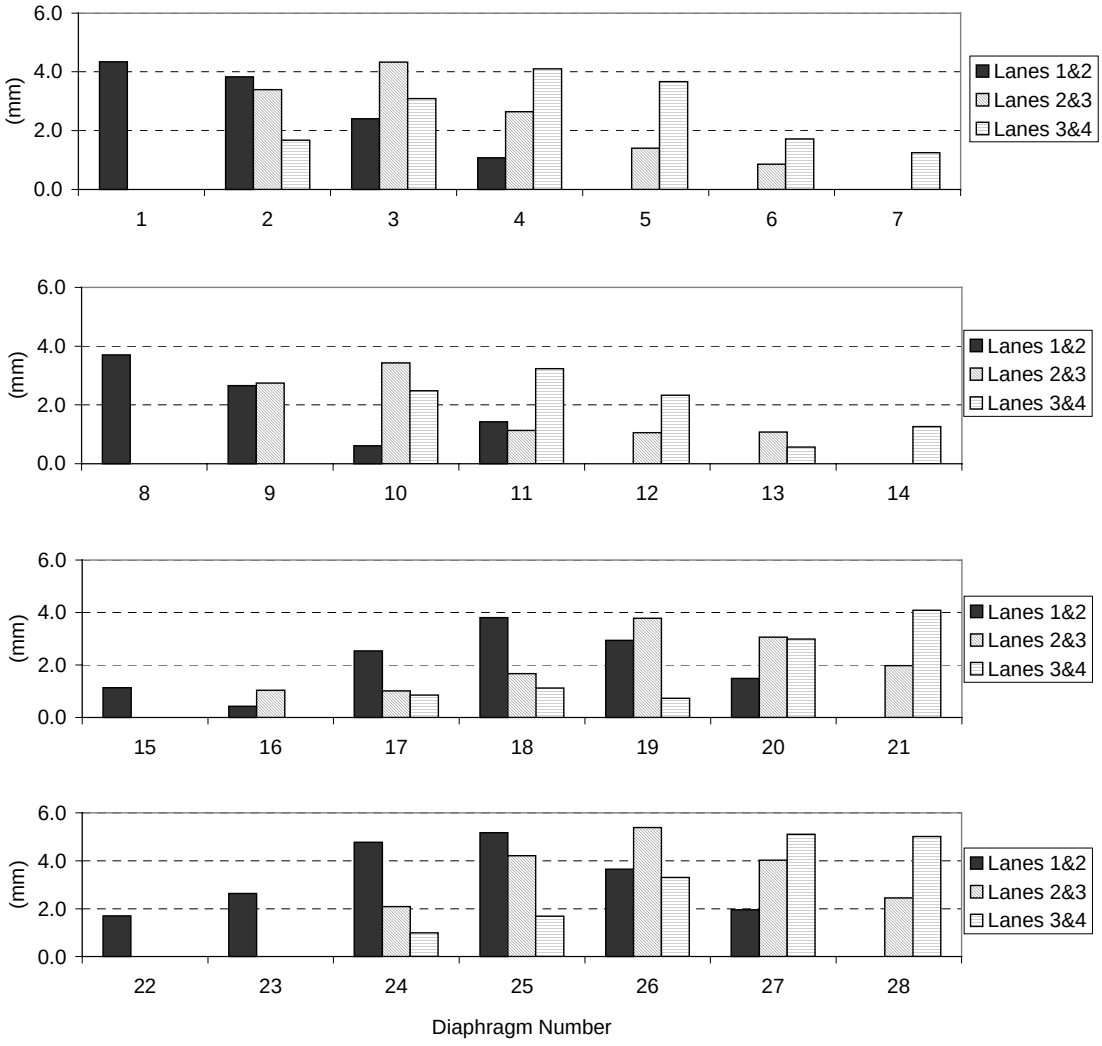

Figure 4.8 West Span Diaphragm Differential Deflection, Dual Truck Loading

It is observed that two trucks, side-by-side in adjacent lanes, do not produce a diaphragm deflection equal to the superimposed deflection of two individual trucks in their respective lanes.

The diaphragm deflection two trucks, side-by-side, also do not produce twice the deflection of an individual truck. In fact, the largest diaphragm deflection under dual truck loading (5.4 mm) is only 59% larger than the largest diaphragm deflection under single truck loading (3.4 mm). This phenomenon arises from the previously described load path in skewed bridges (i.e., obtuse corner effect) in which the loads from the side-by-side trucks flow along discrete parallel paths over different diaphragms. This observation also supports the use of three-dimensional finite element models for accurate calculation of diaphragm deflection. Finally, because the effect of dual trucks on diaphragm deflection is not additive, and since the likelihood of dual truck passage is much lower than that for single trucks, the parameter study was conducted using loading for a single HS-20 truck.

4.3 Bridge Parameter Survey

A thorough investigation of all parameters suspected to have an influence on differential girder deflection was essential to properly determine which parameters to include in the parametric finite element study. The Mn/DOT bridge database contains all roadway bridges in service in the state of Minnesota, including the entire inventory of composite, steel bridges. This inventory was surveyed to find a subset of bridges similar to the three-span, four-lane bridge at the intersection of I-94/I-694. A subset of twenty bridges, similar to the I-94/I-694 bridge and the calibrated finite element model, was identified and surveyed to find the range of values for all variables that may contribute to differential girder deflection. The surveyed bridge data included: number of bridge spans, main span length, adjacent span length, total bridge length, girder depth, girder spacing, skew angle, diaphragm arrangement, diaphragm detail, web gap length, deck thickness, web thickness, edge rail type, concrete strength, and steel strength. Mn/DOT survey data is presented in Table 4.1.

Mn/DOT Bridge No.	No. of Spans	Spans (ft.)	Main Span Length (ft.)	Bridge Width (in.)	No. of Girders	Girder Depth (in.)	Web Height (in.)	Pier Web Thickness (in.)	Pier Top Fl. Width (in.)	Pier Top Fl. Thickness (in.)	Pier Bottom Fl. Width (in.)	Pier Bottom Fl. Thickness (in.)
69021	3	60-2, 60-9, 60-2	60.75	493	5	27.38	25.43	0.605	13.965	0.975	13.965	0.975
19898	3	44.36, 62.14, 44.36	62.14	900	8	30.44	28.31	0.655	14.985	1.065	14.985	1.065
19897	3	45.5, 64, 46.4	64	765.375	7	30.31	28.31	0.615	10.545	1	10.545	1
9775	3	59.75,77.25,59.75	77.25	523	5	33.09	31.38	0.58	11.51	0.855	11.51	0.855
9452	4	38.5,78..83,78.83,53	78.833	552	6	33.09	31.38	0.58	11.51	0.855	11.51	0.855
27015	2	58.5, 80.5	80.5	900	8	38.04	36	0.65	12	1.02	12	1.02
62045	4	63,81-7,71-2,49-10	81.58	592	6	35.85	33.97	0.625	11.975	0.94	11.975	0.94
66809	3	60.667, 83, 60.667	83	536	5	35.85	33.97	0.625	11.975	0.94	11.975	0.94
31023	3	70, 94, 69	94	532	5	46.25	44	0.5	14	1.125	14	1.125
55029	3	78, 98, 78	98	796	7	36.49	33.97	0.765	12.115	1.26	12.115	1.26
69894	3	70 104, 70	104	586	5	47.75	46	0.5	16	0.875	16	0.875
27734	3	108, 138, 80	138	746	7	44.75	40	0.5	18	2.375	18	2.375
62702	3	99.5, 62,109	109.346	752	8	37	33	0.5	18	2	18	2
66001	3	78, 109, 80	109.5	730	8	45	42	0.375	16	1.5	16	1.5
86802	4	2@68,2@115.333	115.333	578	5	52	50	0.5624	16	1	16	1
49011	4	2@75'-6",2@117'-7"	117.58	532	5	56	54	0.5625	14	1	14	1
27106	3	53.333,126, 35.75	126	532	5	62.75	60	0.375	18	1.375	18	1.375
19882	4	2@110.75,138,88.75	138	844	7	64	60	0.5625	16	2	16	2
19816	2	2@151-8	151.667	1325	11	84	80	0.5625	20	2	20	2
19832	4	90,174,149.66,104.5	174	1197	10	75	70	0.5	16	2.5	16	2.5

Mn/DOT Bridge No.	Midspan Web Thickness (in.)	Midspan Top Fl. Width (in.)	Midspan Top Fl. Thickness (in.)	Midspan Bottom Fl. Width (in.)	Midspan Bottom Fl. Thickness (in.)	Deck Thickness (in.)	Girder Spacing (ft.)	Skew Angle (deg.)	Typ. Dia. Spacing (ft.)	Web Gap (in.)	Mn/DOT edge rail	L/d
69021	0.605	13.965	0.975	13.965	0.975	9	8.75	45	25'	2	J	26.63
19898	0.655	14.985	1.065	14.985	1.065	9	9.833	20	20'-24'	2	J	24.50
19897	0.615	10.545	1	10.545	1	9	9.75	26	21'	2	J	25.34
9775	0.58	11.51	0.855	11.51	0.855	9	8	52	20'	2	J	28.01
9452	0.58	11.51	0.855	11.51	0.855	9	8.25	26	19'-8.5"	1.5	W	28.59
27015	0.765	12.115	1.26	12.115	1.26	9	10	56	22'	2	F	25.39
62045	0.625	11.975	0.94	11.975	0.94	8	8.917	49	20-5"	1.5	G	27.31
66809	0.65	12	1.02	12	1.02	7.75	9.25	49	21', 22'	1.5		27.78
31023	0.4375	14	0.625	14	0.875	8	9.5	53	19'	1.5	G	24.39
55029	0.725	12.075	1.18	12.075	1.18	9	10	30	14'-19'	2	F	32.23
69894	0.5	14	0.625	16	1.25	8	10.375	50	stag.	1.5	G	26.14
27734	0.5	14	1	18	1.25	9	9.25	61	23', 24'	2	J	28.96
62702	0.5	14	1	18	2.25	9	8	25	25', 20'	2		35.46
66001	0.375	14	0.625	16	1.125	6.5	8.917	57	21.9'	1.5		29.20
86802	0.5	16	0.75	16	0.75	8.25	10.167	42	23'	1.5	G	26.62
49011	0.5	14	0.75	14	0.875	8	9.5	49	20'-25'	1.5		25.20
27106	0.375	18	0.75	18	1.375	7	9.5	24	21'	1.5		24.10
19882	0.5625	14	1	16	1	9.25	10.75	45	23'	2	F	25.88
19816	0.5625	18	1	20	1	9	10.25	22	25'	2	J	21.67
19832	0.5	16	0.75	16	1.5	9	10.167	55	25'	2	J	27.84

Table 4.1 Mn/DOT Bridge Survey Data

The bridges surveyed typically had three or more lanes and were two-, three-, or four-span bridges. An analysis of trends in the collected data for this survey was conducted to focus the parameter study and streamline the bridge modeling process. Parameters found to have a significant effect on diaphragm deflection would be modeled in a primary parameter study, while parameters with less significant influence on deflection would either be neglected or addressed individually in secondary parameter studies.

4.4 Identifying Parameter Significance

The properties and configurations of the bridges in the Mn/DOT survey were reviewed to determine how they might influence differential deflection. The parameters deemed to have a less significant effect on diaphragm relative deflection included the following:

- Total bridge length and number of bridge spans: The total length of a bridge structure, or having fewer or more distant spans, is believed to have little to no effect on the local phenomenon of diaphragm differential deflection.
- Diaphragm arrangement: Staggered diaphragms in the survey of skewed Mn/DOT steel bridges are at the bridge designer's discretion but appeared to be evenly spaced between supports.
- Diaphragm detail: The rigid, bent plate diaphragm detail that results in fatigue susceptible web gaps was present in the previously studied I-94/I-694 bridge was a prerequisite of the bridges selected from the Mn/DOT inventory for the bridge survey.
- Web gap length, g, and web thickness, t_w: Although web gap dimensions play a significant role in web gap distortional stresses (Eq. 2.1), they have small effects on deflection since web gap length has no effect on section moment of inertia and web thickness does not have a significant influence on moment of inertia.
- Deck thickness: Deck thickness was believed to have less effect on differential deflection than other parameters since deck thickness reductions made would occur to the total composite cross-section above each girder. Deck thickness ranged from 16.5 to 25.4 cm (6.5 in to 10 in), although most bridge decks in the Mn/DOT survey were approximately 22.9 cm (9 in) thick.

- Edge rail type: Although many different types of edge rail exist (e.g., Mn/DOT G-rail, F-rail, and J-rail types), they are all integrally reinforced with the deck and should affect bridge deflection behavior in a similar manner.
- Concrete strength and steel strength: Concrete strength, $f`_c$ = 27 MPa (4 ksi), and steel strength, f_y = 345 MPa (50 ksi), were virtually constant in the Mn/DOT survey of bridges.
- Adjacent span length: Initial models suggested that diaphragm differential deflection is a local phenomenon not affected much by adjacent span length.

4.5 Primary Parameters

Parameters in the survey of multi-girder steel bridges on skew in the Mn/DOT inventory deemed to have significant influence on bridge deflection behavior are as follows:

- Main span length, *L*: Deflection is highly dependent on span length and therefore must be included in any comprehensive analysis of parameters that affect deflection.
- Moment of inertia: Bridge section properties such as girder moment of inertia (i.e., flange width, flange thickness, girder depth) and bridge deck thickness have significant influence on bridge deflection properties.
- Girder spacing, *S*: The original AASHTO load distribution factor was based solely on spacing (e.g., distribution factor = S/5.5, where *S* is girder spacing in ft) and relative deflection between girders are obviously dependent on the spacing between them.
- Angle of skew: A study of bridge differential deflection must include skew since skew bridges, with varying distances to supports, have been observed to have significant differential deflection and distortional fatigue problems.

4.6 Parameter Studies

The primary parameter study included the modeling and analysis of bridges with three principle parameters: span length, angle of skew, and girder spacing. The values for these parameters are as follows:

- Span lengths of 18.3, 30.5, 42.7, and 54.9 m (60, 100, 140, and 180 ft).
- Skew angles of 20°, 40°, and 60° were considered.
- Girder spacing was taken as either 2.44 or 3.20 m (8 or 10.5 ft).

A resolution regarding section moment of inertia as a parameter is addressed in the next section, Section 4.7. Based on the range of values for the bridge parameters surveyed, the full ranges of span length and angle of skew were addressed. The extremes in regard to girder spacing were also chosen for study. Design guidelines indicate that diaphragm staggering is required if the bridge angle of skew is greater than 20°. Bridges with skew less than 20° are designated to have back-to-back diaphragms, which may behave in a manner different than that identified in the previous Mn/DOT research project [1]. Mn/DOT Office of Bridge and Structures expressed interest in the modeling of bridges with no skew. It was decided that zero skew bridges would not be modeled since confidence in the finite element bridge models was the result of calibration with the previously studied I-94/I-694 bridge, which is an extremely skewed bridge that has staggered diaphragms. A bridge with perpendicular abutments will have no skew and back-to-back diaphragms. Future Mn/DOT research is expected to provide more insight into the differences between skewed and non-skewed bridges, as well as staggered and back-to-back diaphragms.

Upon conclusion of the primary parameter study, secondary studies were chosen to determine if diaphragm differential deflection is impacted by: 1) an intermediate value for girder spacing between the extreme values used in the primary study, 2) changes in adjacent span length, 3) rigid plate diaphragm depth, 4) deck thickness, 5) variations in lateral lane position/shoulder width, and 6) changes in web thickness.

4.7 Guidelines for Proportioning Bridge Models

The proportioning "rules" set forth below were established to assure consistent modeling between the parameter studies and the Mn/DOT bridge inventory. These guidelines governed issues related to: length of end spans in the three span models, spacing of girders in relation to bridge width, total width of the bridges, girder depth, depth of rigid plate diaphragms, diaphragm spacing, and the length of the cantilevered bridge deck supporting the edge rail.

- Girder span-to-depth ratio, L/d equal to 27, where L = length of main bridge span, and d = depth of bridge girder, was found to be nearly constant with a median value equal to 27 for the bridges in the Mn/DOT survey (Figure 4.8). Although the L/d data is scattered (i.e.,

coefficient of variation = 14%), most values are between 25 and 30. The modeling of girders in which depth and length vary independently would significantly increase the finite element modeling effort. Assuming L/d = 27, and lengths equal to 18.3, 30.5, 42.7, 54.9 m (60, 100, 140, and 180 ft) requires girder depths equal to 67.7, 113, 158, and 203 cm (26.67, 44.44, 62.22, and 80 in), respectively.

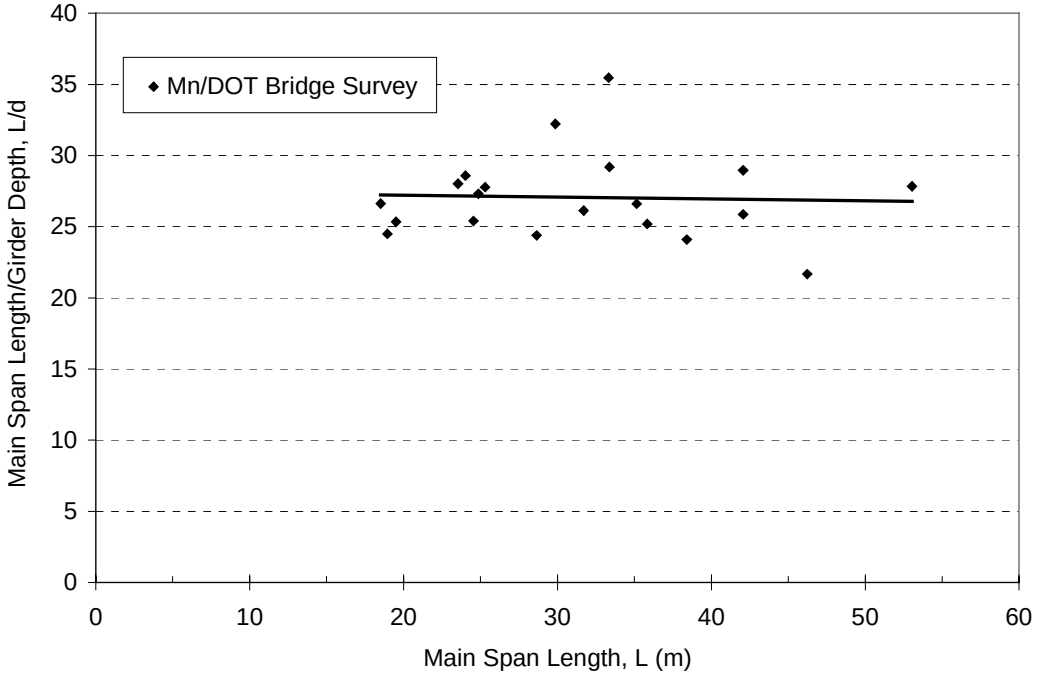

Figure 4.9 L/d Ratio

- Bridges were modeled with three, equal spans, the lengths of which were one of the four values selected for study.
- Diaphragm depth was defined as three-fourths of the girder depth. Based upon girder depths of 67.7, 113, 158, and 203 cm (26.67, 44.44, 62.22, and 80 in), the corresponding depths of the bent plate diaphragms were determined to be 50.8, 83.8, 119, and 122 cm (20, 33, 47, and 48 in), respectively. The maximum diaphragm depth allowed by Mn/DOT is 1.22 m (48 in), and it was used in the bridge models with L = 54.9 m (180 ft) [27]. Diaphragm flange proportions (i.e., diaphragm depth/flange width ratio) were assumed to be identical to those

for the I-94/I-694 bridge, which had a diaphragm depth/flange width ratio equal to 6:1. Diaphragm plate thickness was set equal to a constant 7.9 mm (0.3125 in) for all models.

- For end spans, the diaphragms were evenly spaced along the bridge with a spacing less than or equal to 7.62 m (25 ft), measured from centerline of pier. In actual bridges, diaphragm spacing is selected by the designer and must avoid splice regions, so, it varies much between bridges. Values for the Mn/DOT bridge survey ranged from 4.57 to 7.62 m (15 to 25 ft), with the typical values falling between 6.10 to 7.62 m (20 and 25 ft). For the main (center) span, which had lengths that were integer multiples of 6.10 m (20 ft), diaphragm spacing was held constant at 6.10 m (20 ft) to maintain consistency among the bridges.
- Girder cross-sections that change along bridge length is common in steel bridge design. Although the section may change several times, the bridges studied as part of the Mn/DOT survey typically had two principle cross-sections. Splicing of continuous girders between these sections typically occurs at or near the point of inflection to ensure the splice is subjected to small moments. Bridge engineers at Mn/DOT analyzed the bridges surveyed and found that the location for girder changing cross-sections typically occurs at a distance equal to 0.22L from the pier. Girders were therefore modeled with two cross sections per girder, one at the pier and one at midspan, and the change took place at this location.
- In order to construct finite element bridge models representative of the Mn/DOT bridge inventory, a systematic procedure was needed for the proportioning of the two girder cross sections. Analysis of the Mn/DOT bridge survey data found nearly constant values for the dimensionless parameter given by $L^3W/I_{composite}$ for cross sections at both midspan and at supports, where L is main span length, W is bridge width, and $I_{composite}$ is the moment of inertia of the composite section. Values for this parameter at midspan and pier locations were 4.77×10^6 and 3.78×10^6, respectively, as determined from the survey data for typical bridges with span lengths equal to, or smaller than, 42.7 m (140 ft) (Figure 4.9). Girder cross sections were changed by varying the girder flanges only. Flange thickness ranged from 0.95 to 6.35 cm (0.375 to 2.5 in).
- The finite element bridge models with different girder spacings had similar total bridge widths as well as similar shoulder widths. Bridges were modeled with girder spacing of 2.44 and 3.20 m (8 and 10.5 ft). Nine girders at 2.44 m (8 ft) produce a total roadway width of 20.52 m (67.333 ft). Seven girders at 3.20 m (10.5 ft) produce a total roadway width of

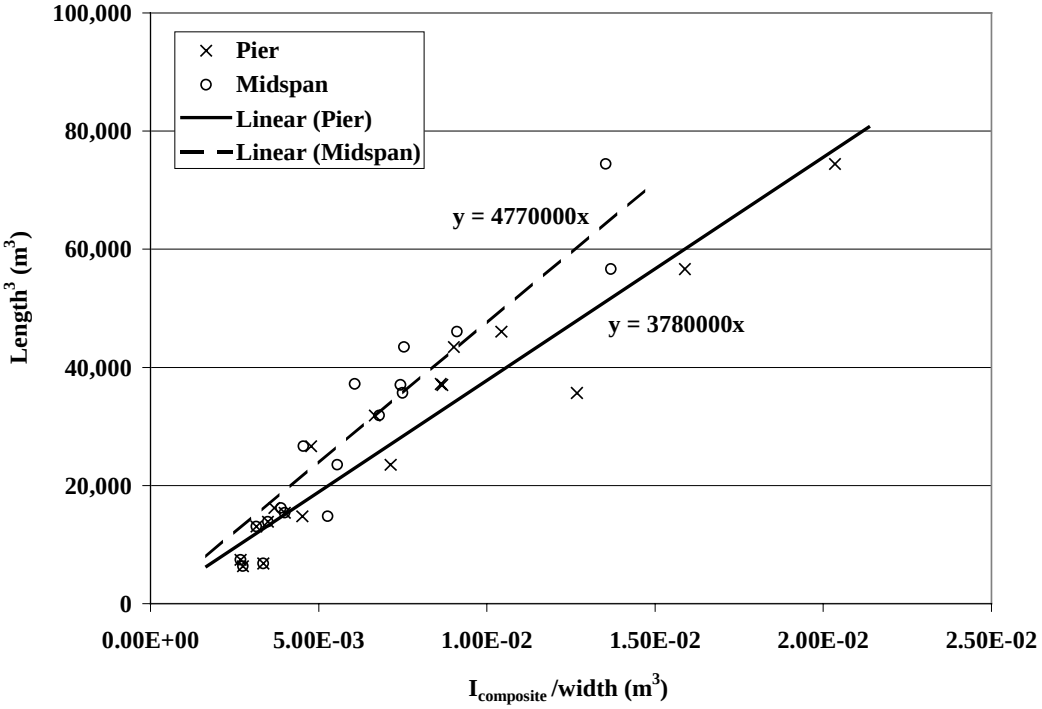

Figure 4.10 Bridge Modeling Dimensionless Parameter

20.27 m (66.333 ft). With four 3.66 m (12 ft) traffic lanes centered on the roadway, this produced shoulder lane widths of 2.95 and 2.79 m (9.667 and 9.167 ft) for the 2.44 and 3.20 m (8 and 10.5 ft) spacing, respectively.

- The length of cantilevered deck supporting the edge rail was 1.02 m (40 in) for all models except for those with span lengths of 18.3 m (60 ft), which had an overhang of 66 cm (26 in). An overhang of 1.02 m (40 in) is the same as that for the I-94/I-694 bridge. According to Mn/DOT guidelines [27], the overhang distance should not exceed the minimum of 0.4 times the girder spacing, girder depth, or 32 in plus 0.5 times the flange width. A cantilevered slab of 1.02 m (40 in) was satisfactory in all cases except for the span length of 18.3 m (60 ft), which were modeled with a 66 cm (26 in) cantilever to the rail. This latter cantilever length produced a shoulder width of 2.59 and 2.44 m (8.5 and 8 ft), respectively, for the 2.44 m and 3.20 m (8 and 10.5 ft) girder spacings.

Chapter 5
Primary Parameter Study

5.1 Primary Parameters

A parametric study into the differential deflection behavior of diaphragms that connect steel girders was conducted to quantify the influence of those variables that impact distortional fatigue directly. With an understanding of the mechanism that causes distortional fatigue, accompanied by proportioning guidelines and modeling methods refined for composite steel bridges, an investigation into the effects of bridge skew angle, span length, and girder spacing on girder differential deflection was conducted. Bridge models for each parametric combination were analyzed. The values of the principle variables in the primary study are as follows:

- Span lengths = 18.3, 30.5, 42.7, 54.9 m (60, 100, 140, and 180 ft),
- Skew angles = 20°, 40°, and 60°, and
- Girder spacing = 2.44 or 3.20 m (8 or 10.5 ft).

All models conformed to the proportioning guidelines outlined in the previous chapter. The model analyses were conducted for HS-20 truck loading in the edge lane, and diaphragm differential deflection was monitored in the obtuse corner region nearest the truck loading in the center span. Primary study model dimensions is shown in Appendix B.

5.2 Primary Modeling Results

Results for differential deflection at Diaphragm A (Figure 4.1) are illustrated in Figures 5.1 and 5.2. The differential deflection data indicates that differential deflection generally decreases with larger bridge span length, increases with larger bridge skew, and increases with larger girder spacing. Figure 5.1 and 5.2 illustrate trends due to skew and span length at a fixed location (i.e., Diaphragm A).

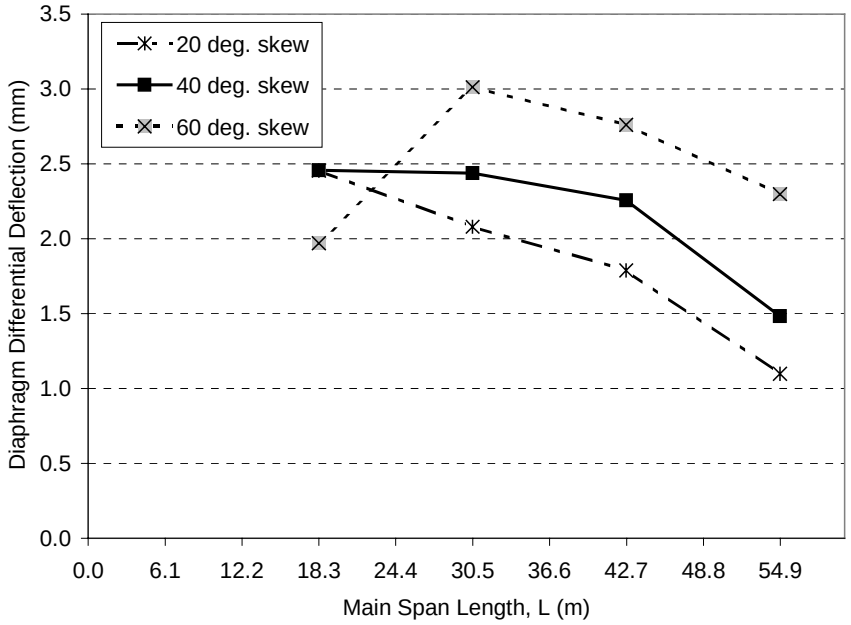

Figure 5.1 Differential Deflection, Diaphragm A, Girder Spacing = 3.20 m (10.5 ft)

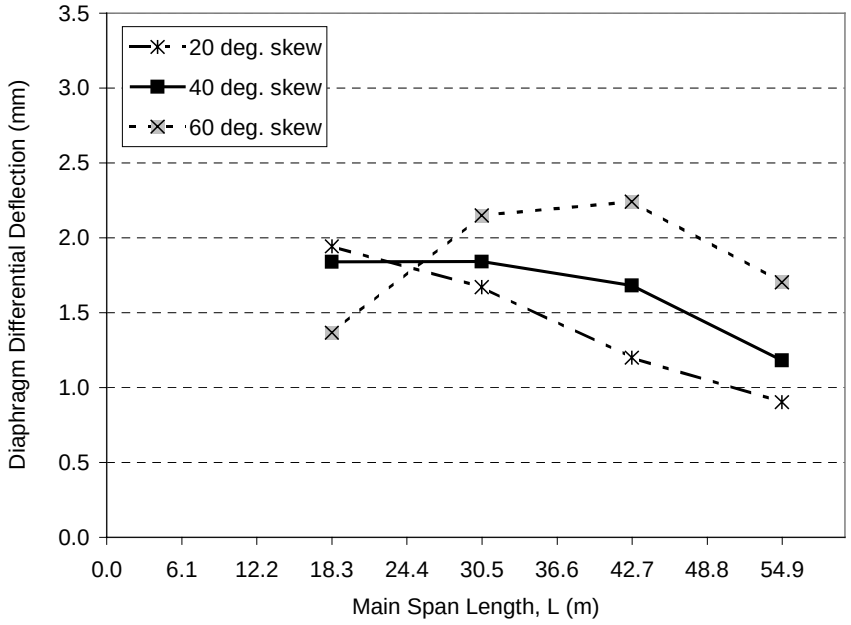

Figure 5.2 Differential Deflection, Diaphragm A, Girder Spacing = 2.44 (8 ft)

Trends in diaphragm differential deflection for bridges with girders spaced at 3.20 m (10.5 ft) are of greater magnitude but are comparable to deflection trends for bridges with girders spaced at 2.44 m (8 ft). Differential deflection generally decreases slightly with larger span length, except for the shortest span length and the largest angle of skew. For this case, maximum differential deflection occurs with a main span length equal to 30.5 m (100 ft) and then decreases for both longer and shorter span lengths. The effects on relative deflection with changes in skew for short spans can be explained by the fact that shorter span lengths approach the 13.4 m (44 ft) total length of an HS-20 truck. As skew angle increases and span length remains constant, the perpendicular distance between supports decrease even further (Figure 5.3). Load transferred along a perpendicular path between supports may explain the observed decrease in relative deflection at the shortest spans.

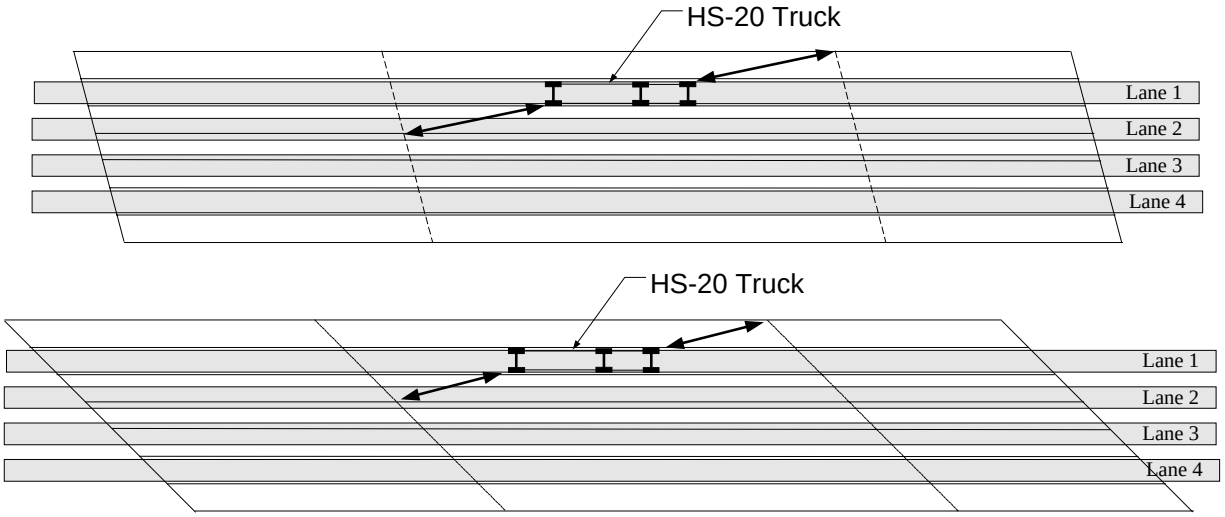

Figure 5.3 Reduction in Distance to Supports at Increased Bridge Skew

Diaphragm A was typically, but not always, the location of maximum differential deflection. Such locations should correspond with the first instances of distortional fatigue cracking if web gap geometry and traffic loading is the same throughout the bridge. In some instances, the location of maximum differential deflection moved from the obtuse corner toward midspan of the center span (e.g., maximum diaphragm differential deflection moving from Diaphragm A to H, Figure 4.2). Plots of maximum differential deflection are shown in Figures 5.4 and 5.5. A comparison of Diaphragm A deflections (Figure 5.1 and 5.2) with diaphragm maximum

deflection (Figure 5.4 and 5.5) indicates that for models with intermediate span lengths (100, 140 ft) and low skew (20°, 40°) , or the long span (180 ft), diaphragm maximum deflection occurred away from the obtuse corner. Mn/DOT bridge inspectors have observed that distortional fatigue cracks typically occur in the web gap at the diaphragm connection in the negative moment region at or near the point of inflection. This result would support that observation. With two diaphragms spaced regularly at 6.10 m (20 ft) intervals between main span supports, the obtuse corner diaphragm of the short, 18.3 m (60 ft) span is already near the point of inflection. Finite element modeling results for skew bridges in Figure 4.1 also indicate a change in maximum diaphragm deflection away from the obtuse corner towards midspan at lesser values of skew.

It appears that as span length increases, the region affected by skew diminishes and becomes a smaller fraction of the span length. This feature allows composite section bending to become the more significant mode of load transfer, and, therefore, deflection. Lesser bridge deflection and diaphragm relative deflection at the longer spans (> 140 ft), or possibly greater bridge aspect ratios (bridge span/bridge width), would concur with the importance of aspect ratio on moment distribution [19]. Although bridge aspect ratio may be a good indicator of this effect, the role of skew and its effect in relation to aspect ratio make it a parameter for which influence is difficult to define. Previous research has also noted less severe out-of-plane distortion in 3-girder bridges as compared with 4- and 5-girder bridges [2]. This deflection behavior appears to indicate that the design provision requiring the moment of inertia of the gross cross-sectional area (i.e., including girders and deck) should be used for computing beam and girder deflection is more applicable to longer spans [23].

The finite element data for maximum relative deflection for the diaphragms also indicate a close range of displacement values. Although the effects of skew and girder spacing are present, values of relative deflection are typically within a 0.6 mm (0.025 in) band for each span length. This tight band of deflection values likely stems from the proportioning rules defined within the parameter study and the uniformity in bridge design for the Mn/DOT inventory.

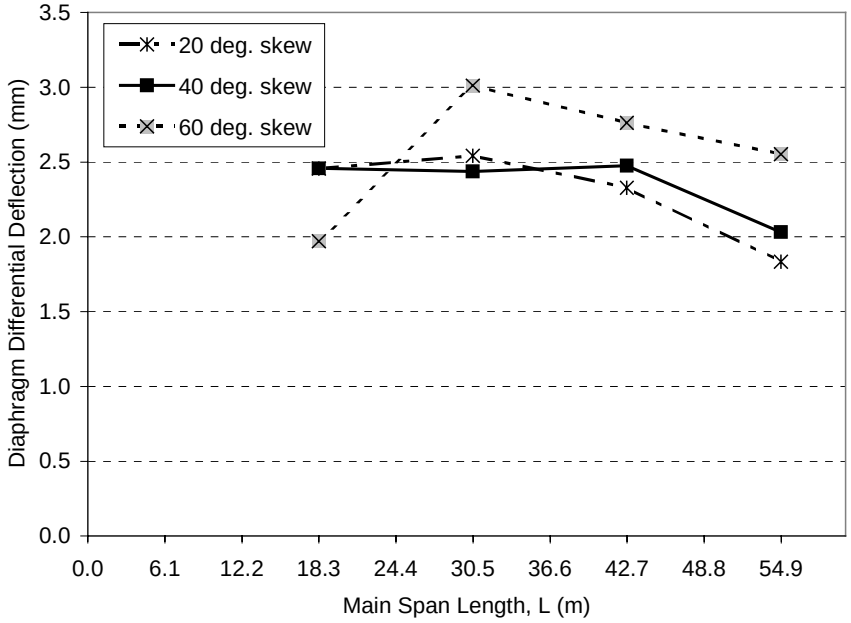

Figure 5.4 Maximum Diaphragm Differential Deflection, Girder Spacing = 3.20 m (10.5 ft)

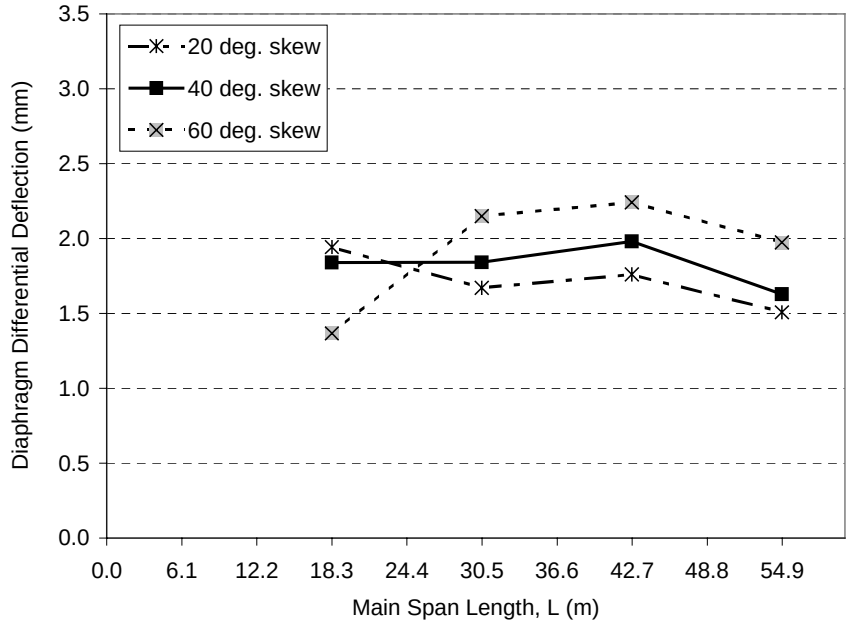

Figure 5.5 Maximum Diaphragm Differential Deflection, Girder Spacing = 2.44 m (8 ft)

Deflection data for all the finite element analyses described in this chapter are summarized in Table 5.1.

Girder Spacing		Span Length		Skew	Diaphragm A Differential Deflection		Max. Diaphragm Differential Deflection		Max. Diaphragm Location
ft.	m	ft.	m	deg.	in.	mm	in.	mm	*
8	2.44	60	18.3	20	0.077	1.94	0.077	1.94	A
8	2.44	100	30.5	20	0.066	1.67	0.066	1.67	A
8	2.44	140	42.7	20	0.047	1.20	0.069	1.76	H
8	2.44	180	54.9	20	0.036	0.90	0.059	1.51	O
8	2.44	60	18.3	40	0.072	1.84	0.072	1.84	A
8	2.44	100	30.5	40	0.072	1.84	0.072	1.84	A
8	2.44	140	42.7	40	0.066	1.68	0.078	1.98	H
8	2.44	180	54.9	40	0.047	1.18	0.064	1.63	O
8	2.44	60	18.3	60	0.054	1.37	0.054	1.37	A
8	2.44	100	30.5	60	0.085	2.15	0.085	2.15	A
8	2.44	140	42.7	60	0.088	2.24	0.088	2.24	A
8	2.44	180	54.9	60	0.067	1.70	0.078	1.97	H
9.25	2.82	60	18.3	20	0.087	2.21	0.087	2.21	A
9.25	2.82	100	30.5	20	0.077	1.96	0.095	2.41	H
9.25	2.82	140	42.7	20	0.054	1.37	0.083	2.11	O
9.25	2.82	100	30.5	60	0.102	2.59	0.102	2.59	A
9.25	2.82	140	42.7	60	0.095	2.41	0.101	2.57	H
9.25	2.82	180	54.9	60	0.083	2.11	0.096	2.44	H
10.5	3.20	60	18.3	20	0.097	2.46	0.097	2.46	A
10.5	3.20	100	30.5	20	0.082	2.08	0.100	2.54	H
10.5	3.20	140	42.7	20	0.070	1.79	0.092	2.33	H
10.5	3.20	180	54.9	20	0.043	1.10	0.072	1.83	O
10.5	3.20	60	18.3	40	0.097	2.46	0.097	2.46	A
10.5	3.20	100	30.5	40	0.096	2.44	0.096	2.44	A
10.5	3.20	140	42.7	40	0.089	2.26	0.097	2.47	H
10.5	3.20	180	54.9	40	0.058	1.48	0.080	2.03	O
10.5	3.20	60	18.3	60	0.078	1.97	0.078	1.97	A
10.5	3.20	100	30.5	60	0.119	3.01	0.119	3.01	A
10.5	3.20	140	42.7	60	0.109	2.76	0.109	2.76	A
10.5	3.20	180	54.9	60	0.090	2.30	0.100	2.55	H

* Diaphragm location A, H, and O (Figure 4.2)

Table 5.1 Parameter Study Differential Deflection Data

Chapter 6
Secondary Parameter Studies

6.1 Overview

A secondary group of finite element models were studied in an effort to expand the previously discussed primary parameter study of composite steel bridges. Some of the trends observed in the primary study and their significance are made more clear in the secondary studies.

6.2 Secondary Parameters

Secondary finite element analyses were conducted to 1) address variables that were held constant in the primary study, 2) include intermediate values for parameters that were varied coarsely in the primary study (i.e., only two values consider), and 3) provide spot checks of the primary parameter study. The secondary studies included research into the effects of an intermediate girder spacing, adjacent span length, diaphragm depth, deck thickness, web thickness, and lateral lane position in relation to girder placement. These secondary modeling studies serve to provide insight into changes in deflection behavior from the variation of parameters held constant in the primary parameter study. They also provide a measure of variability when relating the finite element model studies to actual steel bridges.

6.3 Secondary Modeling Results

- *Girder spacing*: Models were created to study an intermediate girder spacing between the girder spacings of 2.44 and 3.20 m (8 and 10.5 ft) that were used in the primary study. Models with a girder spacing of 2.82 m (9.25 ft) indicate an approximately linear relation for girder differential deflection with girder spacing, within the range of values studied (Figure 6.1). Diaphragm relative deflection data for the intermediate girder spacing is included in Table 5.1.

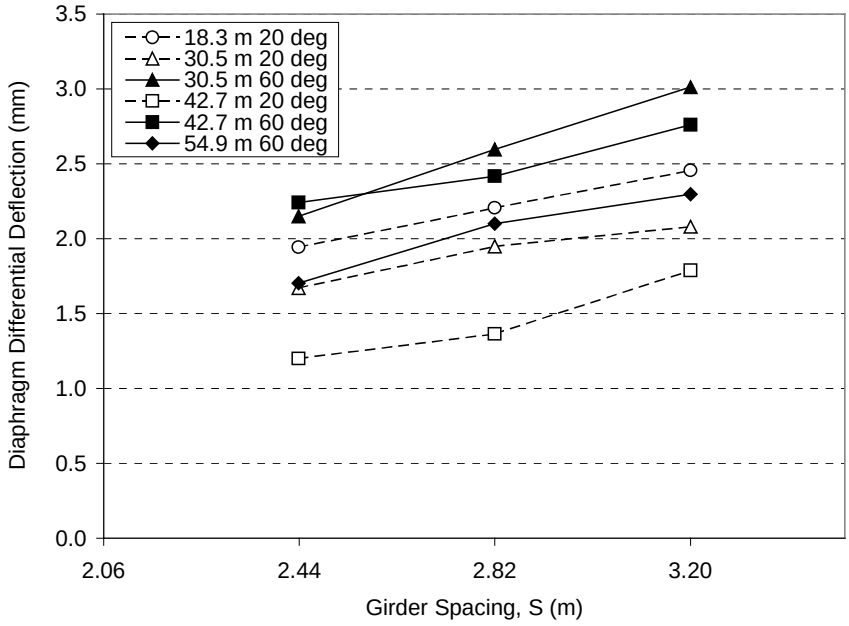

Figure 6.1 Intermediate Girder Spacing, S = 2.82 m (9.25 ft)

- *Adjacent span length*: The primary parameter study utilized bridges with three equal spans. Upon consultation with Mn/DOT, bridges with end spans of different length were investigated. A designer's rule-of-thumb was suggested in which three span bridges should have end span lengths approximately equal to 0.8*L*, where *L* is the main (center) span length. Such a configuration results in girders with more balanced positive and negative bending moments. Four bridge models with this configuration, one at each of the lengths used in the primary parameter study, indicated a small change in maximum diaphragm differential deflection of up to, but not more than, 0.08 mm (0.003 in) (Table 6.1). That change represents 3% of the maximum differential deflections obtained in the primary study. It is concluded, with respect to the ratio of adjacent span length, that the primary study is directly applicable to the bridges in the Mn/DOT inventory. Instances where adjacent span lengths are significantly different from 0.8*L* should be noted when assessing differential deflection.

Primary Parameter Study

Girder Spacing		Span Length		Skew	Diaphragm A Differential Deflection		Max. Diaphragm Differential Deflection		Max. Diaphragm Location
ft.	m	ft.	m	deg.	in.	mm	in.	mm	
8	2.44	60	18.3	20	0.077	1.94	0.077	1.94	A
10.5	3.2	100	30.5	60	0.119	3.01	0.119	3.01	A
8	2.44	140	42.7	40	0.066	1.68	0.078	1.98	H
10.5	3.2	180	54.9	60	0.090	2.3	0.100	2.55	H

Secondary Parameter Study, 0.8L End Spans

Girder Spacing		Span Length		Skew	Diaphragm A Differential Deflection		Max. Diaphragm Differential Deflection		Max. Diaphragm Location
ft.	m	ft.	m	deg.	in.	mm	in.	mm	
8	2.44	60	18.3	20	0.076	1.93	0.076	1.93	A
10.5	3.2	100	30.5	60	0.116	2.94	0.116	2.94	A
8	2.44	140	42.7	40	0.065	1.65	0.078	1.99	H
10.5	3.2	180	54.9	60	0.088	2.22	0.099	2.52	H

Girder Spacing		Span Length		Skew	Diaphragm A Diff. Deflection Difference		Max. Diaphragm Diff. Deflection Difference		Percent Difference	
ft.	m	ft.	m	deg.	in.	mm	in.	mm	Dia. A	Max.
8	2.44	60	18.3	20	0.001	0.02	0.001	0.02	0.9%	0.9%
10.5	3.2	100	30.5	60	0.003	0.08	0.003	0.08	2.5%	2.5%
8	2.44	140	42.7	40	0.001	0.03	0.000	-0.01	1.9%	-0.3%
10.5	3.2	180	54.9	60	0.003	0.07	0.001	0.03	3.3%	1.2%

Table 6.1 Adjacent Span Length Study Differential Deflection Data

- *Diaphragm depth*: In the primary parameter study, diaphragm depth was set equal to three-fourths of girder depth. At the request of Mn/DOT staff, eight finite element bridge models were modified to incorporate a minimum value for diaphragm depth equal to one-half of girder depth. Smaller diaphragm depths were expected to result in more flexible diaphragms and less diaphragm differential deflection and rotation. Diaphragm depth modifications from three-fourths of girder depth to one-half of girder depth resulted in no change in girder differential deflection in any of the models (Table 6.2). Models with the diaphragms removed entirely indicated no change to the nearest 0.025 mm (0.001 in) over those in the primary study. These observations should have been expected since the previous Mn/DOT research indicated that diaphragms rotate essentially as pinned elements with little moment developed since rotation is resisted only by the flexible web and the girder flange displacing out-of-plane. The diaphragm and web gap rotation behavior observed in finite element analysis of the diaphragm detail led to the development of Eq. 2.1. The diaphragms in the finite element models simulate these conditions since the diaphragms were connected solely at one point in the middle of the web (Figure 3.1). A number of field studies have shown that diaphragms are responsible for only a small percentage of load distribution [14, 28].

Primary Parameter Study, Diaphragm Depth = Three/Fourths of Girder Depth

Girder Spacing		Span Length		Skew	Diaphragm A Differential Deflection		Max. Diaphragm Differential Deflection		Max. Diaphragm Location
ft.	m	ft.	m	deg.	in.	mm	in.	mm	
8	2.44	60	18.3	20	0.0765	1.94	0.077	1.94	A
8	2.44	60	18.3	60	0.0538	1.37	0.054	1.37	A
10.5	3.2	100	30.5	40	0.0960	2.44	0.096	2.44	A
10.5	3.2	100	30.5	60	0.1186	3.01	0.119	3.01	A
10.5	3.2	140	42.7	20	0.0704	1.79	0.092	2.33	H
10.5	3.2	140	42.7	60	0.1087	2.76	0.109	2.76	A
8	2.44	180	54.9	40	0.0466	1.18	0.064	1.63	O
8	2.44	180	54.9	60	0.0670	1.70	0.078	1.97	H

Secondary Parameter Study, Diaphragm Depth = Half of Girder Depth

Girder Spacing		Span Length		Skew	Diaphragm A Differential Deflection		Max. Diaphragm Differential Deflection		Max. Diaphragm Location	
ft.	m	ft.	m	deg.	in.	mm	in.	mm		
8	2.44	60	18.3	20	0.0765	1.94	0.077	1.94	A	
8	2.44	60	18.3	60	0.0538	1.37	0.054	1.37	A	
10.5	3.2	100	30.5	40	0.0960	2.44	0.096	2.44	A	
10.5	3.2	100	30.5	60	0.1186	3.01	0.119	3.01	A	
10.5	3.2	140	42.7	20	0.0704	1.79	0.092	2.33	H	
10.5	3.2	140	42.7	60	0.1087	2.76	0.109	2.76	A	
8	2.44	180	54.9	40	0.0466	1.18	0.064	1.63	O	
8	2.44	180	54.9	60	0.0670	1.70	0.078	1.97	H	
Girder Spacing		Span Length		Skew	Diaphragm A Diff. Deflection Difference		Max. Diaphragm Diff. Deflection Difference		Percent Difference	
ft.	m	ft.	m	deg.	in.	mm	in.	mm	Dia. A	Max.
8	2.44	60	18.3	20	0.0000	0.00	0.0000	0.00	0.0%	0.0%
8	2.44	60	18.3	60	0.0000	0.00	0.0000	0.00	0.0%	0.0%
10.5	3.2	100	30.5	40	0.0000	0.00	0.0000	0.00	0.0%	0.0%
10.5	3.2	100	30.5	60	0.0000	0.00	0.0000	0.00	0.0%	0.0%
10.5	3.2	140	42.7	20	0.0000	0.00	0.0000	0.00	0.0%	0.0%
10.5	3.2	140	42.7	60	0.0000	0.00	0.0000	0.00	0.0%	0.0%
8	2.44	180	54.9	40	0.0000	0.00	0.0000	0.00	0.0%	0.0%
8	2.44	180	54.9	60	0.0000	0.00	0.0000	0.00	0.0%	0.0%

Table 6.2 Diaphragm Depth Study Differential Deflection Data

- *Deck thickness, t_d*: Finite element bridge models from the primary study, with 22.9 cm (9 in) decks, were modified to study deck thickness. Changes in deck thickness of ± 1 in. resulted in changes in average differential deflection of 15% or 0.3 mm (0.012 in), and 18% or 0.38 mm (0.015 in), respectively, for deck thicknesses of 25.4 and 20.3 cm (10 and 8 in) (Table 6.3). The influence of deck thickness on girder relative deflection indicates that deck thickness should not be neglected when assessing diaphragm differential deflection. A correction factor, β_d (Eq. 6.1), should be applied when assessing differential deflection, Δ, between bridge girders with decks other than 22.9 cm (9 in),

$$\beta_d = 1 + \left[0.15 \left(\frac{D - t_d}{\alpha} \right) \right] \qquad \text{Eq. 6.1}$$

where t_d is deck thickness, D is equal to 9 inches or 22.86 cm, and α is equal to 1 inch or 2.54 cm.

Primary Parameter Study, Concrete Deck Thickness = 9 inches

Girder Spacing		Span Length		Skew	Diaphragm A Differential Deflection		Max. Diaphragm Differential Deflection		Max. Diaphragm Location
ft.	m	ft.	m	deg.	in.	mm	in.	mm	
10.5	3.2	100	30.5	40	0.096	2.44	0.096	2.44	A
8	2.44	140	42.7	20	0.047	1.20	0.069	1.76	H
10.5	3.2	180	54.9	60	0.090	2.30	0.100	2.55	H

Secondary Parameter Study, Deck Thickness

Girder Spacing		Span Length		Skew	Diaphragm A Differential Deflection		Max. Diaphragm Differential Deflection		Max. Diaphragm Location
ft.	m	ft.	m	deg.	in.	mm	in.	mm	
Deck Thickness = 20.3 cm (8 inches)									
10.5	3.2	100	30.5	40	0.114	2.88	0.114	2.88	A
8	2.44	140	42.7	20	0.056	1.42	0.087	2.21	H
10.5	3.2	180	54.9	60	0.101	2.57	0.119	3.02	H
Deck Thickness = 25.4 cm (10 inches)									
10.5	3.2	100	30.5	40	0.081	2.07	0.081	2.07	A
8	2.44	140	42.7	20	0.040	1.02	0.055	1.39	H
10.5	3.2	180	54.9	60	0.082	2.08	0.086	2.18	H

Girder Spacing		Span Length		Skew	Diaphragm A Diff. Deflection Difference		Max. Diaphragm Diff. Deflection Difference		Percent Difference	
ft.	m	ft.	m	deg.	in.	mm	in.	mm		
Deck Thickness = 20.3 cm (8 in.)									Dia. A	Max.
10.5	3.2	100	30.5	40	-0.018	-0.45	-0.0176	-0.45	-18.4%	-18.4%
8	2.44	140	42.7	20	-0.009	-0.22	-0.0178	-0.45	-18.2%	-25.6%
10.5	3.2	180	54.9	60	-0.011	-0.27	-0.0183	-0.46	-11.8%	-18.2%
				Average Percent Difference:					-18%	
Deck Thickness = 25.4 cm (10 in.)									Dia. A	Max.
10.5	3.2	100	30.5	40	0.015	0.37	0.0146	0.37	15.2%	15.2%
8	2.44	140	42.7	20	0.007	0.18	0.0144	0.37	15.2%	20.8%
10.5	3.2	180	54.9	60	0.009	0.22	0.0145	0.37	9.6%	14.5%
				Average Percent Difference:					15%	

Table 6.3 Deck Thickness Study Differential Deflection Data

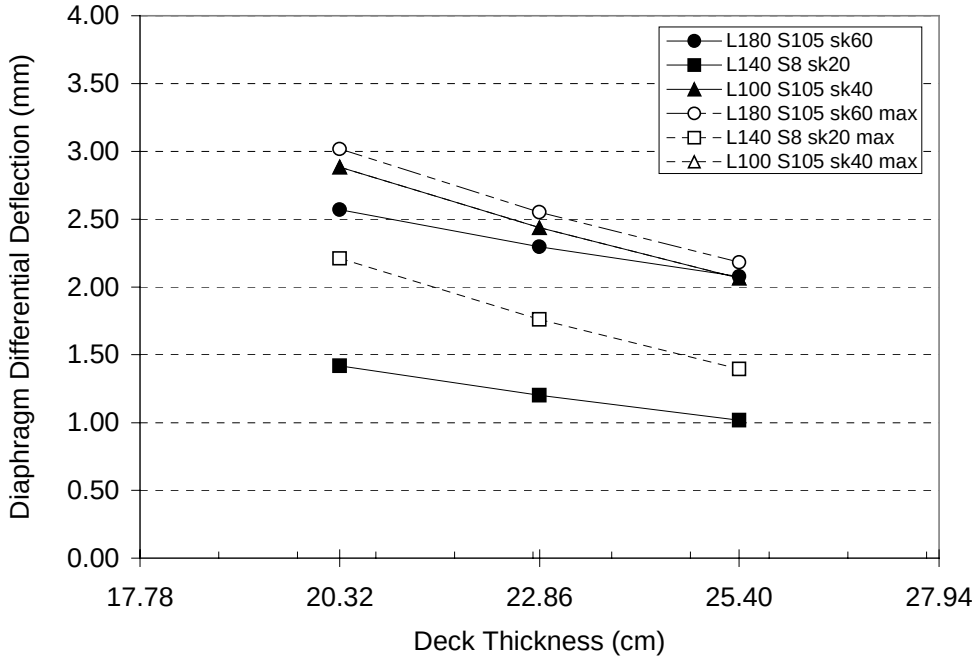

Figure 6.2 Deflection Variation due to Deck Thickness

- *Shoulder width*: In studying the effect of different girder spacing, approximately, but not exactly, equal bridge widths were assumed for all models. The roadway included four 3.66 m (12 ft) lanes centered on the bridge. Since the girder spacing and number of girders varied between models, bridge shoulder widths varied from 2.44 to 2.95 m (8 to 9.667 ft). This prompted a study into the effects of shoulder width on differential deflection due to loading in the edge lane. Shoulder widths above and below the range of shoulder widths in the primary parameter study were included in this study to ascertain the effects of a more broad range of values. The case of a truck axle straddling a girder could result in differences in computed differential deflection when compared with an axle that loads the deck on only one side of a girder, or an axle that loads the deck between two girders. However, finite element results (Table 6.4) indicated negligible changes in girder differential deflection over the range of shoulder widths included in the parameter study (Figures 6.3 and 6.4).

Secondary Parameter Study, Shoulder Width

Girder Spacing		Span Length		Skew	Shoulder Width		Diaphragm A Differential Deflection	
ft.	m	ft.	m	deg.	ft.	m	in.	mm
8	2.44	140	42.7	60	0.667	0.203	0.041	1.035
8	2.44	140	42.7	60	6.667	2.032	0.082	2.079
8	2.44	140	42.7	60	9.667	2.946	0.088	2.242
8	2.44	140	42.7	60	11.667	3.556	0.085	2.160
8	2.44	140	42.7	60	14.667	4.470	0.078	1.984
10.5	3.2	100	30.5	60	3.042	0.927	0.084	2.139
10.5	3.2	100	30.5	60	6.250	1.905	0.111	2.829
10.5	3.2	100	30.5	60	9.167	2.794	0.118	2.998
10.5	3.2	100	30.5	60	10.917	3.327	0.118	2.990
10.5	3.2	100	30.5	60	13.542	4.128	0.110	2.792

Table 6.4 Shoulder Width Study Differential Deflection Data

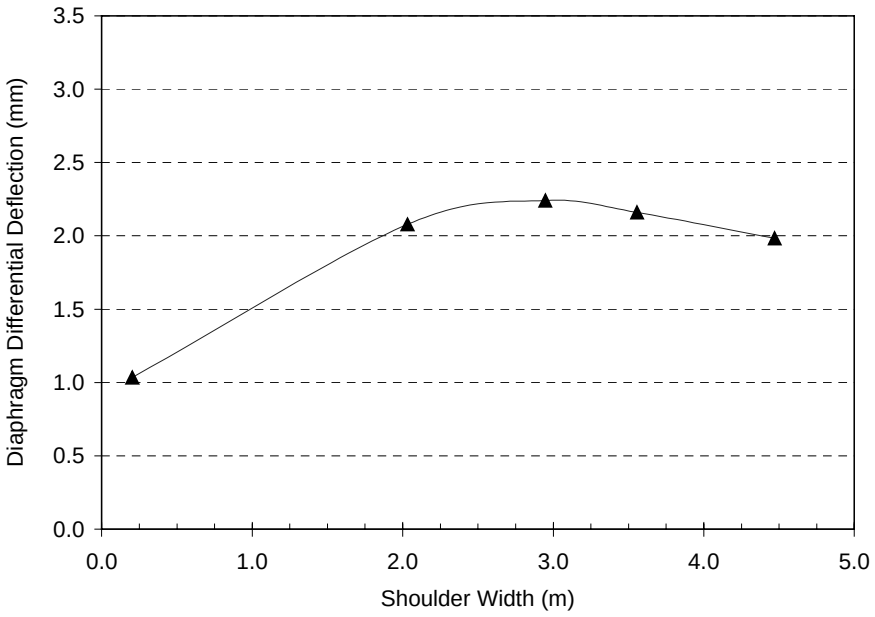

Figure 6.3 Effect of Shoulder Width, Diaphragm A, Girder Spacing = 2.44 m (8 ft)

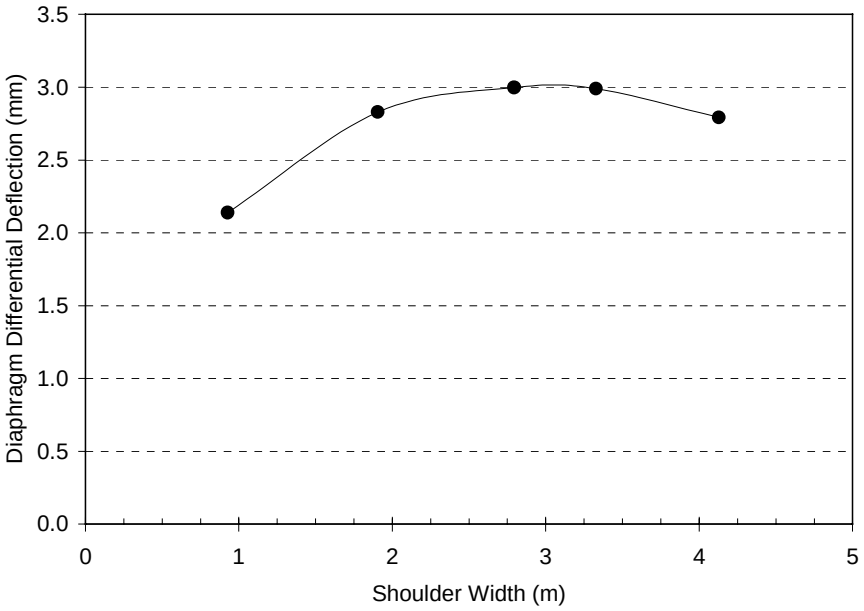

Figure 6.4 Effect of Shoulder Width, Diaphragm A, Girder Spacing = 3.20 m (10.5 ft)

- *Web thickness*: Since the primary parameter study models incorporated only one web thickness (0.5 in), a few other models were defined in order to determine the significance of web thickness on differential deflection. Changes in web thickness of ± 3.2 mm (0.125 in) resulted in changes in differential deflection of approximately ± 3% and is, therefore, deemed negligible in regard to the primary parameter study (Table 6.5).

Primary Parameter Study, Web Thickness = 0.5 inches

Girder Spacing		Span Length		Skew	Girder Web Thickness		Diaphragm A Differential Deflection	
ft.	m	ft.	m	deg.	in.	mm	in.	mm
8	2.44	100	30.5	20	0.5	12.70	0.066	1.67
8	2.44	100	30.5	40	0.5	12.70	0.072	1.84
8	2.44	100	30.5	60	0.5	12.70	0.085	2.15
10.5	3.2	140	42.7	20	0.5	12.70	0.070	1.79
10.5	3.2	140	42.7	40	0.5	12.70	0.089	2.26
10.5	3.2	140	42.7	60	0.5	12.70	0.109	2.76

Secondary Parameter Study, Web Thickness Change

Girder Spacing		Span Length		Skew	Girder Web Thickness		Diaphragm A Differential Deflection		Diaphragm A Diff. Deflection Difference		Percent Difference
ft.	m	ft.	m	deg.	in.	mm	in.	mm	in.	mm	Dia. A
8	2.44	100	30.5	20	0.625	15.88	0.064	1.63	0.002	0.04	2.4%
8	2.44	100	30.5	40	0.625	15.88	0.071	1.80	0.002	0.04	2.1%
8	2.44	100	30.5	60	0.625	15.88	0.083	2.11	0.002	0.04	1.9%
10.5	3.2	140	42.7	20	0.625	15.88	0.068	1.73	0.002	0.06	3.3%
10.5	3.2	140	42.7	40	0.625	15.88	0.086	2.19	0.003	0.07	2.9%
10.5	3.2	140	42.7	60	0.625	15.88	0.106	2.69	0.003	0.07	2.6%
8	2.44	100	30.5	20	0.375	9.53	0.068	1.72	-0.002	-0.05	-2.7%
8	2.44	100	30.5	40	0.375	9.53	0.075	1.90	-0.002	-0.06	-3.0%
8	2.44	100	30.5	60	0.375	9.53	0.087	2.21	-0.002	-0.06	-2.6%
10.5	3.2	140	42.7	20	0.375	9.53	0.074	1.88	-0.003	-0.09	-4.9%
10.5	3.2	140	42.7	40	0.375	9.53	0.093	2.35	-0.004	-0.10	-4.3%
10.5	3.2	140	42.7	60	0.375	9.53	0.113	2.86	-0.004	-0.10	-3.7%

Table 6.5 Web Thickness Study Differential Deflection Data

Chapter 7
Parameter Study Stresses

7.1 Overview

The finite element models in the present study, while quite large (e.g., 15,000 nodes, 4,900 frame elements, 13,000 shell elements, calibrated Bridge No. 27734), were developed to provide realistic assessments of deflections, but did not have a sufficiently fine mesh to capture local response to loading or provide realistic estimates of web gap stress. The previous phase of the Mn/DOT research program provided the equation (Eq. 2.1) that approximates values of web gap stress. These stresses are due to out-of-plane distortion and are computed given differential deflection (Δ) and bridge properties (web thickness, t_w, web gap length, g, steel modulus, E, and girder spacing, S). Stress estimates were computed using the diaphragm deflections from the finite element primary parameter study, and actual bridge parameters for web gap geometry (t_w and g) were used. Assumptions made in the analysis of the stress equation and factors that were observed to affect web gap stress are discussed.

7.2 Stress Estimates

Before applying Eq. 2.1 to all bridges in the parameter study, characterizations of t_w and t_w/g values were established using data from the Mn/DOT bridge survey. A range for web thickness, t_w, was required to represent the spread of the data (Figure 7.1) and to include the possible effects of the ratio t_w/g (Figure 7.2) on fatigue stress. Figure 7.2 illustrates the range of t_w/g values for web gap lengths of 3.8 and 5.1 cm (1.5 and 2 in) for all surveyed bridges. Utilizing a range of t_w/g from 0.25 to 0.4167 and applying it to Eq. 2.1, along with finite element model differential deflection Δ for a given girder spacing S (Table 5.1), web gap stresses for the parameter study were calculated. Modulus of elasticity, E, for steel was taken equal to 200 GPa (29,000 ksi) in all cases.

Figures 7.3 to 7.5 show three-dimensional plots of estimated stress for the bridge models in the parameter study with girder spacing equal to 3.20 m (10.5 ft). The plot illustrates stress as a function of both bridge skew and main span length. Differential deflection data from the finite

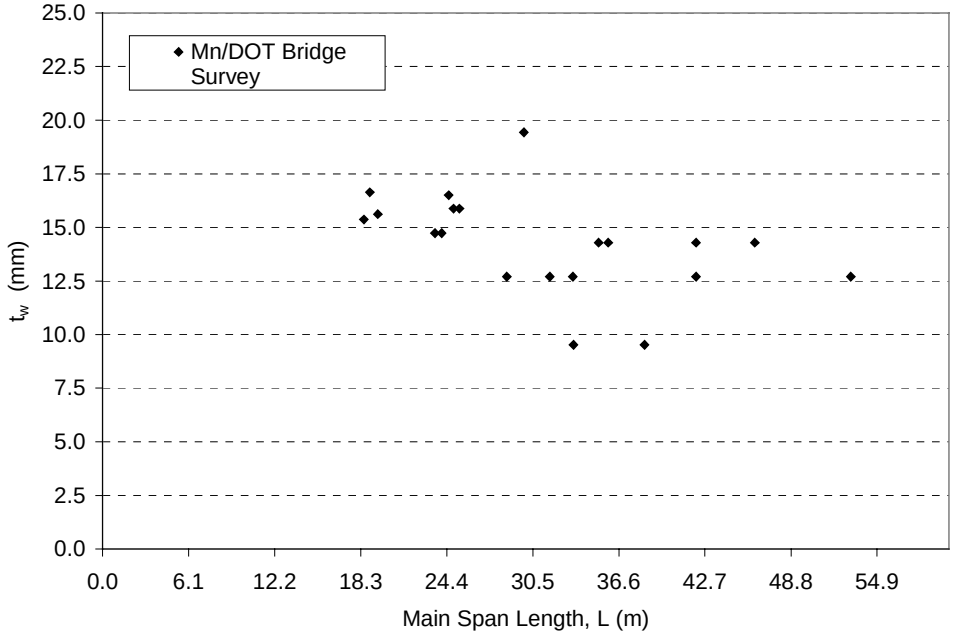

Figure 7.1 Values of t_w

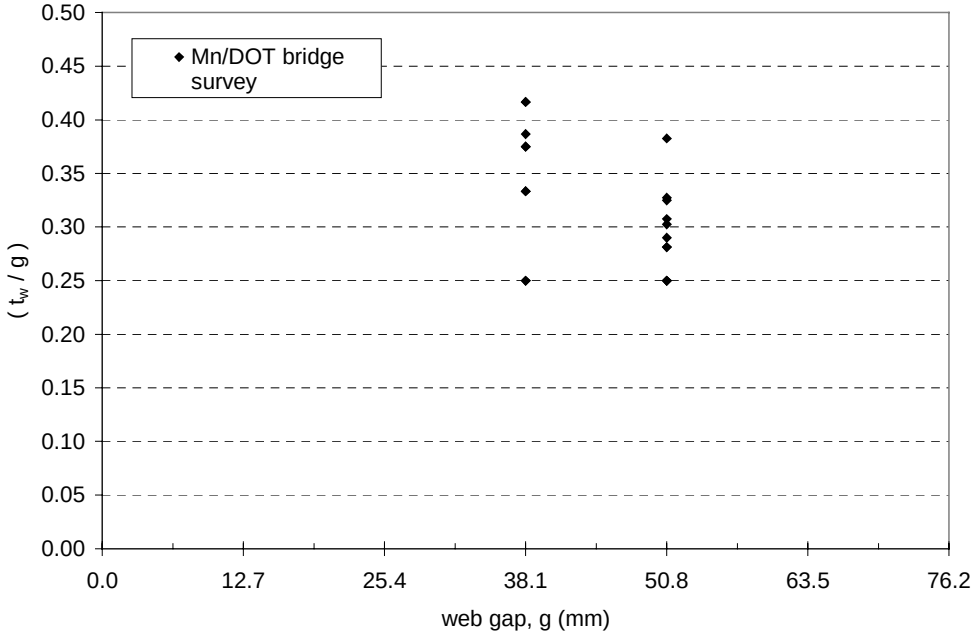

Figure 7.2 Values of t_w/g

element analyses were obtained in response to an HS-20 truckload, so stress is reported based upon that loading. Each three-dimensional plots is for a single ratio of web gap geometric parameters t_w/g. Plots for smaller t_w/g values are similar to those for large t_w/g values except the stresses are scaled to a lesser magnitude.

Plots for models with girder spacing at 2.44 m (8 ft) (Figure 7.6 to Figure 7.8) are comparable to plots for models with girder spacing at 2.82 m (9.25 ft) (Figure 7.9 to 7.11). Only half of all possible combinations of skew and length were modeled in the secondary studies with a girder spacing of 2.82 m (9.25 ft). Data for bridges that were not analyzed in the intermediate spacing parameter study were interpolated from the deflection data for the two extreme girder spacings in the primary study. Angle of skew, followed by span length, increase stresses as they themselves increase. This observation holds for spans up to 30.5 m, above which stress decreases with increasing length.

Comparing plots at equivalent t_w/g values indicate that, although girder spacing has significant effect on differential deflection (Figures 6.3 and 6.4), this effect of spacing on stress is small due to the presence of spacing in the stress calculations. This small difference is evident in calculated stress at different girder spacings and equal t_w/g values (e.g., Figures 7.3, 7.6, and 7.9). The difference in magnitude between points on this stress surface is small for low t_w/g and greatest at the largest t_w/g values. The effects of skew and length on differences in diaphragm relative deflection and stress become most pronounced at large values of t_w/g. The narrow range of differential deflection values, Δ, is in contrast to the broad range of computed stress values due to the role t_w/g plays in the magnitude of out-of-plane stress. The maximum stress for the range of span length and skew with $t_w/g = 0.4167$ (Figure 7.3) is approximately 159 MPa (23 ksi), while the smallest maximum stress in the corresponding plot with $t_w/g = 0.25$ (Figure 7.5) is approximately 56 MPa (8 ksi). The strong influence of t_w/g on web gap stress reinforces the AASHTO provisions for web gap length (not less than $4t_w$ or more than $6t_w$, [23]) and emphasizes that designers should be mindful of this requirement, although web gap distortion is not a problem in new design since stiffeners are required to be rigidly attached to both girder flanges. The importance of web gap dimensions on stress emphasizes the relevance of the detail retrofit that reduces web gap stress by increasing the web gap length.

Fatigue stress for remaining fatigue life analysis according to AASHTO can be taken directly as three-fourths of the stresses calculated in this study. This reduction in truck load is easily handled since the AASHTO fatigue truck has the same axle configuration as the HS-20 truck but weighs 25% less. This weight correction factor, β_w, may be applied and is equal to fatigue truck weight/HS-20 truck weight of 320 kN (72 kips), provide the axle configurations are the same.

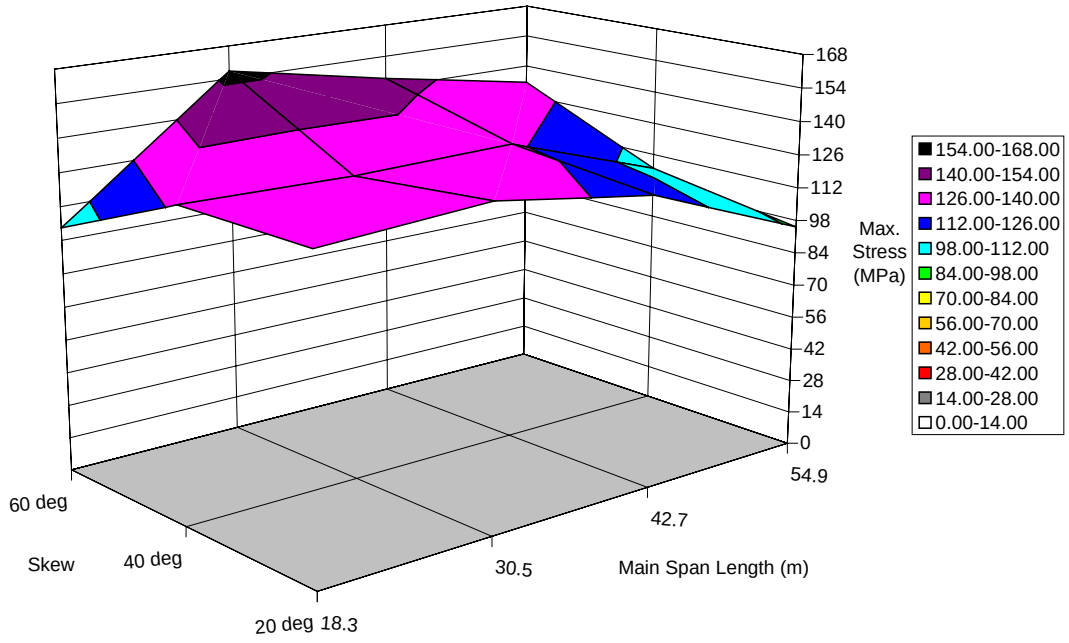

Figure 7.3 Estimated Maximum Fatigue Stress, S = 3.20 m (10.5 ft), t_w/g = 0.4167

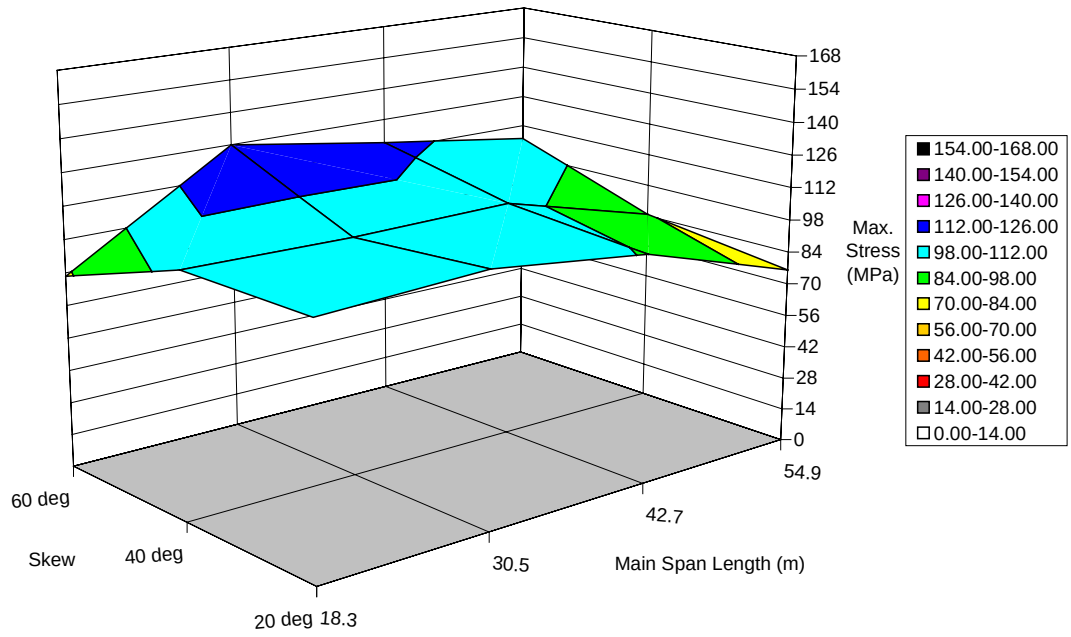

Figure 7.4 Estimated Maximum Fatigue Stress, S = 3.20 m (10.5 ft), t_w/g = 0.333

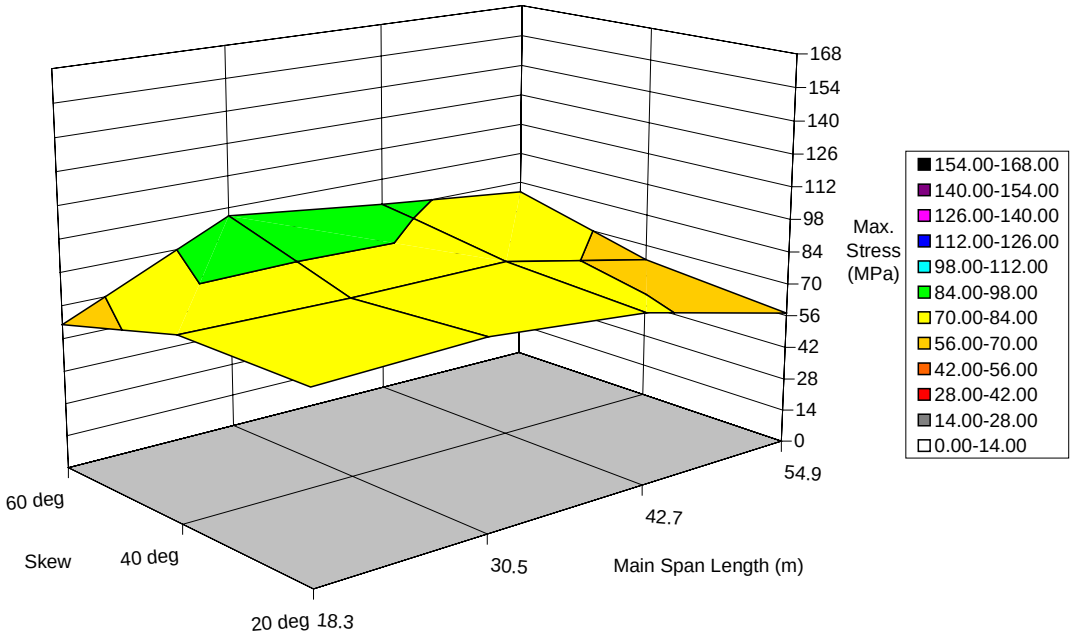

Figure 7.5 Estimated Maximum Fatigue Stress, S = 3.20 m (10.5 ft), t_w/g = 0.25

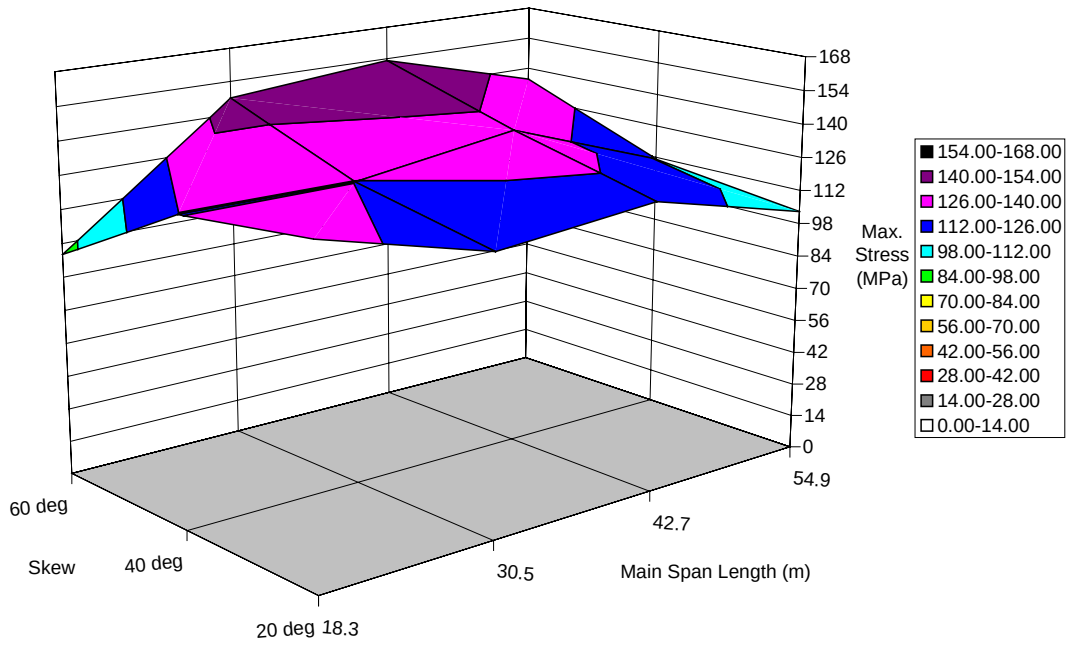

Figure 7.6 Estimated Maximum Fatigue Stress, S = 2.44 m (8 ft), t_w/g = 0.4167

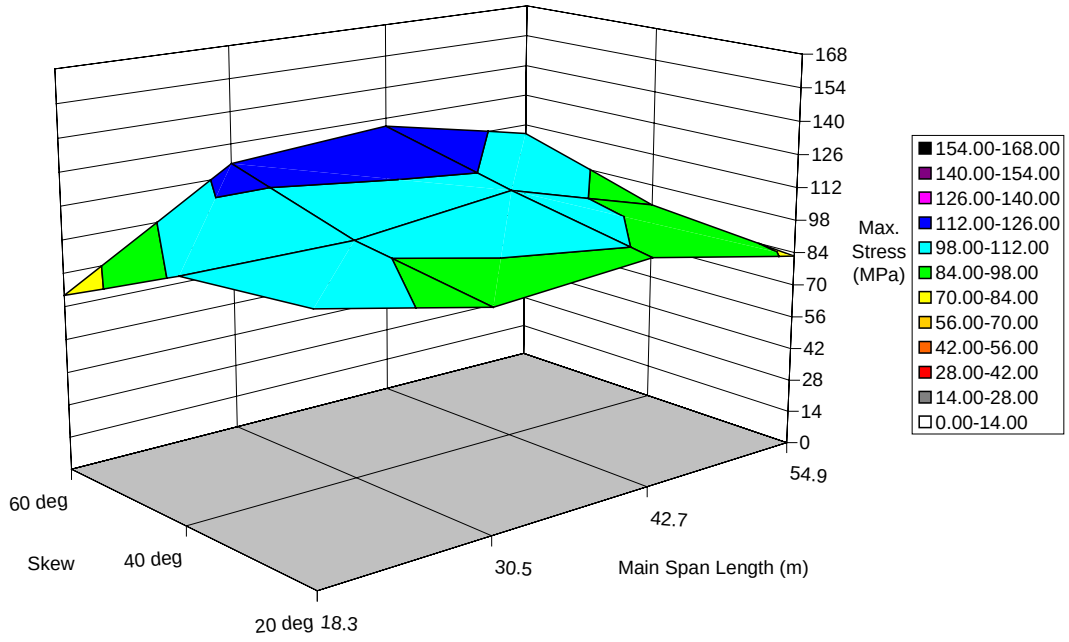

Figure 7.7 Estimated Maximum Fatigue Stress, S = 2.44 m (8 ft), t_w/g = 0.333

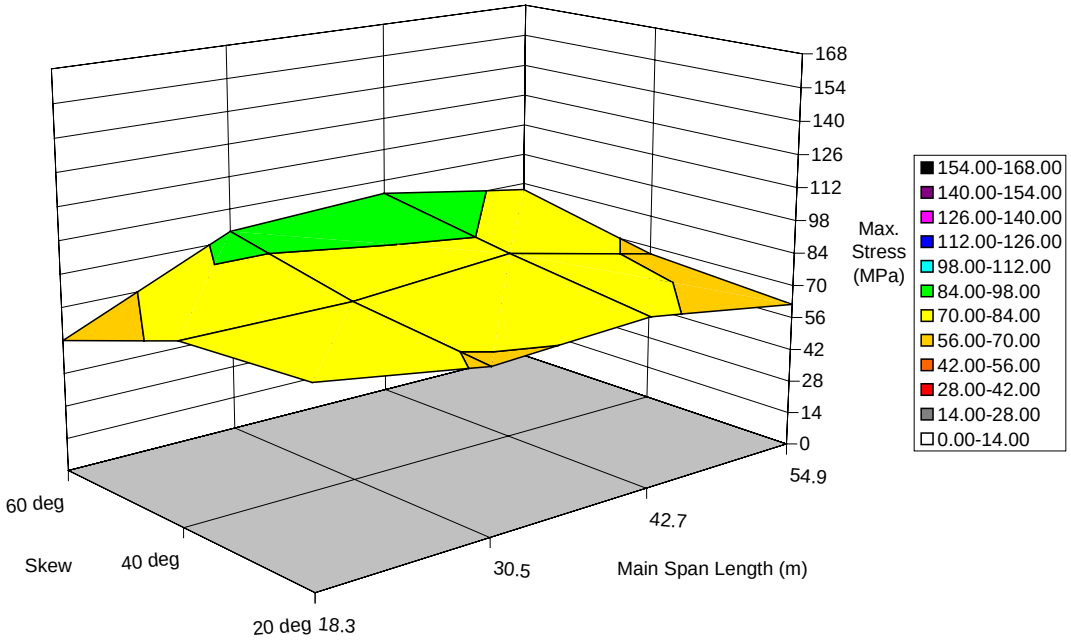

Figure 7.8 Estimated Maximum Fatigue Stress, S = 2.44 m (8 ft), t_w/g = 0.25

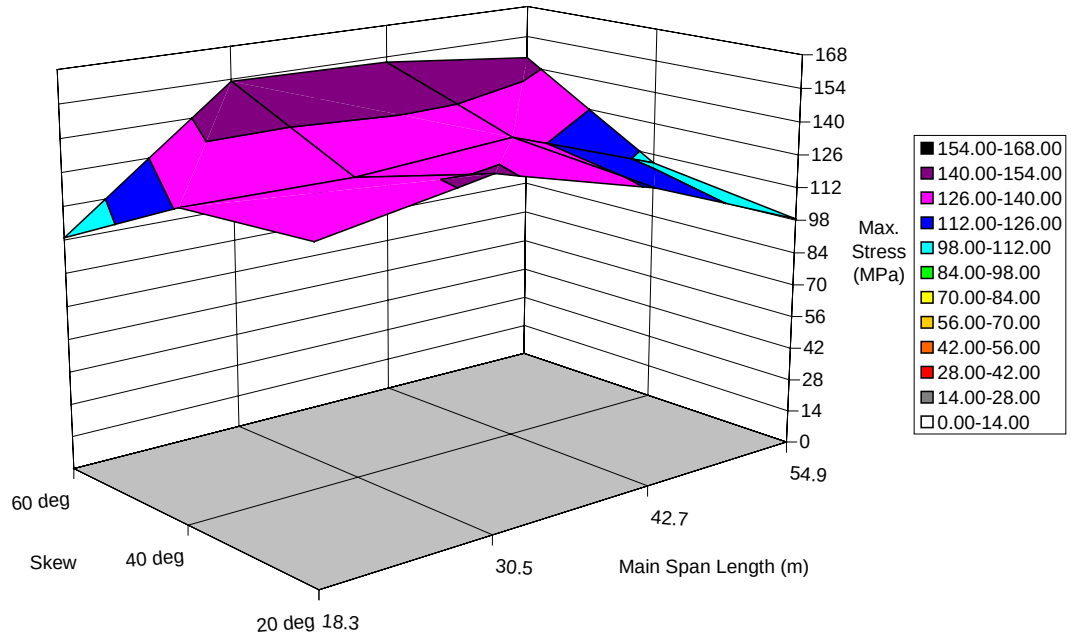

Figure 7.9 Estimated Maximum Fatigue Stress, S = 2.82 m (9.25 ft), t_w/g = 0.4167

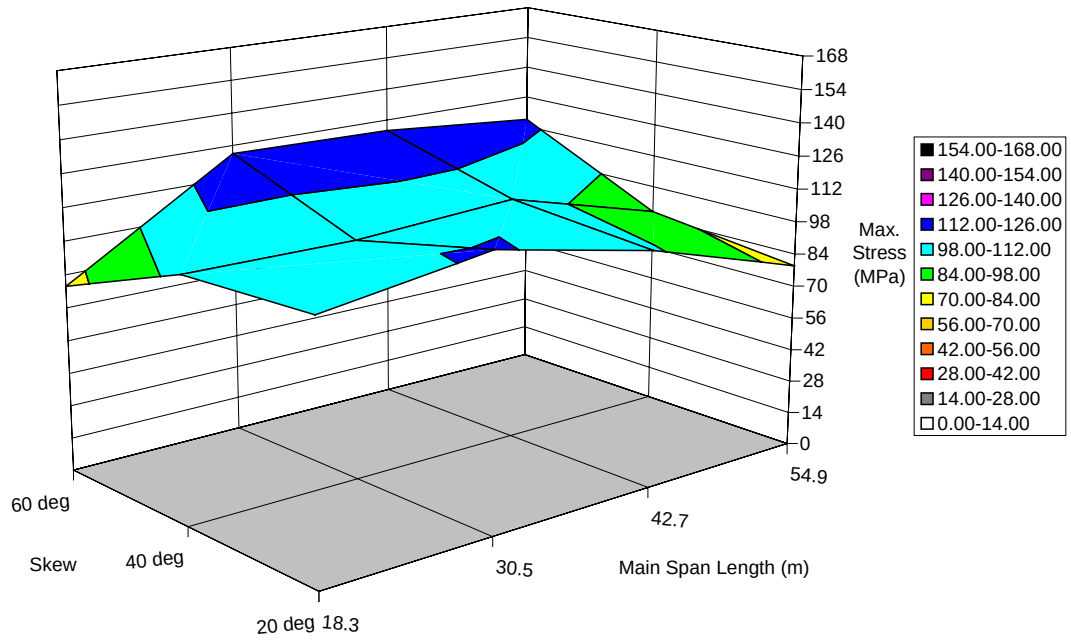

Figure 7.10 Estimated Maximum Fatigue Stress, S = 2.82 m (9.25 ft), t_w/g = 0.333

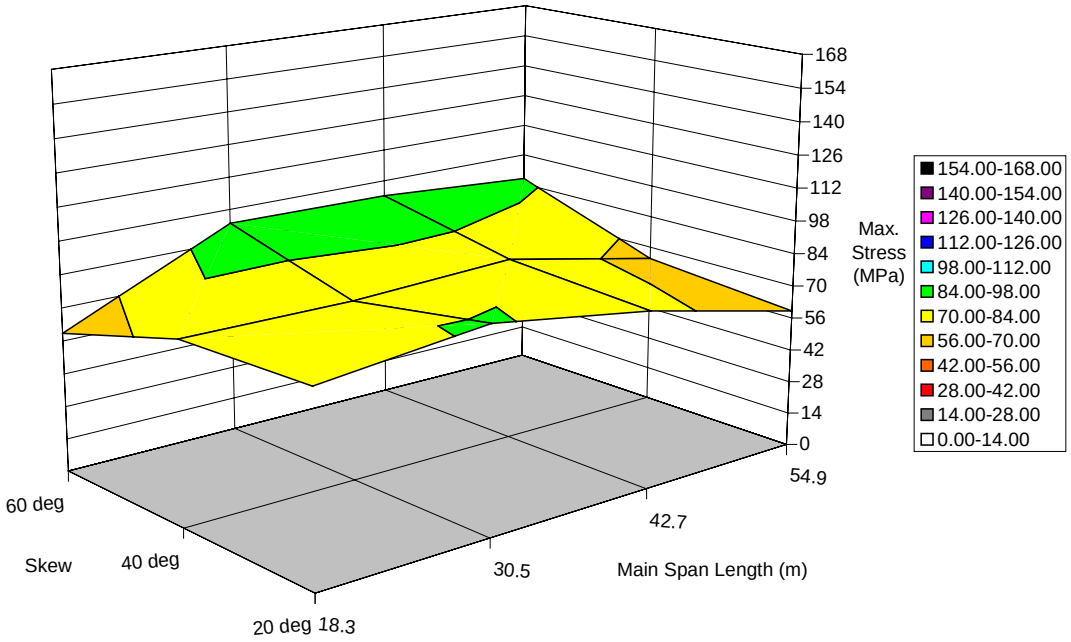

Figure 7.11 Estimated Maximum Fatigue Stress, S = 2.82 m (9.25 ft), t_w/g = 0.25

				Web Gap Stress (MPa)		
Girder Spacing (m)	Span Length (m)	Skew (deg.)	Max. Diaphragm Differential Deflection (mm)	Web Gap Geometric Parameter: tw/g		
				0.2500	0.3333	0.4167
2.44	18.3	20	1.94	79.7	106.2	132.8
2.44	30.5	20	1.67	68.5	91.3	114.2
2.44	42.7	20	1.76	72.1	96.2	120.2
2.44	54.9	20	1.51	61.8	82.4	103.0
2.44	18.3	40	1.84	75.4	100.5	125.7
2.44	30.5	40	1.84	75.5	100.6	125.8
2.44	42.7	40	1.98	81.2	108.3	135.3
2.44	54.9	40	1.63	66.8	89.0	111.3
2.44	18.3	60	1.37	56.0	74.7	93.4
2.44	30.5	60	2.15	88.1	117.5	146.9
2.44	42.7	60	2.24	91.9	122.5	153.2
2.44	54.9	60	1.97	80.9	107.9	134.9
2.82	18.3	20	2.21	78.2	104.3	130.3
2.82	30.5	20	2.42	85.9	114.5	143.2
2.82	42.7	20	2.10	74.5	99.3	124.2
2.82	54.9	20	1.67	59.2	79.0	98.7
2.82	18.3	40	2.15	76.2	101.6	126.9
2.82	30.5	40	2.14	75.8	101.1	126.4
2.82	42.7	40	2.23	79.0	105.3	131.6
2.82	54.9	40	1.83	64.9	86.5	108.1
2.82	18.3	60	1.67	59.2	78.9	98.6
2.82	30.5	60	2.60	92.0	122.7	153.4
2.82	42.7	60	2.58	91.4	121.8	152.3
2.82	54.9	60	2.44	86.5	115.3	144.1
3.2	18.3	20	2.46	76.7	102.3	127.8
3.2	30.5	20	2.54	79.4	105.9	132.3
3.2	42.7	20	2.33	72.7	96.9	121.2
3.2	54.9	20	1.83	57.3	76.4	95.5
3.2	18.3	40	2.46	76.7	102.3	127.9
3.2	30.5	40	2.44	76.1	101.5	126.9
3.2	42.7	40	2.47	77.3	103.1	128.8
3.2	54.9	40	2.03	63.4	84.6	105.7
3.2	18.3	60	1.97	61.5	82.1	102.6
3.2	30.5	60	3.01	94.1	125.4	156.8
3.2	42.7	60	2.76	86.2	115.0	143.7
3.2	54.9	60	2.55	79.7	106.3	132.9

Table 7.1 Parameter Study Stress Data

Chapter 8

Estimating Web Gap Distortional Stresses

8.1 Overview

The primary purpose of this project was to provide a means to assess web gap stresses that produce distortional fatigue. The accurate identification of bridges that are susceptible to out-of-plane web distortion and fatigue cracking should provide significant benefits to bridge maintenance and inspection. Consequently, tools were sought to provide a simple and accurate means by which distortional stress may be estimated in actual bridges. In the previous Mn/DOT research project, Jajich, et al. [1] used a detailed finite element model of a small portion of Mn/DOT Bridge No. 27734 (e.g., 2,150 shell elements, 12,220 equilibrium equations), in order to get accurate values for stress response to loading. However, in this research project, a simple formula for estimating web gap distortional stresses was derived which avoids the computational cost and complexity of the finite element models. Procedures are recommended in this chapter for assessing web gap distortional stress in bridges similar in configuration to those in this study. The web gap stress assessment procedures and an example problem are outlined in detail in Appendix A. Observations from the parameter studies regarding differential deflections and their impact on web gap stress estimates are also made.

8.2 Differential Deflection per Unit Girder Spacing

The results of the finite element study were investigated to identify trends in differential deflection with the important variables. In Figure 8.1, parameter study differential deflection, Δ, is multiplied by L/S. The polynomial trend lines (Eq. 8.1) shown in Figure 8.1 were found to offer the most accurate estimates of differential deflection per unit girder spacing where L, S, and Δ are measured in meters. The constants A, B, and C, are given in Table 8.1.

$$L \cdot \left(\frac{\Delta}{S} \right) = A \cdot L^2 + B \cdot L + C \qquad \text{Eq. 8.1}$$

	Constants (L in meters)		
(deg.)	A	B	C
20	-0.00001327	0.001486	-0.008639
40	-0.00001227	0.001522	-0.01034
60	-0.00001714	0.002185	-0.02328
	Constants (L in inches)		
(deg.)	A	B	C
20	-3.370E-07	0.001486	-0.3399
40	-3.115E-07	0.001522	-0.4065
60	-4.352E-07	0.002185	-0.9156

Table 8.1 Polynomial Equation Constants

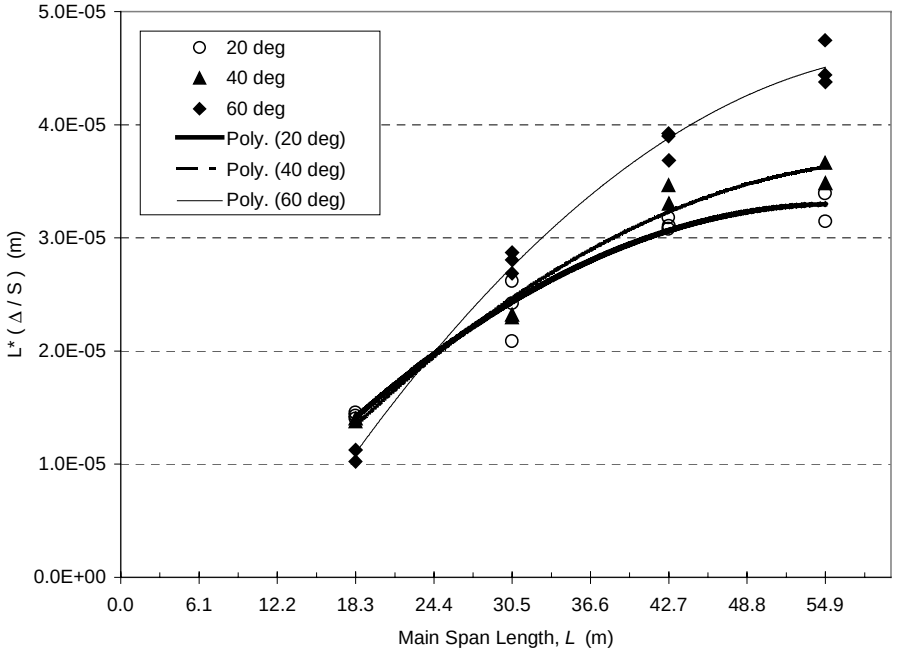

Figure 8.1 Modeling Data Trends for Predicting Δ and Δ/*S*

The polynomial formulas given by Eq. 8.1 may be manipulated algebraically and solved for Δ/*S* to yield a solution for Δ/*S* that is solely a function of main span length and skew. This formula is given in Eq. 8.2. The scatter between alternate girder spacing data at each skew angle trend does not allow further identification of more accurate trends for each girder spacing. This agrees with the previous observation that the significant effects of girder spacing on diaphragm differential deflections is rendered insignificant when computing web gap stress. Coefficients for bridges with skew angles between 20°, 40°, and 60° would be interpolated from the values in Table 8.1.

$$\left(\frac{\Delta}{S}\right) = \frac{A \cdot L^2 + B \cdot L + C}{L} \qquad \text{Eq. 8.2}$$

The constants in Table 8.1 necessary for determining diaphragm differential deflection per unit girder spacing are significantly influenced by skew. Figures 8.2, 8.3, and 8.4 illustrate the profound parameter sensitivity for bridge angles of skew greater than 40°.

The differential deflection in all thirty finite element models at all three girder spacings compared well with the differential deflection predicted using the polynomial equations. The predicted deflections yielded an average deviation of 5% from the finite element deflections with only one value having more than 10% error (Figure 8.5).

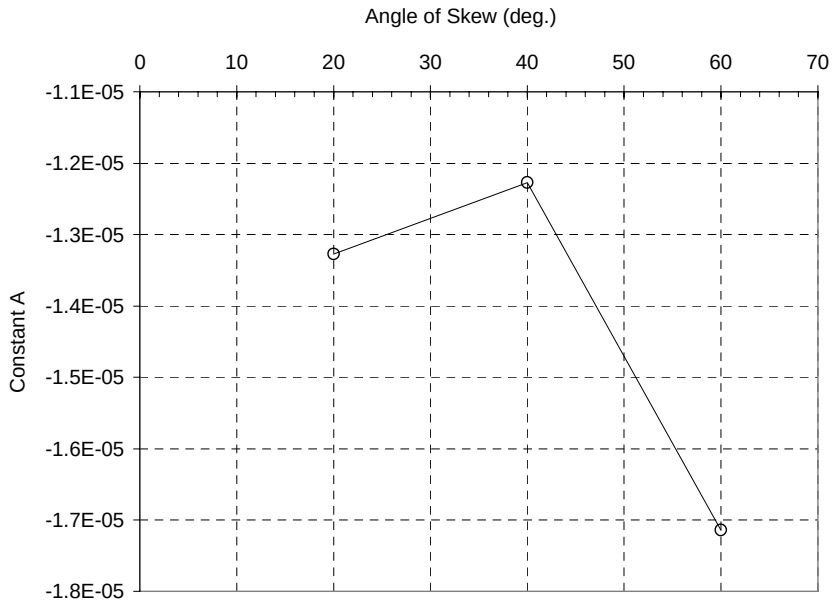

Figure 8.2 Skew Effects on Constant A

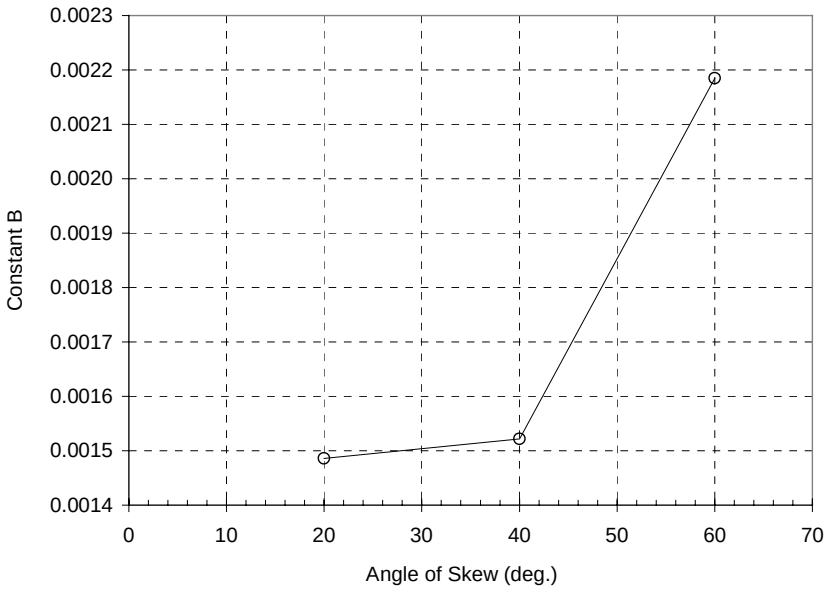

Figure 8.3 Skew Effects on Constant B

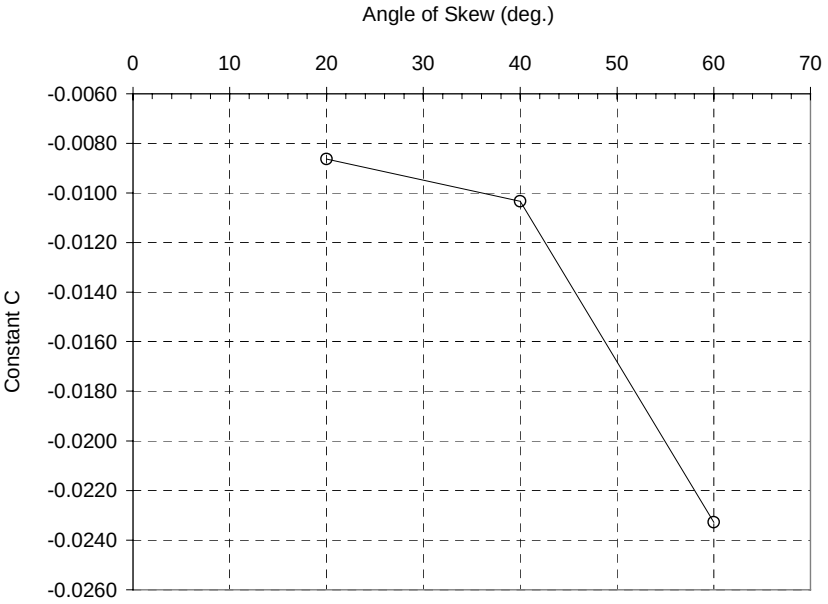

Figure 8.4 Skew Effects on Constant C

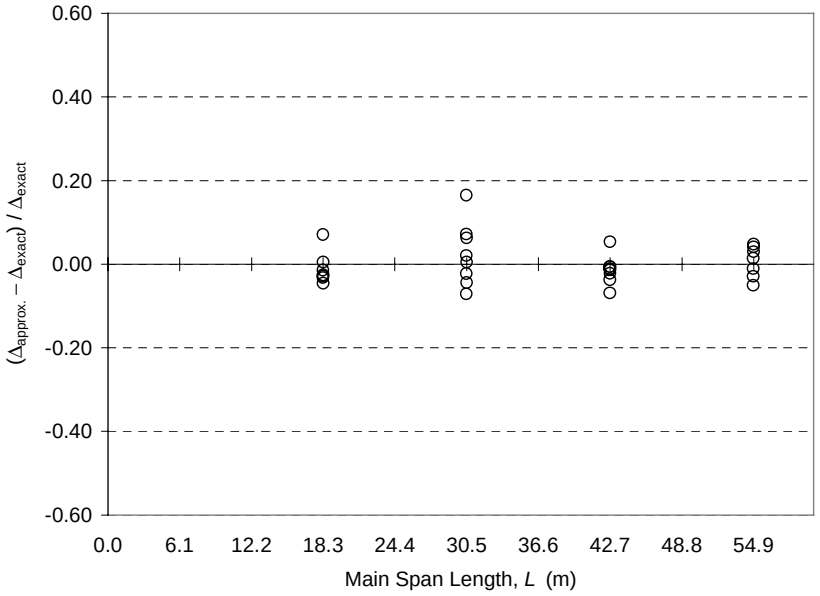

Figure 8.5 Error Predicting Differential Deflection with Polynomial Trend

8.3 Web Gap Geometry Parameter

The ratio of web thickness, t_w, to web gap length, g, is another important parameter in the estimation of web gap stress using Eq. 2.1. All promising trends were sought to characterize girder web gap and thickness. Web gap length appears to be arbitrarily assigned by the design engineer and no specific rationale was found for its designation. Trends of the web gap geometry parameter t_w/g were thoroughly researched and the simple linear regression (Eq. 8.3)

$$\left(\frac{t_w}{g}\right) = K \cdot L + 0.4091 \qquad \text{Eq. 8.3}$$

shown in Figure 8.6 was chosen to best approximate values of t_w/g if actual values for t_w and/or g are unknown, where K is –0.002858 or –0.00007260 when L is in meters or inches, respectively. This linear best-fit equation represents most of the t_w/g range and is applicable over the entire range of span lengths considered in the Mn/DOT bridge survey. The error of the linear trend prediction with respect to the survey of actual bridges had a standard deviation of 15% (Figure 8.7).

Equation 8.3 for t_w/g is a simple vehicle whereby an estimation of the web gap geometry parameter t_w/g may be made if actual values are not available. It is more accurate, and therefore more desirable, to use field measurements, or at least as-built bridge plan values for t_w and g. Work on the previously instrumented Mn/DOT bridge [1] indicated that the actual value of the web gap length, 64 mm (2.5 in), was larger than that indicated on the plans, 51 mm (2 in), and often web gap length is not even indicated on older bridge plans. If, in assessing a specific bridge, an effort is made to determine exact span lengths or exact angle of skew, then further investigation into determining actual values for t_w and g is warranted to increase confidence in the assessment of web gap distortional stresses.

Procedures for estimating distortional stress in actual composite steel bridges are discussed in Appendix A.

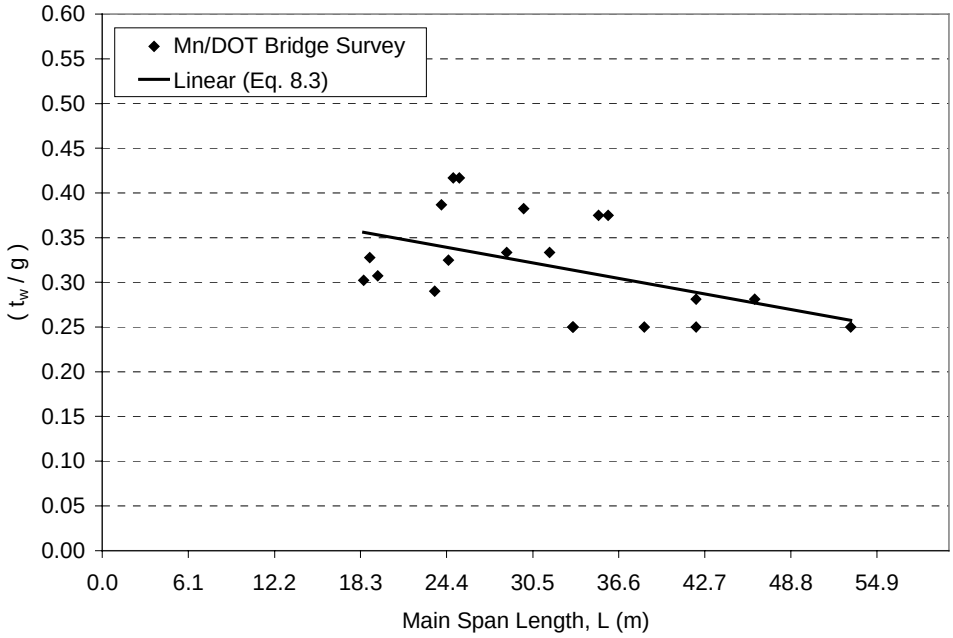

Figure 8.6 Linear Trend for Predicting t_w/g

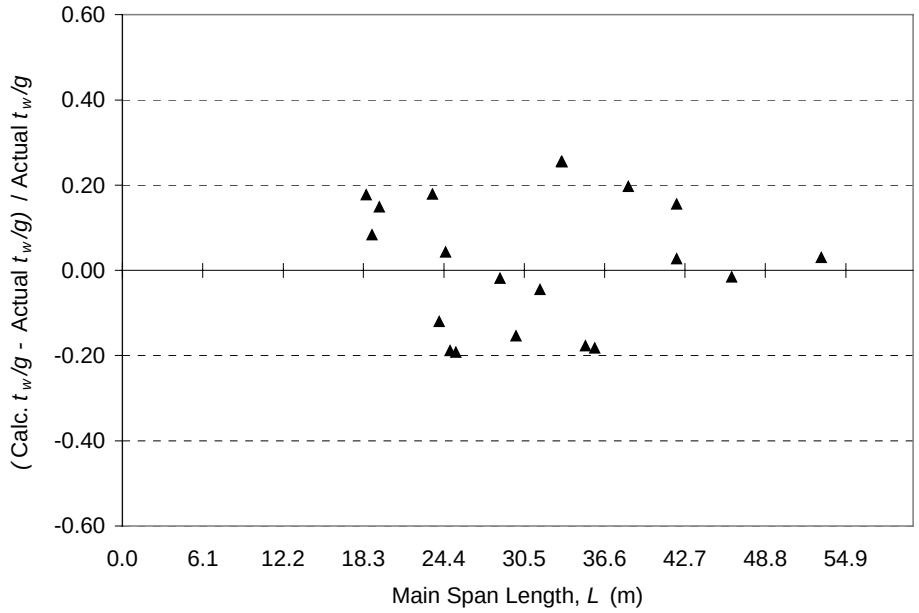

Figure 8.7 Error Predicting t_w/g from Linear Trend

8.4 Additional t_w and g Trend

One of the more interesting identified trends of note is that values of the web gap geometry parameter t_w/g separate for the two web gaps of 3.8 and 5.1 cm (1.5 and 2 in) when plotted versus span length, L (Figure 8.5). The reason for this distinction is unknown and does not appear to be related to any of the bridge geometry information gathered in the Mn/DOT bridge survey. A possible reason for the disparity could be due to similarities between web gap and design years, or changing AASHTO requirements on values of web gap length. The average construction year of bridges with web gaps of 3.8 and 5.1 cm (1.5 and 2 in) was 1971 and 1979, respectively, or from changing design standards, but there is no uniform correlation between the year constructed and the web gap parameter. It is possible specific types of spans were addressed during differing construction periods of federal and state construction. Neither trend in Figure 8.5 addresses both the full range of t_w/g found in the Mn/DOT bridge survey, nor does it reach all values of span length, L. Selection of either of these trends for estimating the web gap geometric parameter t_w/g requires knowing values for web gap length, g. If g is known, then no estimation is required and, therefore, these identified trends do not aid in predicting t_w/g values.

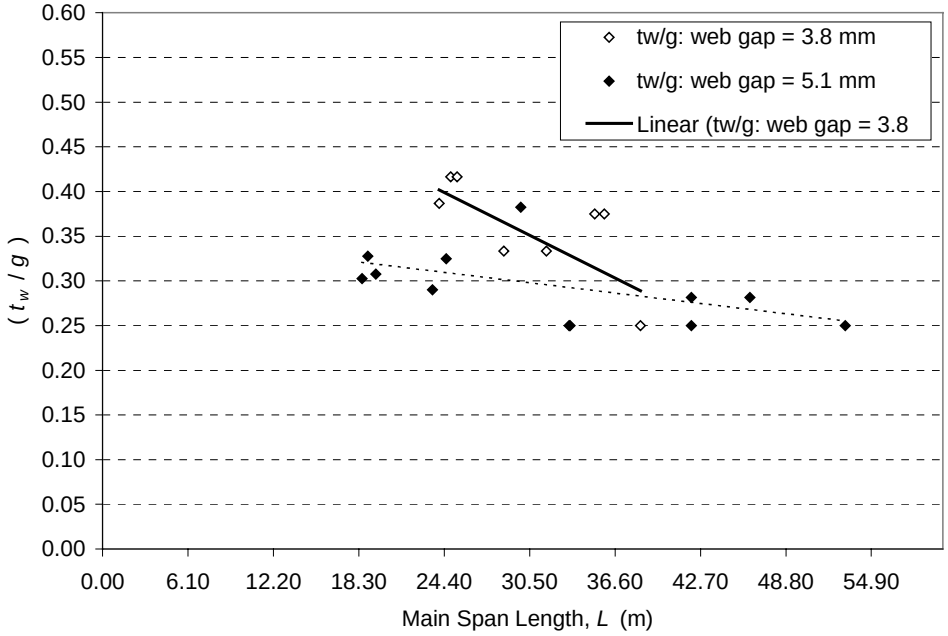

Figure 8.8 Separate t_w/g Trends for g = 3.8 cm (1.5 in) and g = 5.1 cm (2 in)

Trends identified in the Mn/DOT bridge survey data that were unserviceable or less successful in predicting values for web gap parameters included plots of t_w/g vs g, $d{\cdot}g/t_w$ vs L, $d{\cdot}g/t_w/L$ vs L, and $d{\cdot}g/t_w/S$ vs L.

8.5 Conclusions

This chapter details the procedures to estimate web gap stress in skewed, composite steel bridge girders. To evaluate web gap distortional stress utilizing Eq. 2.1, use the polynomial equation (Eq. 8.2) to determine diaphragm differential deflection per unit girder width, Δ/S. When appropriate, apply the two differential deflection correction factors, β_d and β_w, where β_d corrects for deck thickness that deviates from the deck thickness used in the parameter studies (Eq. 6.1), and β_w corrects for truck weight. When correcting for truck weight, the axle configuration must be the same as that for an AASHTO HS-20 truck, causing β_w to be the ratio of fatigue truck weight/HS-20 truck weight, 320 kN (72 kips). Use actual values for the web gap parameters t_w and g. If actual web gap geometry is unobtainable, use the linear formula for t_w/g (Eq. 8.3). A check of results may be performed by comparing the computed stress with parameter study stress

in Table 7.1 and the three-dimensional stress surface plots in Chapter 7. With the differential deflection correction factors incorporated in the deflection estimate, Eq. 2.1 becomes Eq. 8.4.

$$\sigma_{wg} = 2E \cdot \left(\frac{t_w}{g}\right)\left(\beta_d \beta_w \frac{\Delta}{S}\right) \qquad \text{Eq. 8.4}$$

Chapter 9
Summary and Conclusions

The present Mn/DOT research study furthers the understanding of bridge diaphragm deflection behavior and advances the ability to estimate distortional stress in web gaps and assess bridges susceptible to distortional fatigue from large, secondary stresses. Distortion-induced fatigue in unstiffened web gaps is a well-documented problem often addressed in field and laboratory research. A literature review of past research aids in identifying the problem, helps to define its behavior, and addresses the effectiveness of a variety of retrofitting solutions.

A previous Mn/DOT research project significantly advanced the understanding of web gap behavior in skewed, multi-girder composite steel bridges with staggered, rigid plate diaphragms [1]. A simple equation for estimating the magnitude of web gap stress was proposed (Eq. 2.1). This equation can be used to obtain accurate estimates of web gap stress given bridge detail geometry and the magnitude of diaphragm differential deflection. However, predicting the relatively small magnitudes of relative deflection between adjacent steel bridge girders is a difficult task. In addition, little to no research effort has been expended to model and predict diaphragm relative deflection or determine parameters that influence differential deflection. Such parameters should correlate directly with parameters that affect distortional stress in fatigue-prone webs.

The present Mn/DOT research project addressed the deflection behavior of skewed, multi-girder composite steel bridges. Three-dimensional finite element models were formulated and refined in an attempt to model the recorded behavior of a previously studied Mn/DOT bridge [1]. Behavior in bridges with differing configurations may be analyzed using the finite element modeling techniques used in this study. Once calibrated, these finite element models were incorporated in a parametric study to evaluate the impact of bridge variables on relative deflection between bridge girders. Parameters were separated into two categories: primary and secondary. Primary parameters were thought to have a significant effect on differential deflection and all possible parametric combinations were incorporated in the primary parameter

study. Secondary parameters were believed to have less influence on bridge deflection behavior. Their importance was investigated in smaller, secondary modeling studies. Observations made regarding 1) bridge characteristics in the Mn/DOT inventory of bridges, and 2) from the finite element parameter studies differential deflection characteristics provide a strong knowledge base from which to develop methods for assessing out-of-plane distortional stresses.

Diaphragm differential deflection behavior observed in the finite element studies indicates that:

- Girder spacing, bridge skew, main span length, and deck thickness influence diaphragm deflection behavior.
- Transverse load distribution properties play the most significant role in determining the magnitude of differential deflection.
- Maximum differential deflection occurs at the diaphragm in the obtuse corner of a loaded lane or near the obtuse corner toward the point of inflection of the girder.
- Greater bridge skew results in greater differential deflection. This, however, is not that case when spans are so short that truck length begins to approach the main span length.
- Long bridge spans (> 140 ft), or bridges with large aspect ratios (bridge span length/bridge width), deflect as a composite unit. Therefore, girders in long spans do not undergo as significant differential deflection and out-of-plane distortion as do those in shorter bridges.

Out-of-plane distortional stress in fatigue prone web gaps is primarily dependent on:

- The magnitude of the web gap geometric parameter, t_w/g.
- Bridge properties affecting differential deflection: Main span length, skew angle, and deck thickness.
- Loading characteristics: Truck weight and axle configuration.

Spacing plays a significant role in determining out-of-plane distortion, but values of Δ/S, and, therefore, web gap distortional stress estimates using Eq. 2.1, are approximately constant for bridges with equivalent values of skew and span length (Figure 8.1). Secondary modeling studies indicate potential parameters that can affect stress and relative differential deflection in varying magnitudes.

Distortional stress assessment in existing bridges may be performed by means of Eq. 2.1 using:

- Equations for Δ/S as a function of span length and skew (Eq. 8.2), based upon trends found within the parameter study.
- Equation 8.2 estimates of Δ/S for bridges with skew values between 20°-40° and 40°-60° should be interpolated from the given values at 20°, 40°, and 60°.
- A deck thickness correction factor, β_d (Eq. 6.1), must be applied to the computed differential deflection when assessing web gap stress in bridges with deck thickness other than 22.9 cm (9 in).
- A truck weight correction factor, β_w, equal to truck weight/HS-20 truck weight, 320 kN (72 kips), must be applied to differential deflection when assessing web gap stress due to trucks with different weight (e.g., an AASHTO fatigue truck) but the same axle configuration as the AASHTO HS-20 truck.
- Actual web dimensions for t_w and g are preferred to evaluate web gap stress. If actual web dimensions are not known, the linear formula for approximate t_w/g as a function of span length may be utilized (Eq. 8.3). Web thickness and web gap length are not presently in the Mn/DOT bridge database and determining actual t_w/g values might prove to be laborious. However, actual values for t_w and g enhance the accuracy of stress estimates.

Proposed procedures for evaluating out-of-plane stress should prove practical and aid in assessing bridges vulnerable to fatigue cracking of web gaps. Incorporating this procedure in a bridge management system should allow for the identification and screening of bridges in jeopardy of developing web gap cracks to assist bridge maintenance and biennial inspections. Furthermore, remaining fatigue life estimates may be made for high-risk structures if truck loads and lane loading frequencies are known or estimated. Future modifications to the stress equation may be required, since the mode of distortion likely differs for straight bridges with back-to-back diaphragms, bridge with differently configured diaphragms (e.g., X-diaphragm), or short span rolled section girders with a thick web. Regardless of stress equation adjustments, trends concerning differential deflection and large t_w/g values should still be applicable to a more varied spectrum of bridge configurations.

References

1. Jajich, D., Schultz, A. E., Bergson, P.M., and Galambos, T.V. "Distortion-Induced Fatigue in Multi-Girder Steel Bridges." Dept. of Civil Engineering, University of Minnesota, Minneapolis, March 2000.

2. Fisher, John W., Jin, Jian, Wagner, David, and Yen, Ben. "Distortion Induced Fatigue Cracking in Steel Bridges." NCHRP Report 336, Transportation Research Board, National Research Council, Washington D.C., Dec. 1990.

3. Keating, Peter. "Focusing on Fatigue." Civil Engineering, Nov. 1994, 54—57.

4. Åkesson, Björn, and Edlund, Bo. "Fatigue Cracking in a Steel Railway Bridge." Structural Engineering International, Feb. 1997, 118—121.

5. Cousins, T. E., et al. "Field Evaluation of Fatigue Cracking in Diaphragm-Girder Connections." Journal of Performance of Constructed Facilities, 12(1), 1998, 25—32.

6. DeWolf, John T., Lindsay, Tod, and Culmo, Michael. "Fatigue Evaluation in Steel Bridges Using Field Monitoring Equipment." Building to Last Proceedings of Structures Congress XV, ASCE, Portland, Oregon, April 13th-16th, 1997.

7. Fisher, John W. Fatigue and fracture in steel bridges: Case Studies New York: Wiley, 1984

8. Fisher, John W., Yen, Ben, and Wagner, David. "Review of Field Measurements for Distortion Induced Fatigue Cracking in Steel Bridges." Transportation Research Record, n1118, 1987, 49—55.

9. Nishikawa, Kazuhiro, et al. "Study on the Fatigue of Steel Highway Bridges in Japan." Construction and Building Materials, 12(2-3), 1998, 133—141.

10. Fisher, John W. "Fatigue Cracking in Bridges from Out-of-Plane Distortion." Canadian Journal of Civil Engineering, 5(4), 1978, 542—556.

11. Fisher, John W., Hausammann, Hans, Sullivan, Michael D., and Pense, Allan W. "Detection and Repair of Fatigue Damage in Welded Highway Bridges." NCHRP Report 206, Transportation Research Board, National Research Council, Washington D.C., June 1979.

12. Keating, Peter and Fisher, John W. "Fatigue Behavior of Variable Loaded Bridge Details Near the Fatigue Limit." Transportation Research Record n1118, 1987, 56—64.

13. Stallings, J.M. and Cousins, T.E. "Laboratory Tests of Bolted Diaphragm-Girder Connections." Journal of Bridge Engineering, May 1998.

14. Wipf, T.J., Greimann, L.F., Wood, D., Tarries, D., McDonald, N., and Brakke, B. "Preventing Out-of-Plane Distortion Fatigue Cracking in Multiple Steel Girder Bridges." Proceedings of the Fifth National Workshop on Bridge Research in Progress, Oct. 8-10th, Minneapolis, MN, University of Minnesota, 289—294.

15. Stallings, J.M., Cousins, T.E., and Stafford, T.E. "Effects of Removing Diaphragms from a Steel Girder Bridge." Transportation Research Record, n1541, Nov 1996, 183—188.

16. Moses, F., Schilling, C.G., and Raju, K.S. "Fatigue Evaluation Procedures for Steel Bridges." NCHRP Report 299, Transportation Research Board, National Research Council, Washington D.C., Nov. 1987.

17. Bishara, Alfred G., Liu, Maria Chuan, and El-Ali, Nasser D. "Wheel Load Distribution on Simply Supported Skew I-Beam Composite Bridges." Journal of Structural Engineering, ASCE, 119(2), Feb. 1993, 399—419.

18. Schilling, Charles G. "Lateral-Distribution Factors for Fatigue Design." Journal of the Structural Division, Vol. 108, No. ST9, Sept. 1982, 2015—2033.

19. Ebeido, Tarek, and Kennedy, John B. "Girder Moments in Continuous Skew Composite Bridges." Journal of Bridge Engineering, ASCE, 1(1), Feb. 1996.

20. Mabsout, Mournir E., Tarhini, Kassim M., Frederick, Gerald R., and Tayar, Charbel. "Finite-Element Analysis of Steel Girder Highway Bridges." Journal of Bridge Engineering, ASCE, 2(3), Aug. 1997, p. 83—87.

21. *Guide Specifications for Distribution of Loads for Highway Bridges*, AASHTO, Washington, D.C., 1994

22. Nutt, R.V., Schamber, R.A., and Zokaie, T. "Distribution of Wheel Loads on Highway Bridges." Project No. 12-26, NCHRP, Transportation Research Board, National Research Council, Imbsen & Associates Inc., Sacramento, CA, 1988.

23. *Standard Specifications for Highway Bridges*, AASHTO, 16th Edition, Washington, D.C., 1996.

24. Mabsout, Mournir E., Tarhini, Kassim M., Frederick, Gerald R., and Kesserwan, Abbas. "Effect of Continuity on Wheel Load Distribution in Steel Girder Bridges." Journal of Bridge Engineering, ASCE, 3(3), Aug. 1998.

25. Mabsout, Mournir E., Tarhini, Kassim M., Frederick, Gerald R., and Kobrosly, Marwan. "Influence of Sidewalks and Railings on Wheel Load Distribution in Steel Girder Bridges." Journal of Bridge Engineering, ASCE, 2(3), Aug. 1997, p. 88-96.

26. Computers and Structures Inc. SAP2000 Analysis Reference, Berkley, 1996.

27. "Mn/DOT Bridge Design Manual." Mn/DOT Office of Bridges and Structures, Mn/DOT, Sept. 1998.

28. Stallings, J.M., Cousins, T.E. "Evaluation of Diaphragm Requirements in Existing Bridges," Proceedings of the 15th Structures Congress, Part 2, 1997, 1494—1498.

Appendix A
Estimating Web Gap Stress in Existing Bridges

Equation 2.1 may be utilized to determine distortional stress in skewed, composite steel girder bridges.

$$\sigma_{wg} = 2E \cdot \left(\frac{t_w}{g}\right)\left(\frac{\Delta}{S}\right) \qquad \text{Eq. 2.1}$$

where E = steel modulus of elasticity, t_w = girder web thickness, g = web gap length, Δ = diaphragm differential deflection, and S = girder spacing. The girder spacing is also the diaphragm length. The modulus of elasticity is a constant value, regardless of steel yield strength, equal to 200 GPa (29000 ksi).

A.1 Evaluating Web Gap Dimensions (t_w and g):

Actual values for web thickness, t_w, and web gap length, g, are preferred to reduce approximation error when evaluating web gap distortional stress. Existing values may be obtained either from field measurements or bridge plans. Actual bridge web gap values have been known to differ from plan values, and web gap dimensions are sometimes not included or specified in older bridge plans. If actual web gap dimensions are not available, a simple estimation, based upon data from a survey of Mn/DOT bridges, is possible utilizing Eq. 8.3 where L is the main span length and K is –0.002858 or –0.00007260 when L is in meters or inches, respectively.

$$\left(\frac{t_w}{g}\right) = K \cdot L + 0.4091 \qquad \text{Eq. 8.3}$$

A.2 Evaluating Girder Differential Deflection per unit Girder Spacing (Δ/S):

Values for Δ/S may be estimated based solely upon main span length, L, and bridge skew angle using Eq. 8.2 and values from Table 8.1 for constants A, B, and C. Bridges with values of skew between 20°, 40°, and 60° must be interpolated linearly from adjacent skew values.

$$\left(\frac{\Delta}{S}\right) = \frac{A \cdot L^2 + B \cdot L + C}{L} \qquad \text{Eq. 8.2}$$

The appropriate deflection correction factors, β_d and β_w, must be applied to estimated differential deflection when deck thickness is not equal to 22.9 cm (9 in) or when truck weight differs from that of an HS-20 truck, 320 kN (72 kips).

A.3 Example Bridge Web Gap Distortional Stress Assessment:

Mn/DOT Bridge No. 22734 at the intersection of Interstate 694 over Interstate 94 is a skewed, composite, multi-girder steel bridge built in 1980 with a fatigue prone web gap detail. The bridge has three spans of lengths 108, 138, and 80 ft. and a girder spacing of 9 ft.-3 in. The bridge support angle of skew is 60°-27'-25.5", measured from a line perpendicular to the roadway centerline. Bridge plans indicate that in the negative moment region the girder web has a thickness of 0.5 in. and a web gap of 2 in. Web gap measurements made in the field indicate the web gap has an actual length of 2.5 in.

Analysis of actual values from Bridge No. 27734 with L = 1656 in. and skew angle of 60°, along with Eq. 8.2 and constants from Table 8.1, yields:

$$\left(\frac{\Delta}{S}\right) = \frac{-4.352 \cdot 10^{-7}(1656)^2 + 2.185 \cdot 10^{-3}(1656) - 0.9156}{(1656)} = 9.114 \cdot 10^{-4}$$

$$\Delta = 9.114 \cdot 10^{-4}(S) = 9.114 \cdot 10^{-4}(111in) = 0.101in$$

This value for differential deflection Δ matches the measured deflection from truck testing of Bridge No. 27734 reported by Jajich, et al. [1].

Using Eq. 2.1, the distortional stress estimate is made knowing that E = 29000 ksi, t_w = 0.5 in., deck thickness = 9 in. (i.e., $\beta_d = 1$), truck loading = HS-20 (i.e., $\beta_w = 1$), and Δ/S = 9.114E-04. Web gap stress is

$$\sigma_{wg} = 2E \cdot \left(\frac{t_w}{g}\right)\left(\frac{\Delta}{S}\right) \qquad \text{Eq. 2.1}$$

$$\sigma_{wg} = 2(29000ksi)\left(\frac{0.5in}{2.5in}\right)\left(9.114 \cdot 10^{-4}\right) = 10.6ksi$$

This value for web gap stress corresponds reasonably well with 12 ksi from finite element analysis of the unbraced web-gap detail [1]. Stress from strain gage measurements during the truck test, modified for strain gage location and horizontal stress gradients, was 12.9 ksi.

To illustrate the importance of knowing actual values of t_w and g, if web-gap dimensions were not known from field measurements, plan values for t_w and g would have been required for use in Eq. 2.1. The plan value for t_w was correct, 0.5 in., but for g the plan indicated 2 in. Thus

$$\left(\frac{t_w}{g}\right) = \left(\frac{0.5in}{2in}\right) = 0.25$$

$$\sigma_{wg} = 2(29000ksi)(0.25)\left(9.114 \cdot 10^{-4}\right) = 13.2ksi$$

If web gap dimensions were not known from both plan and field measurements, an estimate of t_w/g would have been required using Eq. 8.3. The stress estimate changes to

$$\left(\frac{t_w}{g}\right) = -7.260 \cdot 10^{-5}(1656) + 0.4091 = 0.289$$

$$\sigma_{wg} = 2(29000ksi)(0.289)\left(9.114 \cdot 10^{-4}\right) = 15.3ksi$$

If an AASHTO fatigue truck (HS-15) was selected to determine web gap stress, and bridge plans indicated t_w = 0.5, g = 2 in., and a deck thickness of 10 in., both deflection correction factors, β_d and β_w, would be required to properly assess differential deflection. For Eq. 6.1, knowing D = 9 in., α = 1 in., HS-15 truck weight = 54 kips, and HS-20 truck weight = 72 kips, the correction factors become

$$\beta_d = 1 + \left[0.15 \left(\frac{D - t_d}{\alpha} \right) \right] = 1 + \left[0.15 \left(\frac{9in - 10in}{1in} \right) \right] = 0.85 \qquad \text{Eq. 6.1}$$

$$\beta_w = \frac{HS15}{HS20} = \frac{54kip}{72kips} = 0.75$$

and the web gap stress estimate becomes

$$\sigma_{wg} = 2E \cdot \left(\frac{t_w}{g} \right) \left(\beta_d \beta_w \frac{\Delta}{S} \right)$$

$$\sigma_{wg} = 2(29000ksi)(0.25)\left[(0.85)(0.75)\left(9.114 \cdot 10^{-4}\right)\right] = 8.42ksi$$

Appendix B

Parameter Study

Finite Element Model Dimensions

Primary Parameter Study	West Span Length	Main (Center)	East Span Length	Girder Depth	No. of Girders	Diaphragm Depth	Diaphragm Fl. Width	Deck Thickness	Deck Width	Girder Web Thickness	Deck Cantilever to	Pier		Midspan	
												Flange Width	Flange Thickness	Flange Width	Flange Thickness
Main Span-Spacing-Skew	ft.	ft.	ft.	in.		in.	in.	in.	ft.	in.	in.	in.	in.	in.	in.
P-L060-S8-sk20	60	60	60	26.67	9	20	3.33	9	68.333	0.5	26	13.8	0.375	7.25	0.375
P-L060-S8-sk40	60	60	60	26.67	9	20	3.33	9	68.333	0.5	26	13.8	0.375	7.25	0.375
P-L060-S8-sk60	60	60	60	26.67	9	20	3.33	9	68.333	0.5	26	13.8	0.375	7.25	0.375
P-L100-S8-sk20	100	100	100	44.44	9	33	5.5	9	70.667	0.5	40	15.2	1	9.75	1
P-L100-S8-sk40	100	100	100	44.44	9	33	5.5	9	70.667	0.5	40	15.2	1	9.75	1
P-L100-S8-sk60	100	100	100	44.44	9	33	5.5	9	70.667	0.5	40	15.2	1	9.75	1
P-L140-S8-sk20	140	140	140	62.22	9	47	7.83	9	70.667	0.5	40	15.55	1.75	10.35	1.75
P-L140-S8-sk40	140	140	140	62.22	9	47	7.83	9	70.667	0.5	40	15.55	1.75	10.35	1.75
P-L140-S8-sk60	140	140	140	62.22	9	47	7.83	9	70.667	0.5	40	15.55	1.75	10.35	1.75
P-L180-S8-sk20	180	180	180	80	9	48	8	9	70.667	0.5	40	17.9	2.25	12.15	2.25
P-L180-S8-sk40	180	180	180	80	9	48	8	9	70.667	0.5	40	17.9	2.25	12.15	2.25
P-L180-S8-sk60	180	180	180	80	9	48	8	9	70.667	0.5	40	17.9	2.25	12.15	2.25
P-L060-S105-sk20	60	60	60	26.67	7	20	3.33	9	68.333	0.5	26	12.75	0.625	7.75	0.625
P-L060-S105-sk40	60	60	60	26.67	7	20	3.33	9	68.333	0.5	26	12.75	0.625	7.75	0.625
P-L060-S105-sk60	60	60	60	26.67	7	20	3.33	9	68.333	0.5	26	12.75	0.625	7.75	0.625
P-L100-S105-sk20	100	100	100	44.44	7	33	5.5	9	70.667	0.5	40	17	1.25	11.475	1.25
P-L100-S105-sk40	100	100	100	44.44	7	33	5.5	9	70.667	0.5	40	17	1.25	11.475	1.25
P-L100-S105-sk60	100	100	100	44.44	7	33	5.5	9	70.667	0.5	40	17	1.25	11.475	1.25
P-L140-S105-sk20	140	140	140	62.22	7	47	7.83	9	70.667	0.5	40	18.4	2	12.7	2
P-L140-S105-sk40	140	140	140	62.22	7	47	7.83	9	70.667	0.5	40	18.4	2	12.7	2
P-L140-S105-sk60	140	140	140	62.22	7	47	7.83	9	70.667	0.5	40	18.4	2	12.7	2
P-L180-S105-sk20	180	180	180	80	7	48	8	9	70.667	0.5	40	21.5	2.5	15	2.5
P-L180-S105-sk40	180	180	180	80	7	48	8	9	70.667	0.5	40	21.5	2.5	15	2.5
P-L180-S105-sk60	180	180	180	80	7	48	8	9	70.667	0.5	40	21.5	2.5	15	2.5

Table B.1 Primary Parameter Study Model Dimensions

Secondary Parameter Study	West Span Length	Main Span Length	East Span Length	Girder Depth	No. of Girders	Diaphragm Depth	Diaphragm Fl. Width	Deck Thickness	Deck Width	Girder Web Thickness	Deck Cantilever to	Pier Flange Width	Pier Flange Thickness	Midspan Flange Width	Midspan Flange Thickness
Main Span-Spacing-Skew	ft.	ft.	ft.	in.		in.	in.	in.	ft.	in.	in.	in.	in.	in.	in.
2-L060-S925-sk20	60	60	60	26.67	8	20	3.33	9	69.083	0.5	26	16.4	0.375	9.2	0.375
2-L100-S925-sk20	100	100	100	44.44	8	33	5.5	9	71.417	0.5	40	18.2	1	12	1
2-L140-S925-sk20	140	140	140	62.22	8	47	7.83	9	71.417	0.5	40	18.27	1.75	18.27	1.75
2-L100-S925-sk60	100	100	100	44.44	8	33	5.5	9	71.417	0.5	40	18.2	1	12	1
2-L140-S925-sk60	140	140	140	62.22	8	47	7.83	9	71.417	0.5	40	18.27	1.75	18.27	1.75
2-L180-S925-sk60	180	180	180	80	8	48	8.0	9	71.417	0.5	40	20.9	2.25	14.4	2.25

Table B.2 Secondary Parameter Study Model Dimensions: Girder Spacing = 2.82 m (9.25 ft.)

Secondary Parameter Study	West Span Length	Main Span Length	East Span Length	Girder Depth	No. of Girders	Diaphragm Depth	Diaphragm Fl. Width	Deck Thickness	Deck Width	Girder Web Thickness	Deck Cantilever to	Pier Flange Width	Pier Flange Thickness	Midspan Flange Width	Midspan Flange Thickness
Main Span-Spacing-Skew	ft.	ft.	ft.	in.		in.	in.	in.	ft.	in.	in.	in.	in.	in.	in.
2-08L060-S8-sk20	48	60	48	26.67	9	20	3.33	9	68.333	0.5	26	13.8	0.375	7.25	0.375
2-08L100-S105-sk60	80	100	80	44.44	7	33	5.5	9	69.667	0.5	40	17	1.25	11.475	1.25
2-08L140-S8-sk40	112	140	112	62.22	9	47	7.83	9	70.667	0.5	40	15.55	1.75	10.35	1.75
2-08L180-S105-sk60	144	180	144	80	7	48	8.0	9	69.667	0.5	40	21.5	2.5	15	2.5

Table B.3 Secondary Parameter Study Model Dimensions: End Span Lengths = 0.8L

Secondary Parameter Study	West Span Length	Main Span Length	East Span Length	Girder Depth	No. of Girders	Diaphragm Depth	Diaphragm Fl. Width	Deck Thickness	Deck Width	Girder Web Thickness	Deck Cantilever to	Pier Flange Width	Pier Flange Thickness	Midspan Flange Width	Midspan Flange Thickness
Main Span-Spacing-Skew	ft.	ft.	ft.	in.		in.	in.	in.	ft.	in.	in.	in.	in.	in.	in.
2dd-L060-S8-sk20	60	60	60	26.67	9	13.33	2.22	9	65	0.5	26	13.8	0.375	7.25	0.375
2dd-L060-S8-sk60	60	60	60	26.67	9	13.33	2.22	9	65	0.5	26	13.8	0.375	7.25	0.375
2dd-L100-S105-sk40	100	100	100	44.44	7	22.22	3.7	9	66.33	0.5	40	17	1.25	11.475	1.25
2dd-L100-S105-sk60	100	100	100	44.44	7	22.22	3.7	9	66.33	0.5	40	17	1.25	11.475	1.25
2dd-L140-S105-sk20	140	140	140	62.22	7	31.11	5.2	9	66.33	0.5	40	18.4	2	12.7	2
2dd-L140-S105-sk60	140	140	140	62.22	7	31.11	5.2	9	66.33	0.5	40	18.4	2	12.7	2
2dd-L180-S8-sk40	180	180	180	80	9	40	7	9	67.33	0.5	40	17.9	2.25	12.15	2.25
2dd-L180-S8-sk60	180	180	180	80	9	40	7	9	67.33	0.5	40	17.9	2.25	12.15	2.25

Table B.4 Secondary Parameter Study Model Dimensions: Diaphragm Depth = Half of Girder Depth

Secondary Parameter Study	West Span Length	Main Span Length	East Span Length	Girder Depth	No. of Girders	Diaphragm Depth	Diaphragm Fl. Width	Deck Thickness	Deck Width	Girder Web Thickness	Deck Cantilever to	Pier Flange Width	Pier Flange Thickness	Midspan Flange Width	Midspan Flange Thickness
Main Span-Spacing-Skew	ft.	ft.	ft.	in.		in.	in.	in.	ft.	in.	in.	in.	in.	in.	in.
2dk8-L100-S8-sk40	100	100	100	44.44	9	33	5.5	8	67.33	0.5	40	18.375	1.25	12.5	1.25
2dk8-L140-S105-sk20	140	140	140	62.22	7	47	7.83	8	66.33	0.5	40	16.65	1.75	11.185	1.75
2dk8-L180-S105-sk60	180	180	180	80	7	48	8	8	66.33	0.5	40	22.77	2.5	15.925	2.5
2dk10-L100-S8-sk40	100	100	100	44.44	9	33	5.5	10	67.33	0.5	40	15.75	1.25	10.55	1.25
2dk10-L140-S105-sk20	140	140	140	62.22	7	47	7.83	10	66.33	0.5	40	14.55	1.75	9.6	1.75
2dk10-L180-S105-sk60	180	180	180	80	7	48	8	10	66.33	0.5	40	20.45	2.5	14.15	2.5

Table B.5 Secondary Parameter Study Model Dimensions: Deck Thickness

Secondary Parameter Study	West Span Length	Main Span Length	East Span Length	Girder Depth	No. of Girders	Diaphragm Depth	Diaphragm Fl. Width	Deck Thickness	Deck Width	Girder Web Thickness	Deck Cantilever to	Pier Flange Width	Pier Flange Thickness	Midspan Flange Width	Midspan Flange Thickness
Main Span-Spacing-Skew	ft.	ft.	ft.	in.		in.	in.	in.	ft.	in.	in.	in.	in.	in.	in.
2sh-L140-S8-sk60	140	140	140	62.22	9	47	7.83	9	67.33	0.5	40	15.55	1.75	10.35	1.75
2sh-L100-S105-sk60	100	100	100	44.44	7	33	5.5	9	66.33	0.5	40	17	1.25	11.475	1.25

Table B.6 Secondary Parameter Study Model Dimensions: Shoulder Width

Secondary Parameter Study	West Span Length	Main Span Length	East Span Length	Girder Depth	No. of Girders	Diaphragm Depth	Diaphragm Fl. Width	Deck Thickness	Deck Width	Girder Web Thickness	Deck Cantilever to	Pier Flange Width	Pier Flange Thickness	Midspan Flange Width	Midspan Flange Thickness
Main Span-Spacing-Skew	ft.	ft.	ft.	in.		in.	in.	in.	ft.	in.	in.	in.	in.	in.	in.
2tw38-L100-S8-sk20	100	100	100	44.44	9	33	5.5	9	67.33	0.375	40	16.8	1	11.4	1
2tw38-L100-S8-sk40	100	100	100	44.44	9	33	5.5	9	67.33	0.375	40	16.8	1	11.4	1
2tw38-L100-S8-sk60	100	100	100	44.44	9	33	5.5	9	67.33	0.375	40	16.8	1	11.4	1
2tw38-L140-S105-sk20	140	140	140	62.22	7	47	7.83	9	66.33	0.375	40	19.375	2	13.7	2
2tw38-L140-S105-sk40	140	140	140	62.22	7	47	7.83	9	66.33	0.375	40	19.375	2	13.7	2
2tw38-L140-S105-sk60	140	140	140	62.22	7	47	7.83	9	66.33	0.375	40	19.375	2	13.7	2
2tw58-L100-S8-sk20	100	100	100	44.44	9	33	5.5	9	67.33	0.625	40	13.65	1	8.125	1
2tw58-L100-S8-sk40	100	100	100	44.44	9	33	5.5	9	67.33	0.625	40	13.65	1	8.125	1
2tw58-L100-S8-sk60	100	100	100	44.44	9	33	5.5	9	67.33	0.625	40	13.65	1	8.125	1
2tw58-L140-S105-sk20	140	140	140	62.22	7	47	7.83	9	66.33	0.625	40	17.475	2	11.68	2
2tw58-L140-S105-sk40	140	140	140	62.22	7	47	7.83	9	66.33	0.625	40	17.475	2	11.68	2
2tw58-L140-S105-sk60	140	140	140	62.22	7	47	7.83	9	66.33	0.625	40	17.475	2	11.68	2

Table B.7 Secondary Parameter Study Model Dimensions: Girder Web Thickness